Birzeit University

Master Thesis

Analysis and Optimization of Microwave Links in Palestine Using Artificial Neural Networks

Joint Master in Electrical Engineering

Department of Electrical Engineering

Mohammad S. AbuRub

Supervised by

Mohammad Jubran, Ph.D.
Mohammad Hussein, Ph.D.

January 31, 2021

MASTER THESIS

Analysis and Optimization of Microwave Links in Palestine Using Artificial Neural Networks

Birzeit University

By

Mohammad S. AbuRub

This thesis was successfully defended On Tuesday November 3, 2020

Supervisors:

Dr. Mohammad Jubran _____

Dr. Mohammad Hussein _____

Examiners:

Dr. Wael Hashlamoun _____

Dr. Abdelkarem Awad _____

This Master Thesis is prepared by Mohammad AbuRub as in part fulfillment of the degree requirements for the Joint Master in Electrical Engineering, JMEE Program.

Declaration of Authorship

I, Mohammad S. AbuRub, declare that this thesis titled, "Analysis and Optimization of Microwave Links in Palestine Using Artificial Neural Networks" and the work presented in it are my own. I confirm that:

- This work was done wholly or mainly while in candidature for a research degree at Birzeit University.
- I hereby declare that all information was collected and provided in compliance with academic rules and ethical standards in this thesis I also declare that I have thoroughly cited and referenced all material and findings which are not original to this research as provided by these rules and conduct.
- I hereby declare that the present Dissertation can be processed and made available electronically by the Birzeit University, Institute of Graduate Studies and Science.
- I have identified all of the key sources of support.

Signature: ..... Date: .....

Contents

Declaration i

Table of Contents ii

List of Figures iii

List of Tables v

List of Abbreviations vii

Acknowledgement vii

English Abstract ix

Arabic Abstract x

1 Introduction 1
- 1.1 Overview of Radio Wave Propagation . . . 1
- 1.2 Wireless Communication . . . 2
- 1.3 Microwave . . . 2
- 1.4 Motivation . . . 4
- 1.5 Problem Statement . . . 4
- 1.6 Research Aim and Objectives . . . 4
- 1.7 Challenges . . . 5
- 1.8 Research Methods . . . 5
- 1.9 Main Contributions . . . 6
- 1.10 Scope of Work . . . 6

2 Related Works 7
- 2.1 Primer on Path Loss . . . 7
  - 2.1.1 Reflection . . . 8
  - 2.1.2 Diffraction . . . 8
  - 2.1.3 Scattering . . . 9
- 2.2 Primer on Path Loss with Machine Learning . . . 11
- 2.3 Primer on Rain Attenuation . . . 12

3 Primer on Artificial Neural Networks 14
- 3.1 Artificial Neuron . . . 16
- 3.2 Artificial Neural Networks . . . 17
  - 3.2.1 Feed-forward Artificial Neural Networks . . . 18

3.2.2 Recurrent Artificial Neural Networks . . . 19
3.2.3 Hopfield Artificial Neural Network . . . 19
3.2.4 Elman and Jordan Artificial Neural Networks . . . 19
3.2.5 Long Short Term Memory . . . 21
3.2.6 Bi-directional Artificial Neural Networks (Bi-ANN) . . . 21
3.2.7 Self-Organizing Map (SOM) . . . 22
3.2.8 Stochastic Artificial Neural Network . . . 22
3.2.9 Physical Artificial Neural Network . . . 22
3.3 Learning . . . 22
3.3.1 Supervised learning . . . 22
3.3.2 Unsupervised learning . . . 22
3.3.3 Reinforcement learning . . . 23
3.4 Usage of Artificial Neural Networks . . . 23

4 Problem Formulation **24**
4.1 Path Loss Prediction Based on ML . . . 24
4.2 Field measurement Environment and tools . . . 27
4.2.1 Data Collection . . . 28
4.3 Selecting Representative Propagation Models . . . 29
4.3.1 Free Space Path loss for LOS Environment . . . 29
4.3.2 ITU-R Rain Attenuation Model . . . 30
4.3.3 Crane Global Model . . . 32
4.4 Adapting the Selected Propagation Models . . . 32
4.5 Optimizing a Propagation Model . . . 35
4.5.1 NN Feed Forward Fitting Tool optimization . . . 35
4.6 Implementation of the Selected Models . . . 39
4.6.1 Model Validation . . . 39
4.7 Implementation of the Optimized Model . . . 42
4.7.1 Implementation of the NN Feed Forward . . . 42

5 Experimental Evaluation **46**
5.1 Results and Discussion . . . 46
5.1.1 Descriptive statistics of scenario One . . . 46
5.1.2 Descriptive statistics of scenario Two . . . 53
5.1.3 Regression Model . . . 58

6 Conclusion and Perspectives **67**
6.1 Conclusion . . . 67
6.2 Perspectives . . . 68

Appendices **69**

A Antenna Specification **70**

List of Figures

1.1 A communication system. 2
1.2 Different layers of the atmosphere. 3
1.3 A schematic illustration of a microwave link. 3
1.4 Research methods deployed in pursue of research objectives. 5

2.1 Path loss model family tree. Individual templates appear as circles and categories are shown as rectangles. Main categories are green. Smaller categories are blue. 8
2.2 test caption 9
2.3 Free Space Path Loss. 10

3.1 Working principle of an artificial neuron. 15
3.2 Simple artificial neural network. 15
3.3 Biological and artificial neuron design. 16
3.4 Feed-forward and recurrent topology of an ANN. 17
3.5 Feed-forward artificial neural network 18
3.6 Fully recurrent artificial neural network. 19
3.7 Simple one neuron Hopfield artificial neural network. 20
3.8 Elman ANN. 20
3.9 Jordan ANN. 20
3.10 Long Short Term Memory ANN. 21

4.1 test caption 25
4.2 test2 caption 26
4.3 Network Topology 27
4.4 Map of Transmitter Location using GCOM software. 28
4.5 test caption 31
4.6 Flowchart of the propagation models algorithms 34
4.7 Path loss prediction as a regression problem 35
4.8 Machine Learning optimization Framework using Neural Nets 35
4.9 The Levenberg-Marquardt Backpropagation Algorithm 36
4.10 Flowchart of NN Feed Forward Fitting Tool optimization 38
4.11 Implementation of Free Space Path loss Model. 39
4.12 Implementation of ITU-R Attenuation Model. 40
4.13 Implementation of Crane Attenuation Model. 40
4.14 A comparison between the Three Models at Frequency 15GHz. 41
4.15 A comparison between the Three Models at Frequency 18GHz. 41
4.16 A comparison between the Three Models at Frequency 23GHz. 42
4.17 Input and target vectors settings using the MATLAB NN fitting tool. 43

4.18 Defining optimum number of Neurons using the MATLAB NN fitting tool. 44
4.19 Training and measuring MSE using the MATLAB NN fitting tool. . . 44
4.20 Evaluating parameter performance using the MATLAB NN fitting tool. 45

5.1 ANN model diagram. 47
5.2 Histogram of hidden layers at training 51
5.3 Histogram of hidden layers at testing 52
5.4 Histogram of hidden layers at validation 52
5.5 ANN model diagram 53
5.6 Histogram of hidden layers at training 57
5.7 Histogram of hidden layers at testing 57
5.8 Histogram of hidden layers at validation 58
5.9 Histogram of scenario one testing data under 15GHz frequency 60
5.10 Histogram of scenario one testing data under 18GHz frequency 61
5.11 Shows Histogram of scenario one testing data under 23GHz frequency 61
5.12 Histogram of scenario two testing data under frequency 15GHz 63
5.13 Histogram of scenario two testing data under frequency 18GHz 64
5.14 Histogram of scenario two testing data under frequency 23GHz 64
5.15 Absolute Error of the predictive results ANN model and Theoretical models 65
5.16 Mean squared error (MSE), for ANNs models and theoretical models 66

List of Tables

2.1 ITU categorization of environments influenced by radio wave propagation. 10

4.1 The values of parameters k and α given by ITU-R 30
4.2 Percentage of Training, Validation, Testing, and Input Output parameters 43

5.1 Descriptive statistics for output variables in training, testing, and validation data-set at different layers 48
5.2 descriptive statistics for output variables in training, testing, and validation data-set at different layers. 54
5.3 Scenario one path loss prediction based on different layers 58
5.4 scenario one testing data under different frequency. 60
5.5 Scenario two path loss prediction based on different layers. 62

A.1 Antennas specification used in JAWWAL at 15 GHz 70
A.2 Antennas specification used in JAWWAL at 18 GHz 71
A.3 Antennas specification used in JAWWAL at 23 GHz 71

List of Abbreviations

PL Path loss

MSE Mean Squared Errors

LOS Line of sight

ML Machine Learning

ANNs Articial neural networks

FFNNs Feed-Forward Neural Network

GHz Gigahertz

Tx Transmitter

Rx Receiver

RF Radio frequency

ITU International Telecommunication Union

RMSE Root Mean Square Error

MSE Mean Square Error

RSS Received Signal Strength

RSL Received Signal Level

QoS Quality of service

5G Fifth Generation

Acknowledgements

I would like to thank my thesis advisors, Dr. Mohammad Jubran and Dr. Mohammad Hussein from Faculty of Engineering and Technology at Birzeit University (BZU). They consistently allowed this thesis to be my own work, but steered me in the right direction whenever I thought I needed it. Without your close support and follow up this thesis wouldnt be in the shape it has today.

I would also like to thank BZU committee who were involved in the validation proposal for this research project till its defense. A deep thanks to thesis final defense comittee from BZU for their advices and valuable feedback.

I would like to express my very profound gratitude to my parents and family, for providing me with support and continuous encouragement throughout my years of study and through the process of researching and writing this thesis. This accomplishment would not have been possible without them.

Special thanks to my spouse Sally for her every moment support, you have been a continuous source of support and encouragement during the challenges of graduate school and life. I am truly thankful for having you in my life. For my little child Aram who inspire me with joy and love.

Thank you.

Author
Mohammad S. AbuRub

Abstract

Telecommunication operators rely heavily on sophisticated simulation tools to design mobile and wireless networks. These tools depend on path loss models to simulate network performance and produce many reports such as coverage and interference. An accurate path loss models and hence simulation reports are necessary to enable operators to maintain efficient and reliable networks. The aim of this research is to develop and tune path loss model suitable for the Palestinian terrain using machine learning. First we will select appropriate path loss models. Then we will implement a process to tune them in order to model specific wireless environment (urban, suburban, open areas) in Palestine. The parameters of these models will be tuned based on real measured data. This research will focus on the microwave links in Palestinian Telecommunication Company network (PALTEL) and JAWWAL. Particularly, we will analyze the received signal power from a set of active microwave links at different frequencies (15GHz, 18GHz, and 23GHz) covering all geographical locations in the west bank. We will compare the measured received signal power with the tuned theoretical propagation models.

Using the Feed-Forward Neural Network (FFNNs) algorithm an optimal model is developed in this thesis for path loss predictions. Data-set was applied in Palestine to collect path loss data from nineteen different locations at various distances. Multi-layered FFNNs were trained with terrain profile data (transmitting power, frequencies, distance, and ITU-R p.530) to produce corresponding path loss values based on the Levenberg Marquardt algorithm. The number of neurons in the hidden layer was varied (2, 4, 6, 8, 10) with the best predictive accuracy to evaluate the Artificial Neural Network (ANN) model based on different metrics.

The output of the ANN models was evaluated: mean squared error (MSE) and standard deviation. Results of the machine learning processes show that the tangent activation function of the FNN architecture and 4 hidden neurons produced the least predictive error, with MSE and standard deviation values of 0.0032 dB, and 13.74 dB, respectively. In terms of generalization, the predictions of the optimal ANN model were given MSE, and standard deviation values of 0.0022 dB, and 13.84 dB, respectively, when checked with new data not used before

Keywords: Propagation, Path loss, Model, Machine Learning, Artificial Neural Networks, Feed-Forward Neural Network.

المستخلص

تعتمد شركات الاتصالات بشكل كبير على أدوات المحاكات المتطورة لتصميم شبكاتهم، يتيح استخدام نماذج فقدان المسار الدقيقة في هذه الادوات للمشغلين الاحتفاظ بشبكات موثوق بها و باستخدام الحد الأدنى من الموارد. يهدف هذا البحث الى تطوير وضبط نماذج فقدان المسار المناسبة للتضاريس الفلسطينية. سنقوم أولا باختيار نماذج فقدان المسار المناسبةز ثم سنقوم بتنفيذ عملية لضبطها من أجل تصميم بيئة لاسلكية محدده (المناطق الحضربة، الضواحي، المناطق المفنوحه) في فلسطين. سيتم ضبط معلمات هذه النماذج استنادا الى البيانات المقاسة الحقيقية. سيركز هذا البحث على وصلات المايكرويف في شبكة شركات الاتصالات الفلسطينة وبشكل خاص بالتل و جوال، سنقوم بتحليل قدرة الاشارة المستقبلة من مجموعة من وصلات المايكرويف النشطة بترددات مختلفة ١٥ جيجاهرتز، ١٨ جيجاهرتز، ٢٣ جيجاهرتز. لتغطي جميع المواقع الجغرافية في الضفة الغربية. سنقوم بمقارنه قوة الاشارة المستلمة المقاسة مع نماذج الانتشار النظرية المضبوطة. ثم سيتم ادخال افضلها الى التعلم الالي.

باستخدام خوارزمية التغذية إلى الأمام للشبكة العصبية ، تم تطوير نموذج مثالي في هذه الأطروحة للتنبؤ بخسارة المسار. تم تطبيق مجموعة البيانات في فلسطين لجمع بيانات فقدان المسار من تسعة عشر موقعًا مختلفًا على مسافات مختلفة. تم تدريب الشبكة العصبية متعددة الطبقات ذات التغذية الأمامية على بيانات ملف تعريف التضاريس : طاقة الإرسال ، والترددات ، والمسافة ، و ITU-R p.530 لإنتاج قيم خسارة المسار بناءً على خوارزمية Marquardt Levenberg ، تتنوع عدد الخلايا العصبية في الطبقة المخفية (٢ ، ٤ ، ٦ ، ٨ ، ١٠) و بأفضل دقة تنبؤية لتقييم نموذج الشبكة العصبية الاصطناعية بناءً على مقاييس مختلفة .

تم تقييم ناتج نموذج الشبكة العصبية من خلال متوسط الخطأ التربيعي والانحراف المعياري. تظهر نتائج عمليات التعلم الآلي أن وظيفة التنشيط لهيكل الشبكة العصبية الأمامية و ٤ خلايا عصبية مخفية أنتجت أقل خطأ تنبؤي، بمتوسط خطأ تربيعي وقيم انحراف معياري

تبلغ 0.0032 ديسيبل و 13.74 ديسيبل على التوالي. أعطيت تنبؤات نموذج الشبكة العصبية الاصطناعية الأمثل متوسط الخطأ التربيعي ، وقيم الانحراف المعياري 0.0022- ديسيبل ، و 13.84 ديسيبل ، على التوالي ، عند التحقق من البيانات الجديدة غير المستخدمة من قبل.

Chapter 1

Introduction

Contents

1.1 Overview of Radio Wave Propagation 1
1.2 Wireless Communication 2
1.3 Microwave 2
1.4 Motivation 4
1.5 Problem Statement 4
1.6 Research Aim and Objectives 4
1.7 Challenges 5
1.8 Research Methods 5
1.9 Main Contributions 6
1.10 Scope of Work 6

1.1 Overview of Radio Wave Propagation

These days wireless communication technology becomes more popular and it is used in several applications in our lives. Before installing the equipment, detailed planning and detailed analysis of the radio wave system is required in order to build a stable and reliable microwave network [1]. This is because poor design can lead to the periodic system outage, increase system delay, and reduce flow or total system failure.

An exemplary communication system comprises of three main systems: the transmitter (Tx), the receiver (Rx) and the transmission channel as portrayed in Figure 1.1. It is vital to comprehend the channels statistical characteristics for the purpose of predicting the channel behavior. The signal processing techniques then will be evolved and utilized properly to guarantee that the transmission channel between the Tx and the Rx is as credible as possible. Therefore, understanding the channel features plays an important role in designing and optimizing a communication system.

The channel is susceptible to noise, distortion and other interventional sources leading to the variation of the received signal power. On the one hand, the models

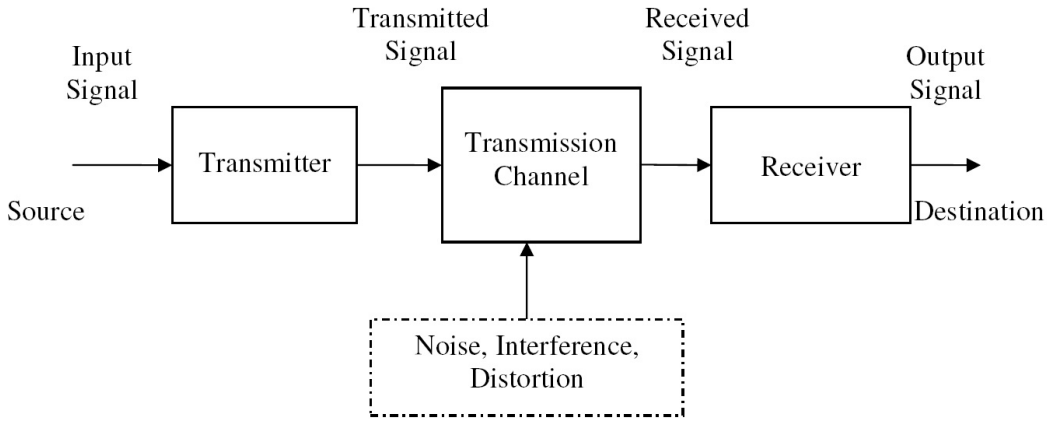

Figure 1.1: A communication system.

that depict the signal fluctuations and fluxes over small distances in the order of the wavelength or short-time duration are called small-scale models. On the other hand, the propagation models that foresee the mean signal strength over the large distances between the TX and the RX or long-time duration are called large-scale or path loss models [2].

Path loss entails that the signal power lost as a radio wave propagates along a path from the TX to the RX. Standardly, the overall received signal oscillates owing to the constructive and destructive addition of multipath signals along different paths of wave propagation.

1.2 Wireless Communication

The term "wireless communication" was introduced in the nineteenth century, and in the following years, wireless communication technology developed. [3]. This is one of the most paramount information transmission media from one device to other devices. In this technology, information can be transferred by air without need cables or other conductive or electronic conductors with electromagnetic waves, such as infrared, radio waves, satellites, etc. Currently, wireless communication technology refers to different devices and wireless technologies: from smartphone to computers,CDs, laptops, Bluetooth technologies, and printers.

1.3 Microwave

The term "microwave" refers to an alternating signal with a frequency between 300 MHz and 300 GHz, which corresponds to the electrical wavelength between $\lambda = c/f = 1m$ and $\lambda = 1mm$ respectively [4]. Microwave signals propagate along straight paths and on the troposphere. Low frequency waves are refracted or reflected, higher frequency waves travel farther before being reflected, very high frequency waves pass by ionized areas in the upper atmosphere, Figure 1.2 shows the

different layers of the atmosphere. Microwaves do not vary slightly from barriers such as hills, mountains, and large human structures. Some damping occurs when the microwave energy passes through trees and frames. Such radio waves have a smaller effect on the energy of radio waves (RF) in longer wavelengths.

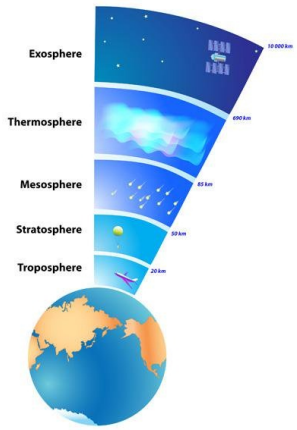

Figure 1.2: Different layers of the atmosphere.

Microwave transition is exceedingly utilized in point-to-point communication systems on the Earths surface as shown in Figure 1.3, in satellite communications, and in space-to-space communications. The other parts of the microwave range are used in radio location stations, radio navigation systems, sensory systems, and radio astronomy. With the development of cellular and satellite technologies, microwave networks are now less frequently used in the era of telecommunications. Communication is dominant in fiber optic data transmission. However, in remote locations where the installation of fiber optic cables is economically impossible, the microwave is still turned on. Microwave data transmission takes place in both analog and digital formats. The digital format is the most advanced type of data transmission for microwave signals.

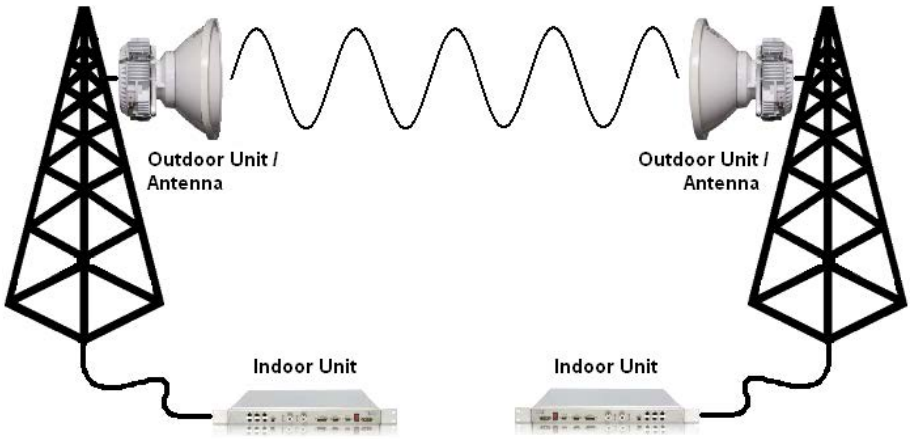

Figure 1.3: A schematic illustration of a microwave link.

1.4 Motivation

The demand for wireless broadband services. The capability for microwave backhaul networks to be expeditiously and cost-effectively deployed is being a critical point for successfully tackling the backhaul bottleneck issue, and it is not a mere coincidence that over 50% of the worlds base transceiver stations are coinjoined using point-to-point microwave technologies [5].

The need to install Microwave links in mobile and wireless networks is important to connect several base stations together and with the core network. Communication Service Providers are eager to keep their Microwave links available and stable. This demands a lot of effort from engineers to design and deploy these microwave link between two sites.The Palestinian terrain and restrictions of access to some locations adds more challenge to this task.

It is anticipated that the machine learning approach to path loss modeling can have a stronger model and can well generalize the propagation process as the model is learned by training with the data obtained from the field. The prediction of loss of the propagation path is seen as a regression problem as mentioned in [6]. The prediction of propagation path loss using ANN models, which provides a more reliable approximation than the empirical models [7].

1.5 Problem Statement

There are innumerable methodologies and mechanisms employed to evolve attenuation models which are later utilized in path loss models. The Global (Crane) model and the ITU model are the most ordinarily used models to compute attenuation by virtue of major atmospheric effects; mainly rain with some discussions regarding water vapor and fog modeling on a terrestrial path link. Conventional techniques for assessing losses due to atmospheric effects focus on the dominant source of fading - rain attenuation. This thesis sheds the light on the study of traffic attribute and their influence on microwave received signal levels using machine learning, not solely on rain attenuation.

1.6 Research Aim and Objectives

The aim of this master research is to optimise a propagation model for point to point microwave connectivity using machine learning technology. Hence, to achieve the research aim, the following research objectives need to be pursued:

Q1. Identification of parameters affecting connectivity of microwave links.

Q2. Selection of propagation models that are suitable.

Q3. Adoption of the selected model in the ML input.

Q4. Evolution of an optimal propagation model using machine learning

Q5. Validation of the optimized models predictions.

1.7 Challenges

Three main challenges can be identified as obstacles to achieving the objectives laid out in Section 1.6:

1. Identifying the most relevant information which can be extracted from the traces of real world experiments to train the machine learning models.
2. Selecting machine learning algorithms for training the models which will be used to generate the new environment specific propagation models.
3. Cleaning and preparing the datasets for the tool of the machine learning algorithms to a specific dataset which will be used to validate the approach.

1.8 Research Methods

1. The first method, Action Research (AR), has been deployed in pursue of Q1, Q2, and Q3. AR aims to build knowledge.

2. The second method, Machine learning (ML), has been deployed in pursue of Q4. There is no generic propagation model which can suit every environment and provide accurate predictions other than those models which have been custom-designed for that. Thus, the ML optimization considered.

3. The third method, the experiment, will deployed in pursue of Q5. Simulations of the optimized and non-optimized propagation models have been mathematically modelled across different environments.

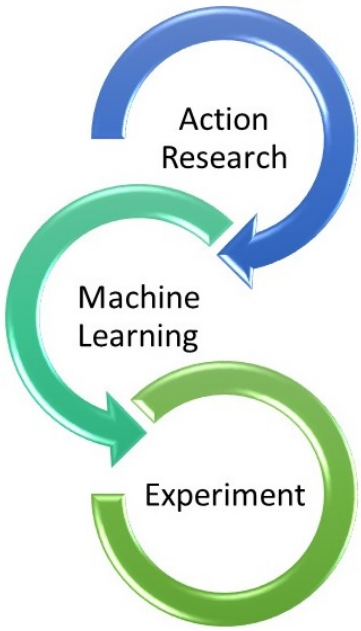

Figure 1.4: Research methods deployed in pursue of research objectives.

1.9 Main Contributions

The main contribution resulting from this thesis can be summarised as follows:

- A machine learning approach to generate optimized path loss models, reflecting the specific characteristics of a given environment, based on traces from real past experiments.
- Adapt the selected empirical propagation models to additionally consider the distance in predicting the ANNs models performance.
- A real Data-Set obtained from PalTel and Jawwal.

1.10 Scope of Work

This thesis is structured as follows.

Chapter 2 Presents related work, discusses and compares existing deterministic and empirical propagation models. Emphasis is placed on the empirical model.

Chapter 3 Introduces artificial neural networks, in order to lighten the area of artificial neural networks we briefly described basic building blocks (artificial neuron) of artificial neural networks and their transformation from single artificial neuron to complete artificial neural network.

Chapter 4 Discusses the design of an optimal propagation model for point to point microwave connectivity. This starts by choosing among existing propagation models those that are representative of their respective types. Then, adapting one model by adding the frequency, distance and transmitted power to predict the performance of link budget parameters. It then evolves using Machine Learning an optimized propagation model.

Chapter 5 Illustrate and analyze the performance of our proposed simulation algorithms.

Chapter 6 Summarizes the research findings and the thesis and makes recommendations for further study and development.

Chapter 2

Related Works

Contents

2.1 Primer on Path Loss 7

2.1.1 Reflection 8

2.1.2 Diffraction 8

2.1.3 Scattering 9

2.2 Primer on Path Loss with Machine Learning 11

2.3 Primer on Rain Attenuation 12

The radio waveform modeling field has been studied by many researchers and from different views. Because the distribution and importance of wireless networks continue to grow, there will also be a need for better methods of modeling and measuring wireless signal propagation. Figure 2.1 shows the path loss models family tree, those models from the last 60 years, most of them are discussed in [8].

2.1 Primer on Path Loss

The radio wave propagation paradigm or path loss model plays a very important role in the planning of any wireless communication systems; the path or depreciation damping is to reduce the power density (decrease) of electromagnetic waves during propagation in space. The purpose of the propagation model is to predict propagation behavior of radio waves in the atmosphere. In the case of microwave line planning, models predict the path loss along with link.

Path loss patterns describe signal attenuation between transmitting and receiving antennas, depending on propagation distance and other parameters. Some models contain many field profile details to evaluate signal attenuation, while others simply take into account frequency and distance of the medium [9]. Loss of a radio signal path is a principally basic element in the design of any radio or wireless system. Studying of radio signal attenuation to determine the number of components of the radio communication system, in particular to enhance the transmitter and antenna power, in particular altitude and overall location. Loss of the radio channel will also affect other elements, such as receiver sensitivity, form of transmission and several

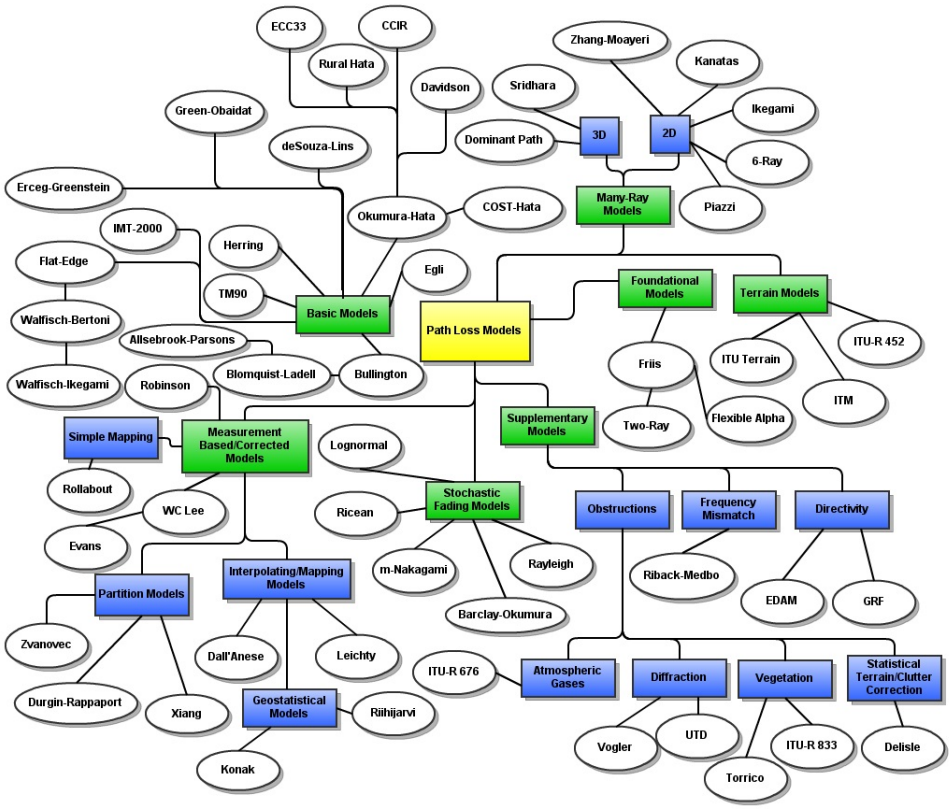

Figure 2.1: Path loss model family tree. Individual templates appear as circles and categories are shown as rectangles. Main categories are green. Smaller categories are blue.

other factors. Therefore, it is necessary to understand the causes of the loss of the radio terminal and to determine the levels of signal loss for the radio channel being broadcast. The three main path loss mechanisms are manifested per the here under narrative:

2.1.1 Reflection

As radio wave stubs on the surface of something that has a large size relative to the wavelength, the object represents a portion of the incident wave and travels in a direction controlled by Snell's law of reflection. The Snell law shows that the angle of incidence is equal to the reflection of the tilt. The reflected wave's electric field amplitude is related to the incident wave by means of the coefficient of reflection. It goes without saying that the coefficient of reflection determines the material characteristics of the media, wave polarization, incident angle and wave frequency [10].

2.1.2 Diffraction

Whilst a radio wave is incident upon an object with a large sharp edge of electrical basis, the wave drags out around the sharp edge into the shadow region of that very object as a result of the propagation mechanism called diffraction [11]. The impact

of diffraction is more significant at high frequencies. Diffraction plays a very major role identical to reflection that allows a transmitted radio signal reaching a receiving antenna even if the direct line of sight between the TX and RX is absent. Huygens principle has explicated the diffraction mechanism. As per this theory, every point in a main wave behaves as a point source radiating secondary spherical wavelets. The totality of these secondary spherical wavelets comprises a secondary wave front of a traveling wave. This is the very mechanism that a radio wave creeps around the sharp edge of an object and infiltrates into the shadow region. Diffraction is obviously fundamental for radio wave propagating in an environment that is full of several random objects. Particularly, diffraction depends on the edge geometry of obstacles, the propagation medium, and the wave characteristics.

2.1.3 Scattering

The scattering effect happens when an electrically rough surface is incidental to a radio wave. It gives rise to various directions for the incident radio wave being reverberated off the earth. A propagating object's roughness refers to the protuberance upon its surface. When the protuberance is of the order of the wavelength the effect of scattering is considerable. The reflected wave moves in a particular direction determined by Snell's law, in the event of reflection. For scattering, the incident wave is reflected in a diffuse behavior resulting in numerous reflected waves traveling in different directions away from the scattering object within some uncommon conical region. Scattering is essentially associated with rough surfaces, or irregularities and abnormalities. Because of scattering, the actual signal obtained may be stronger than predicted by reflection and diffraction only [12]; Figure 2.2 shows scattering of radio signals by rain drops.

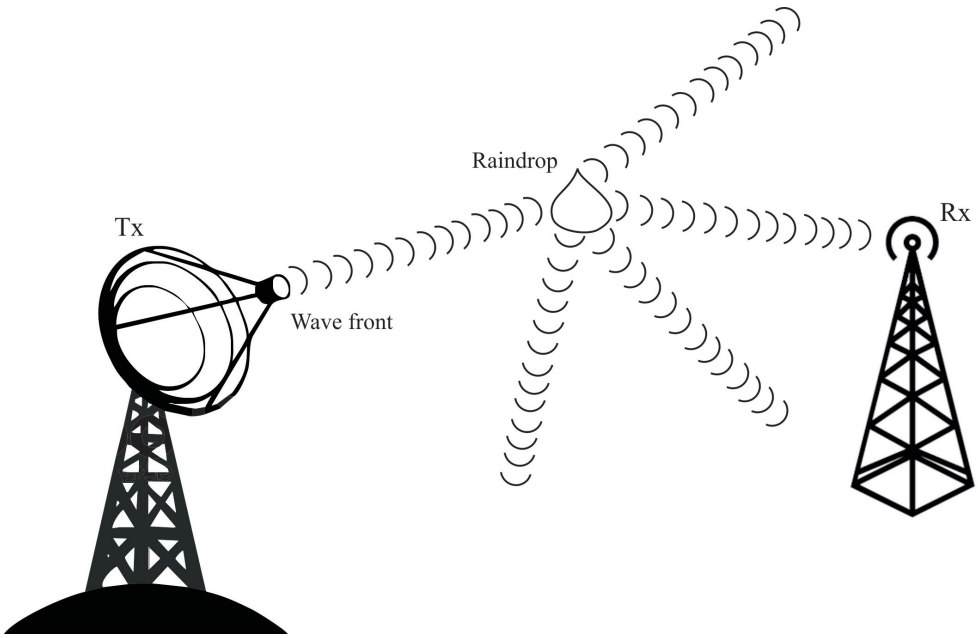

Figure 2.2: Scattering of radio signals by rain drops [13]

The free space path loss (FSPL) is a key factor in the many radio frequency calculations used in various places to predict the radio signal strength that the expected radio system would be expected. The FSPL is essentially a type of signal failure that occurs when an electromagnetic wave changes data on a line path to view free space, as shown in Figure 2.3. In this case, there are no obstacles based on the signal that must be refracted or reflected, or which may become a source of additional mitigation. The FSPL signal is reduced, which is inversely proportional to the square of the distance between the signal sources [14].

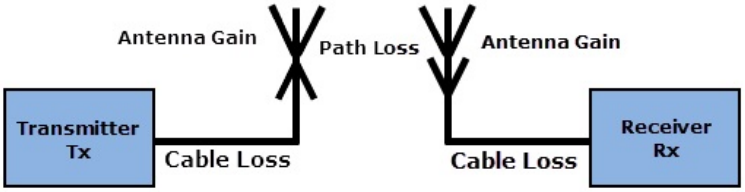

Figure 2.3: Free Space Path Loss.

It is essential to identify the different type of environments that have been categorized by International Telecommunication Union (ITU) namely: Urban, Suburban, and Rural [15]. Table 2.1 lists three environments alongside their characteristics. Besides terrain types, there are several common parameters across propagation models that effect the overall performance, such as frequency of operation, distance between transmitter and receiver (coverage radius), transmitter antenna height, receiver antenna height, as well as antenna gain, and transmission power [16].

Table 2.1: ITU categorization of environments influenced by radio wave propagation.

Environment	**Description and propagation impairments of concern**
Urban	Typified by wide streets Characterized by streets lined with tall buildings with several floors Building height renders contribution to roof-top propagation unlikely Reflections and shadowing from moving vehicles occur Primary effects are long delays
Suburban	Single and double storey dwellings Roads are generally two lanes wide with cars parked along sides Heavy to light foliage possible Motor traffic usually light
Rural	Small houses surrounded by large gardens Influence of topography height Heavy to light foliage possible Motor traffic sometimes high

In [1], a study of popular wireless propagation models was performed. Macrocell (usually a large outer surface), a microcell (a small outer surface) and an internal environment. In the first case, conditions are generally not met. The signal is spread through reflection, diffraction, and refraction. Since there are many factors, it's hard

to make a template, but some have been suggested. The trace element model is easier to formulate from the empirical and physical analysis. For example, an empirical model was proposed in [17]. A theoretical "ray-optical" model was proposed in [18].

Analytical models have been used in several studies. In the radiation tracking model (for example [19]), all possible signal paths are calculated from the transmitter to the receiver. Predictions can be based on the free transfer, reflection, diffraction, diffusion in walls and transmission through different materials.

In models with finite-difference time-domain (FDTD), a numerical solution of the Maxwell equations is made [20]. Maxwell's equations are approximated by a set of difference equations. The numerical solution is achieved by finite differentiation. This is also a method that requires calculation. Only suitable for small areas. For larger dimensions, the radiation pattern is best considered.

2.2 Primer on Path Loss with Machine Learning

Machine learning is an approach to optimize performance on a specific task on the ground of comprehensive data and adjustable model architecture. Recently, it has been extensively used in many fields like computer vision, speech recognition, autonomous driving, and so on. Machine learning tasks can be predominantly classified into supervised learning and unsupervised learning, depending on if data samples are labelled or not. Regarding supervised learning, tasks can be further split into classification problems and regression problems depended on whether the predicted values are detached or constant.

The abstract theoretical models and approaches are very expensive in terms of ability of defining the most advantageous towers locations, fulfilling reasonable data rates and assessing coverage without making a series of propagation measurements and the empirical models are not so precise [21]. These limitations can be controlled by an artificial neural network model. The ETF model with an artificial neural network (ANN) is depended on multilayer conception in combination with a neural network [22]. In the case of a particular environment, the neural network must be readied based on measured data. Even though the training is expensive, it should only be done once.

In [23], Using the Feed- Forward Neural Network (FFNN) algorithm, an advantageous model is built for the path loss expectations. Based on the Levenberg Marquardt algorithm, single-layer FFNNs were trained with standardized terrain profile data (longitude, latitude, elevation, altitude, clutter height) and normalized distances to generate the corresponding path loss values. The number of neurons in the hidden layer was varied (1-50) to determine the best prediction accuracy for the Artificial Neural Network (ANN) model.

The performance of the ANN models was assessed using different metrics: Mean Absolute Error (MAE), Mean Squared Error (MSE), Root Mean Squared Error (RMSE), Standard Deviation, and Coefficient of Regression (R). Machine learning

results show that the FNN architecture adopting a tangent activation function and 48 hidden neurons produced the least predictive error, with MAE, MSE, RMSE, standard deviation and R values of 4.21 dB, 30.99 dB, 5.56 dB, 5.56 dB, and 0.89 respectively. With respect to generalization capability, MAE, MSE, RMSE, standard deviation, and R values of 4.74 dB, 39.38 dB, 6.27 dB, 6.27 dB, and 0.86, respectively, were predicted for the optimal ANN model, When checked on new data not used previously.

The author of [24] developed a new approach for the prediction of the path loss in an urban environment based on dimensionality reduction techniques and learning machines.

Most of the work is dominated by models that extend to the basic principles of electromagnetic suppression with theoretical and empirical corrections. The main attention is given to the development of complex theoretical deterministic models. The next generation of models will probably focus on data.

2.3 Primer on Rain Attenuation

Attenuation can be obtained from direct measurements or could be estimated from rain rate information. Rain attenuation over a terrestrial path is defined as the result of the (dB/km) specific attenuation and the effective (km) propagation path duration. The effective length of the path is determined by knowing the length of the link and by the horizontal distribution of the rain along the path. The $A(dB)$ rain attenuation exceeded by p percent of the time is calculated as follows:

$$A = \gamma R^{d_{eff}} = \gamma R^{dr} \tag{2.1}$$

$$\gamma = kR^{\alpha} \tag{2.2}$$

$$d_{eff} = dr \tag{2.3}$$

Where $R(mm/h)$ approaches the rain rate at p percent of the time, r is the path reduction factor at the same time, $d(km)$ is the radio path range. The k and α variables depend on the frequency, rain temperature, and polarization; their values can be obtained from ITU-R P.838-3 [16]. In most attenuation prediction models, in general, the required inputs are the rainfall rate exceeded at percent p of time, the effective propagation path length, and the operating frequency of the link. It should be remembered that the element of path reduction accounts for the inhomogeneity of rain on the whole propagation path.

The authors present studies on rain attenuation at 18 and 38 GHz microwave connection systems in [25], which defines the minimum output criteria for wireless

radio communication with terrestrial fixed service. The experimental link at 18 and 38 GHz (3.2 km) is used to study effects of rain propagation. Signal data collected for rain attenuation and rain intensity were obtained from 2013 to 2015 at 10s intervals over a 3 year period. The record shows rain intensity of around 50 mm/h and attenuation values of 33.38, 21.88 and 20.89 dB occurred under 18 GHz lateral, vertical and 38 GHz vertical polarization, respectively, for 0.01 percent of the time. This study emphasizes the debate and analysis of models ITU-R P.530-16, Moupfouma, Da Silva Mello, and Abdulrahman. Relative error margin of approximately 71, 60, 38 percent; 64, 49, 42 percent; 3, 38, 42 percent were obtained for 0.1, 0.01, 0.001 percent of the time in 18 GHz horizontal, vertical and 38 GHz vertical polarization respectively from ITU-R P. 530-16, analyzed in conjunction with an appropriate approach to characterizing rain attenuation in microwave interconnections, the efficiency of which was compared with that of prices.

The backpropagation neural network (BPNN) is trained in [26] to predict rainfall rates, and thus attenuation that is likely to be experienced on a link. This research is performed over the Durban subtropical zone of South Africa (29.8587 S, 31.0218 E). The backpropagation neural network is trained using rainfall data collected from 2013 to 2016 to forecast rainfall levels, using the nonlinear mapping capabilities between inputs and outputs. Long-term rain attenuation statistics resulting from predicted rainfall rates are compared to the actual and ITU-R models, and results show a relatively small margin of error between predicted rain attenuation exceeded by 0.01% of an average year.

Advanced models need a more accurate and scalable representation of the path loss for complex Areas such as the urban area. This study suggests an artificial neural network (ANN) that is used to learn from the calculated path loss data and is a function of distance and frequency, the path loss structure. The effect on prediction accuracy of the network architecture parameter (activation function, number of hidden layers and nodes) is analyzed. In this research study , the data was obtained from Palestine 's broad terrestrial lines service , which includes Voice, VoIP, ADSL, VDSL and traffic to corporate customers.

Chapter 3

Primer on Artificial Neural Networks

Contents

3.1 Artificial Neuron 16
3.2 Artificial Neural Networks 17
3.2.1 Feed-forward Artificial Neural Networks 18
3.2.2 Recurrent Artificial Neural Networks 19
3.2.3 Hopfield Artificial Neural Network 19
3.2.4 Elman and Jordan Artificial Neural Networks 19
3.2.5 Long Short Term Memory 21
3.2.6 Bi-directional Artificial Neural Networks (Bi-ANN) 21
3.2.7 Self-Organizing Map (SOM) 22
3.2.8 Stochastic Artificial Neural Network 22
3.2.9 Physical Artificial Neural Network 22
3.3 Learning 22
3.3.1 Supervised learning 22
3.3.2 Unsupervised learning 22
3.3.3 Reinforcement learning 23
3.4 Usage of Artificial Neural Networks 23

An Artificial Neural Network (ANN) can be defined as a Mathematical model that tries to simulate the structure and functionalities of biological neural networks. The main structure that forms the basis of an ANN is the artificial neuron, which is the skeleton of the networks functionality [27]. In order for this model to follow through, three main functions are implemented. The first phase is the multiplication where it occurs at the entrance of the artificial neuron, in this phase the input value is multiplied with individual weight, this input is transferred to the next phase of the cycle the summation phase, where a sum function sums all the weighted inputs and bias, and transfers them to the last phase activation which is where the sum of all previously weighted inputs and bias are outputted Figure 3.1.

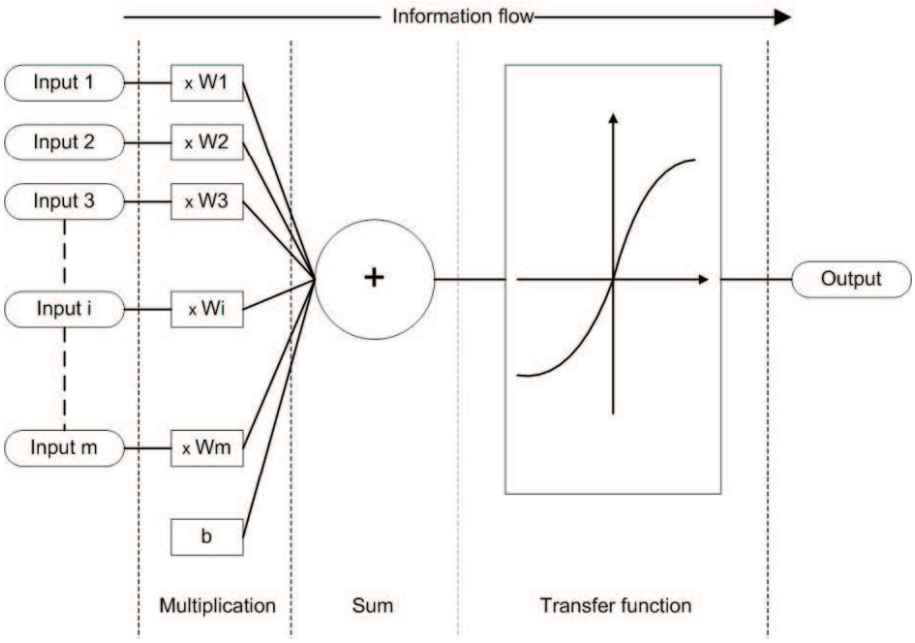

Figure 3.1: Working principle of an artificial neuron.

The main working model and the complexity of the artificial neural network comes to life when all models are interconnected, allowing a simple calculation to grow to a very complex model. Figure 3.2, However random interconnection is not how this model works as it will result in an unmanageable complex structure.

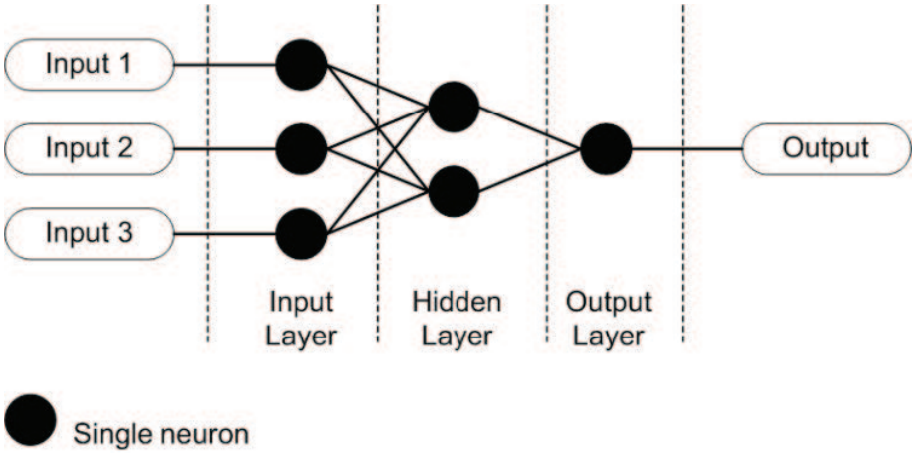

Figure 3.2: Simple artificial neural network.

In order to follow a manageable outline when interconnecting the neurons, two building blocks will need to be followed, the first building block is the predefined standard topographies that were structured to assist in resolving different types of problems. In order to use the topographies correctly, we need to firstly define what the problem is and then we can decided which artificial neural network topology is to be used, after its selection slight modification will need to be made to the topology parameters in order for it to correctly assist in the problem solving.

The second building block is the learning paradigm, this is composed of three learning types, the supervised, the unsupervised and the reinforcement. The basis on how we choose which paradigm is most suitable is based on the problem at hand that we are trying to resolve. The paradigms function on same principality learning data and learning rules based on these two principles the output response is run in parallel to the input signals.

After selecting and editing the topology and choosing the correct paradigm the artificial neural network can be used to resolve the problem. This model has been used in all sectors and for a while now, there is no limitation on where it can be implemented, aerospace, automotive industry, electronics, manufacturing, mechanics, robotics, and telecommunications. [28]

3.1 Artificial Neuron

The artificial neural network is composed in artificial neuron which are based on design and functionality of the biological neuron that composes the biological neural network in the human body Figure 3.3 [29]. Information in a biological neuron enters through the dendrite, and then processed in the soma, the result is then passed on via axon. Artificial neuron functions similarly but through weighted inputs, the body sums the weighted inputs, and processes the sum via the transfer function, the processed information passed then via outputs.

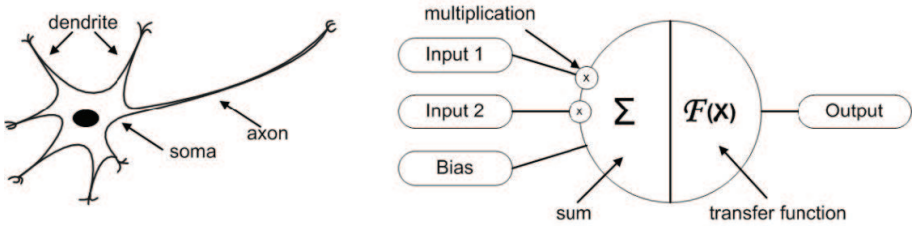

Figure 3.3: Biological and artificial neuron design.

The model of an artificial neuron is composed of two equations; equation 3.1 the transfer function equation, this defines the artificial neuron property in regards to the mathematical functionality. The equation set function can be a, (a) Step function which is used for two possible outputs such as zero and one. This type of transfer function is labelled as neuron perceptron which is used to resolve classification issues which are commonly located in the final layer of the artificial neural networks. (b) Linear transfer function outlines simple neuron linear equations over the sum of weighted inputs and bias or (c) Non-Linear (Sigmoid) which is the most commonly used specifically in the artificial neural network, which allows a calculated derivate. Equation 3.2 describes the situation when the specific threshold listed in step function is not met, resulting in a different value.

$$y(k) = F(\sum_{i=0}^{m} w_i(k).x_i(k) + b) \tag{3.1}$$

Where:

$x_i(k)$ is input value in discrete time k where i goes from 0 to m,

$w_i(k)$ is weight value in discrete time k where i goes from 0to m,

b is bias,

F is a transfer function,

$y_i(k)$ is output value in discrete time k.

$$y = \begin{cases} 1if w_i x_i, & \text{for} \geq threshold \\ 0if w_i x_i, & \text{for} < threshold. \end{cases} \tag{3.2}$$

3.2 Artificial Neural Networks

The Artificial Neural Network is composed of two or more neurons. One artificial neuron is not able to resolve any problems solely on its own. However, when two or more neurons are connected a solution to complex issues and problems can then be generated. The building blocks are able to resolve the issues in the method of distributed, local, nonlinear or parallel way. In the graphs that outline how the topologies interact with each other, the individual neurons are grouped into layers for easier diagram interpretation.

The word, topology is used to describe the architectural interconnection of the neurons with each other. The numerous topologies that can be made are divided to two major classes Figure 3.4 illustrate these two topologies; the first is the feedforward topology (a-cyclic graph), this topology allows the information to flow in one direction and the second is the recurrent topology (semi-cyclic graph) in which the information flows into and in opposite directions.

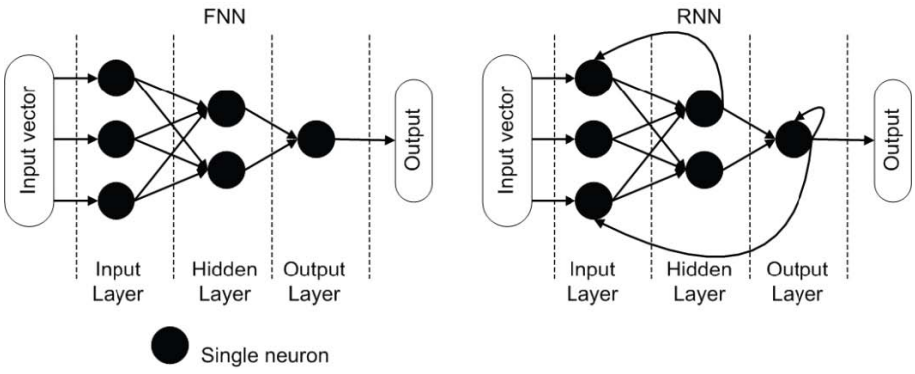

Figure 3.4: Feed-forward and recurrent topology of an ANN.

The topology itself is not the foundation for a working problem solving artificial neural network, the learning method for the proper response that the artificial neural network will output needs to be learnt either through the reinforcement, supervised or un-supervised learning method. The method used the main objective of the learning method is to defines the different variables and decrease the cost function.

3.2.1 Feed-forward Artificial Neural Networks

Artificial neural network that deals with on direction information flow and no back loops is known as Feed-Forward artificial neural network. This type of topology can have an unlimited number connections between artificial neurons, layers, or used transfer functions. The most straightforward network that can be made is a single perceptron with the capability to of linear separable problems Figure 3.5 [30], with the usage of a sets of equations (sets of equations 3.3, 3.4 and 3.5), this type of network can process long mathematical descriptions where solving by hand is impractical.

$$\begin{aligned} n_1 &= F_1(w_1 x_1 + b_1) \\ n_2 &= F_2(w_2 x_2 + b_2) \\ n_2 &= F_3(w_2 x_2 + b_2) \\ n_3 &= F_4(w_3 x_3 + b_3) \end{aligned} \tag{3.3}$$

$$\begin{aligned} m_1 &= F_4(q_1 n_1 + q_2 n_2 + b_4) \\ m_2 &= F_5(q_3 n_3 + q_4 n_4 + b_5) \end{aligned} \tag{3.4}$$

$$y = F_6(r_1 m_1 + r_2 r_2 + b_6) \tag{3.5}$$

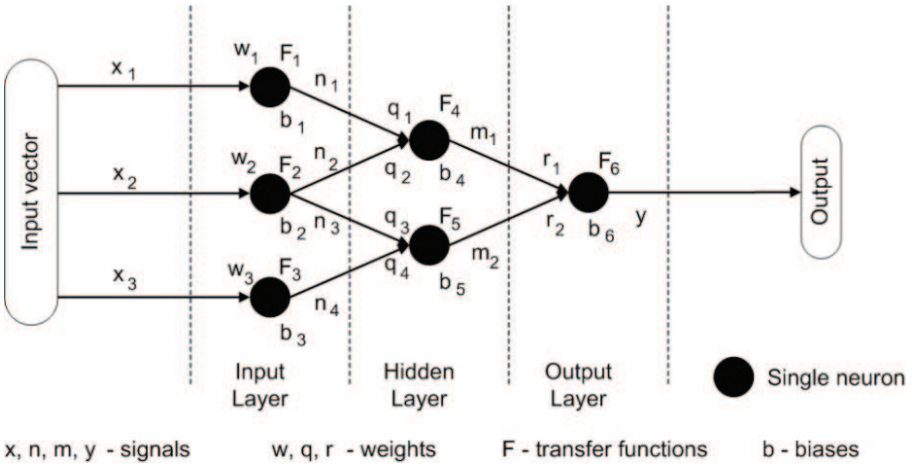

Figure 3.5: Feed-forward artificial neural network

3.2.2 Recurrent Artificial Neural Networks

Artificial neural network that deals with information that is transmitted in forward backward directions is known as the Recurrent artificial neural network. In this type of network there is no limitations regarding back loops, and dynamic temporal behaviour can be exhibited here. Figure 3.6 when all basic building blocks found in the network are directly connected to each other in all directions, this will be the most basic topology. The recurrent artificial neural network is the basis for the bi-directional, Elman, Hopfield, Jordan and others.

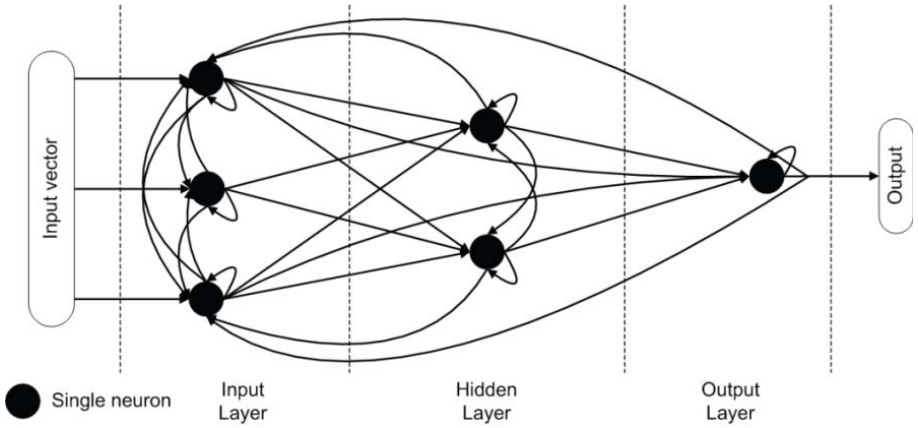

Figure 3.6: Fully recurrent artificial neural network.

3.2.3 Hopfield Artificial Neural Network

A recurrent artificial neural network that has the capability to store one or more memory known as stable target vectors and act a cue to the network memory is known as a Hopfield artificial neural network. This network works on binary nodes i.e. two different value inputs value of 1 or -1 or the value of 1 or 0, with only a possibility for two binary unit activation a_i.

The typically used weights in this network equation is symmetric, this will result in monotonically decrease of the energy function while the activation rule is followed. Non-symmetric weights will result in some periodic or chaotic behaviour. In order to train a Hopfield artificial neural network Figure 3.7 the energy of states will need to be lowered.

3.2.4 Elman and Jordan Artificial Neural Networks

A special case of recurrent artificial neural networks with the ability to detect and generate time-varying patterns such as temporal as well as spatial, with the ability to respond to them, such as network is known as the Elman artificial neural network Figure 3.8 shows a simple three layer network with a context unit (back-loop hidden layer connected to input layer trough). Typically this type of network contains sigmoid artificial neurons in the hidden layer and linear artificial neuron in the output

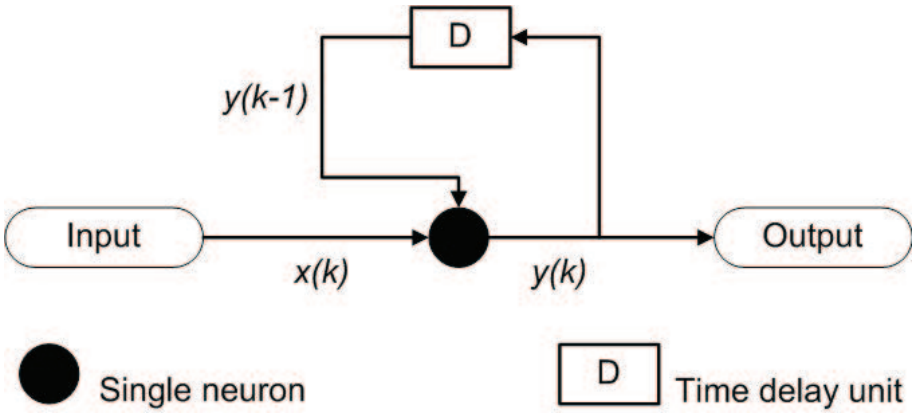

Figure 3.7: Simple one neuron Hopfield artificial neural network.

layer. If there is enough artificial neurons in the hidden layer, this combination will allow approximating the arbitrary accuracy. The Jordan network Figure 3.9 differs from the Elman network by its ability for the context units to be fed from the output layer instead of the hidden layer.

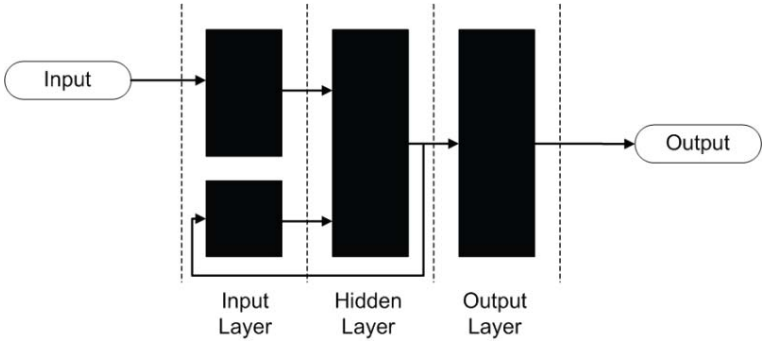

Figure 3.8: Elman ANN.

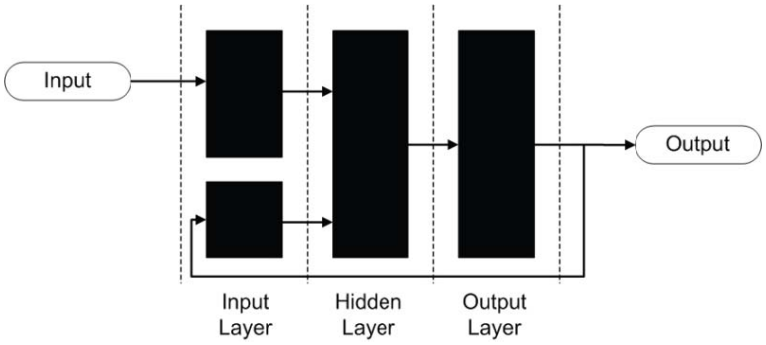

Figure 3.9: Jordan ANN.

3.2.5 Long Short Term Memory

A topology that has the ability to learn from experience in order to classify, predict and process time series that have long time lags and unknown size between important events is a Long Short Term Memory neural network, this is one of the recurrent artificial neural networks typologies that outperforms other neural networks. In this network, hidden Markov Models and other sequence learning methods. The network is composed of (1) gates; that determine the significance to remember an input, when to continue to remember an input or forget it and when to output the value, (2) Long Short Term Memory artificial neural network the building block, that has the ability to remember value for any set period of time.

Network architecture Figure 3.10 consists of sigmoid units. The process that is followed in Figure 3.10 shows the following: Input value is processed in the tope neuron in the input layer, this then might be sent to the memory unit depending on the computed value that was outputted from the second neuron in the input layer. The input layer also has a third neuron that is responsible for deciding how long the memory unit remembers the value. In the bottom layer the neuron here is responsible determining when the output be release from memory. The Figure 3.10 also shows that this network has two hidden layers, the first ones neurons are responsible for simple multiplication, in the second layer the neurons compute simple linear functions of its inputs the output from this layer is directed into the input of the first hidden layer for the decision to be made.

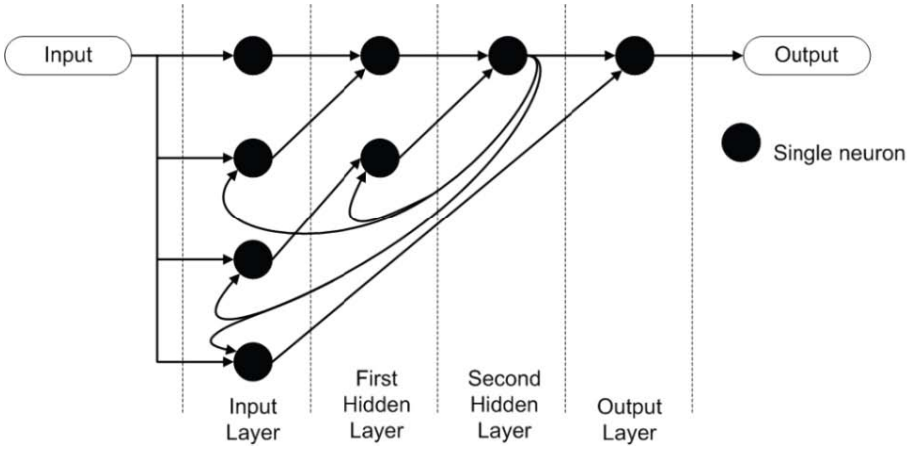

Figure 3.10: Long Short Term Memory ANN.

3.2.6 Bi-directional Artificial Neural Networks (Bi-ANN)

A network that consists of two individual interconnected artificial neural network that performs bidirectional transformation with the ability to increase time series prediction capability is known as Bi-directional artificial neural network. In this type of network two dynamic artificial neurons with the capability to remember their internal state are interconnected. This network topology allows both past and future prediction of values, and thus two learning phases are implemented in the neural

sub network, (1) the future prediction phase and (2) the past prediction phase.

3.2.7 Self-Organizing Map (SOM)

A network that is related to feed-forward networks, with an altered arrangement of neurons and motivation and that uses a neighbourhood functions to preserve the topological properties of the input space in an unsupervised learning paradigm, is known as a Self-organizing Map with the ability to correlate and detect regularities and adapt future responses to that input accordingly . The output result provides a discrete representation, known as a map that allows low-dimensional views of high-dimensional data.

3.2.8 Stochastic Artificial Neural Network

A Stochastic artificial neural network is a type of artificial intelligence tool built with stochastic transfer functions (Boltzmann machine), where its usefulness is shown in resolving optimization problems. It functions on random variations either through the stochastic transfer function or stochastic weights.

3.2.9 Physical Artificial Neural Network

The physical artificial neural network is a physical artificial neural network with adjustable electrical current resistance materials. This type of network uses emulated synapses of artificial neurons known as Memistors.

3.3 Learning

The main learning paradigms are (1) reinforcement, (2) supervised and (3) unsupervised. Each learning paradigm is composed of many training algorithms. The learning paradigm are used by and type of artificial neural network architecture.

3.3.1 Supervised learning

Supervised Learning phase is used to define the usage of wide range of classifiers with different strengths and weaknesses. The task for this phase is then set to define the parameters for the valid input value after seeing the output value. The method of choosing the correct classifiers for a given problem various steps need to be followed: (1) determine type of training example. (2) Gather appropriate training data set. (3) Describe gathered data sat from step 2 in a form that can be understood by the network. (4) Implement the learning phase. (5) Test performance of learned artificial neural network using a data set that was not used in the learning phase.

3.3.2 Unsupervised learning

Unsupervised Learning technique that is based on a given data and a cost function (any function determined but task formulation) which is to be minimized. This type

of learning path is given unlabelled examples (opposed to the labelled examples in the supervised learning path) and is used within blind source separation, clustering (most common form used), compression, filtering and statistical modelling. The main objective of this learning path is to determine data organization. Among above described artificial neural network models, the Self-organizing maps are the ones that the most commonly use unsupervised learning algorithms.

3.3.3 Reinforcement learning

Reinforcement Learning is used when data is usually not provided directly but is extracted from the interactions with the environment. This learning method uses several algorithms in order to select the policy with maximum return and is suited for long-term versus short-term reward trade-off, such as problems involving telecommunications, or games. The main weakness of this learning path is the infinite number of possibilities that can be derived from the environment for the input into the algorithm. The solution to address this weakness is the implementation of the (1) value function approaches which maximizes the return by maintaining a set of estimates of expected returns for one policy or (2) direct policy estimation is similar to the value function approach but with the ability to locate an optimal policy through direct search in policy space to increase computational cost.

3.4 Usage of Artificial Neural Networks

The practicality of using artificial neural networks compared other solutions specifically within complex environments is a major advantage of artificial neural networks. The implementation of artificial neural networks can be seen in a wide range of tasks, such as classification, clustering, decision making, filtering, function approximation, processing, etc. The artificial neural network topology is dependent on the application type and data representation for a problem it is faced with. The degree of artificial neural network processing robustness to a given problem relies on the (1) correct selection of the appropriate network topology and (2) the learning algorithm used.

Chapter 4

Problem Formulation

Contents

4.1 Path Loss Prediction Based on ML 24
4.2 Field measurement Environment and tools 27
4.2.1 Data Collection 28
4.3 Selecting Representative Propagation Models 29
4.3.1 Free Space Path loss for LOS Environment 29
4.3.2 ITU-R Rain Attenuation Model 30
4.3.3 Crane Global Model 32
4.4 Adapting the Selected Propagation Models 32
4.5 Optimizing a Propagation Model 35
4.5.1 NN Feed Forward Fitting Tool optimization 35
4.6 Implementation of the Selected Models 39
4.6.1 Model Validation 39
4.7 Implementation of the Optimized Model 42
4.7.1 Implementation of the NN Feed Forward 42

This chapter discusses the design of an optimal propagation model. At first it presents three empirical propagation models that meet microwave requirements. It then adapts the selected model by adding the transmitting power, distance and frequency to predict the performance of link budget parameters. Finally, it evolves an optimized propagation model for microwave connectivity using a Machine Learning (ML) technique.

4.1 Path Loss Prediction Based on ML

The underlying theory of ML-based path loss predictors is shown in Figure 4.1. We will deploy machine learning methods to find a propitiate estimation algorithm for the path loss prediction after determining the output and the corresponding input features such as transmitting power, frequency, and distance. This algorithm is designed to map input features to loss value of the output path, and it can be either a white box within decision tree based models or a black box within ANN based

models. Path loss predictors based on ML are shown in Figure 4.2. Specific models can be used for the estimation of path loss, and the model selection should consider both precision and complexity criteria. ANN algorithm was selected in this thesis since it has good performance in predicting path loss values [31]. ANN can be used to solve nonlinear regression problems, and has small prediction errors when the sample size is large enough, making it a common path loss prediction [7].

Hyperparameters refer to parameters whose values are set before the learning process starts. Typical hyperparameters are the number of hidden layers and neurons in ANN [32], a set of optimal hyperparameters should be carefully selected to maximize the path loss prediction's efficiency and effectiveness. Hyperparameter optimization approaches primarily include matrix search, random search, and optimization of Bayesian. Parameters of the model are certain parameters obtained from measurements in testing. It is worth noting that different models of learning have different parameters for the pattern. Component parameters such as weights and biases are automatically learned

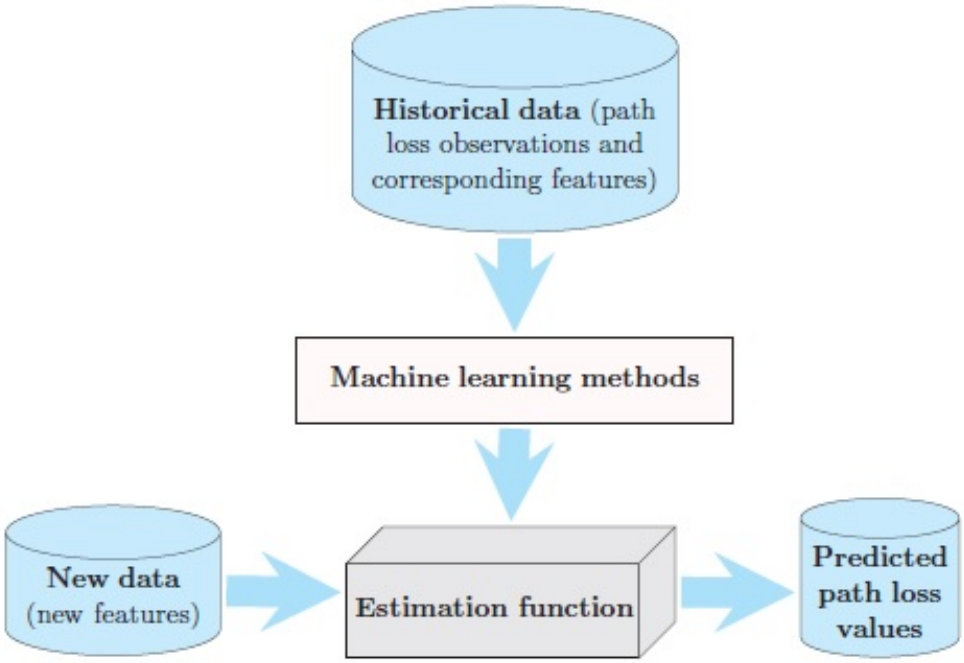

Figure 4.1: Principle of ML based path loss prediction [6]

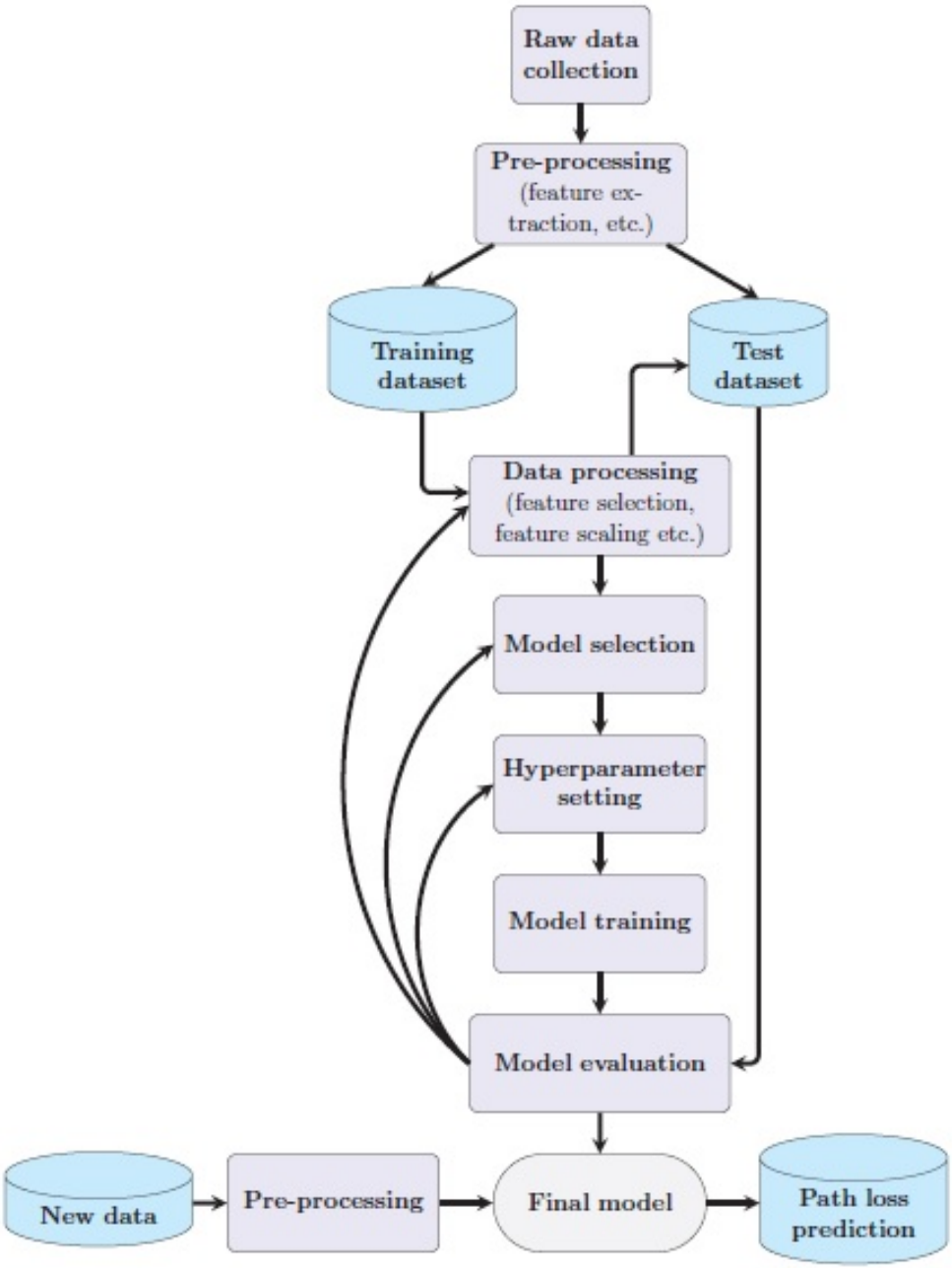

Figure 4.2: Procedure of ML based path loss prediction [6]

4.2 Field measurement Environment and tools

Extensive survey campaigns were carried out in West Bank, Palestine (Latitude N 32 19' 7.70"; Longitude E 35 21' 41.20"); (Latitude N 32 14 0.0; Longitude E 35 18 8.38) and other locations to collect track loss data at various distances from nineteen various 23 GHz, 18GHz and 15GHz base stations. In order to allow adequate variety in the propagation environment , multiple locations were chosen. Typical environments for urban, suburban, and rural spread were covered. A total of nineteen sites (S1-S19) were mapped to cover the propagation of radio waves in the direction of each base station transmitter antenna. Sites S1-S6 are located in Palestine 's northwest bank, Whereas the remaining (S9-S19) are on Palestine's central and southwestern banks. Typical conditions for urban, suburban and rural propagation is covered.

Furthermore, technical insights drawn from Figure 4.3. As illustrated in Figure 4.3 which is represents a simplified network architecture for core network of one of the selected area. The core network is an Internet Protocol (IP) based and SDH network connected by fiber optics transmitting both control signals and data. Core network consists of several components, IP routers, IP switches, and microwaves.

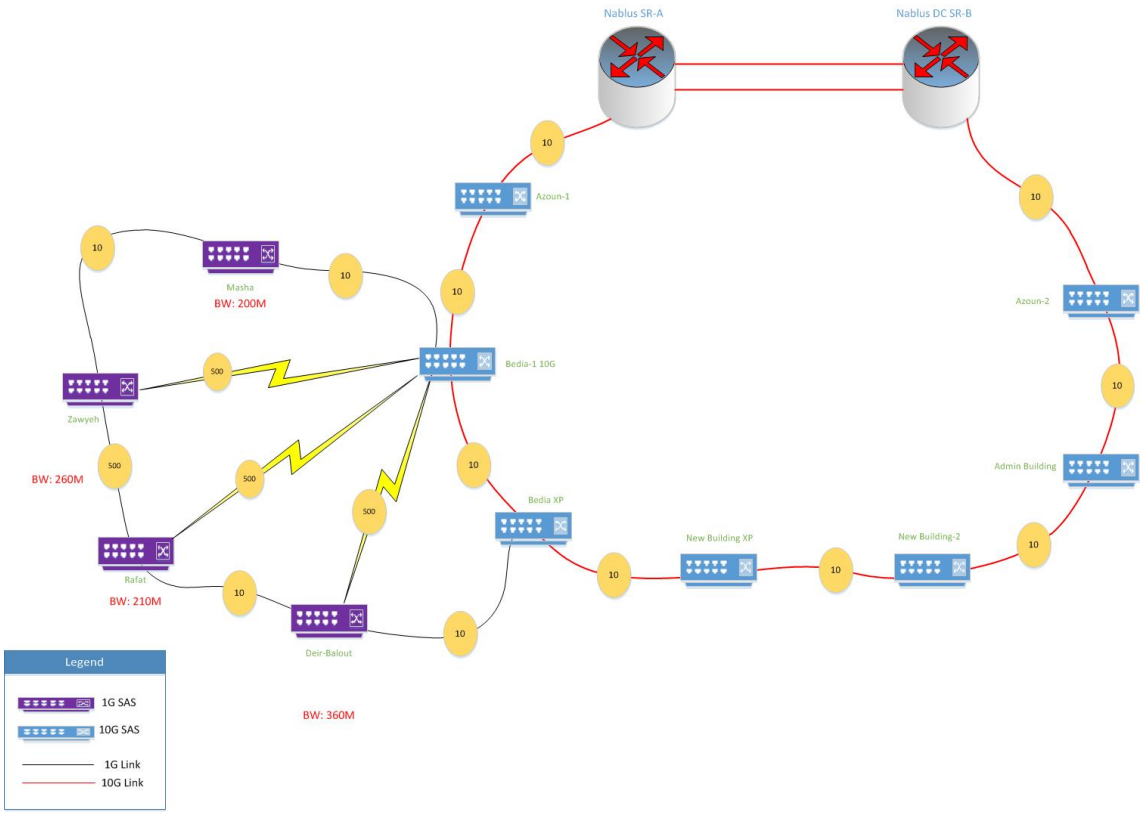

Figure 4.3: Network Topology

4.2.1 Data Collection

The data collected from the measurement should include the value of the path loss and the features of the release input. The input functions can be divided into two categories, parameters dependent on the system, and parameters dependent on environment. System dependent parameters, such as carrier frequency, distance, and heights, are independent of the propagation environment.

Environment dependent parameters are those determined by the geographic environment and the weather conditions. Parameters related to the geographic environment include the terrain, building conditions, and vegetation conditions. Most of them can be obtained from three dimensional (3D) digital maps as shown in Figure 4.4. and topographic databases. An array of software is utilized to acquire data from each site and store it in a format that can be further processed. The RSL data is obtained via Netboss. Netboss is a monitoring system. The data collected were pre-processed in Microsoft Excel 2016.

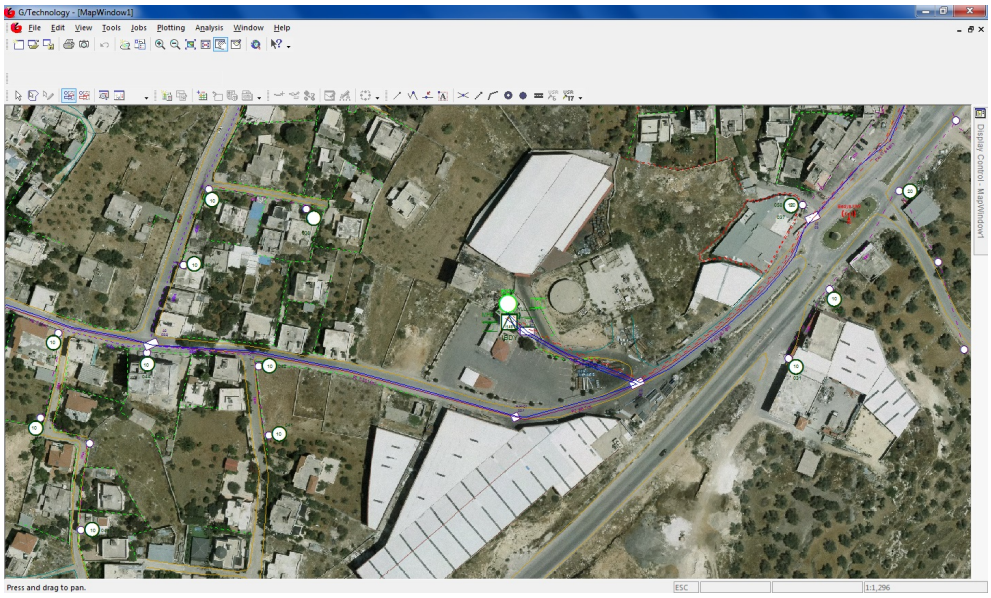

Figure 4.4: Map of Transmitter Location using GCOM software.

4.3 Selecting Representative Propagation Models

Over the years, many rival propagation models have been proposed, but although collectively increasing several shortcomings such as reduced altitude up to a few tens of meters, lack of reach across different environments, low perdition precision, they do have many advantages. Therefore, here a reduction approach is considered in order to narrow down propagation models from tens to three specific models that meet the microwave requirements. There are several common parameters across propagation models that effect the overall performance, such as antenna gain, transmission power, and loss. Other factors include: (f) Frequency of operation, (d) Distance between transmitter and receiver (coverage), (h_t) Transmitter antenna height, (h_r) Receiver antenna height, and Terrain type.

4.3.1 Free Space Path loss for LOS Environment

Free space path loss is a way of estimating the signal power obtained when there is no obstacle that obstructs the LOS path between the TX and the RX. In a LOS setting the model for path loss is clear. The (P_r) obtained power is connected to the (P_t) transmitted power through the [33] Friis transmission formulation.

Free space path loss provides a means to predict the received signal power when there is no object obstructing the LOS path between the TX and the RX.

The model for path loss in a LOS environment is straightforward. The received power (P_r) is related to the transmitted power (P_t) via the Friis transmission formula [33].

$$P_r = \frac{EIRP}{4\pi d^2} A_e = \frac{P_t G_t G_r \lambda^2}{(4\pi d)^2} (W) \tag{4.1}$$

In (4.1), $EIRP = P_t G_t$. The transmitting antenna has gain G_t while the receiving antenna has gain G_r . Distance d is the separation between the TX and the RX. The RX has an effective aperture given by $A_e = G_r \lambda^2 / 4\pi$, where λ is the signal wavelength. The path loss is defined by the term

$$L = \frac{P_r}{P_t G_t G_r} = \frac{A_e}{4\pi G r d^2} = (\frac{\lambda}{4\pi d})^2 \tag{4.2}$$

It is shown that for the LOS environment, the power received will fall off with the square of the distance between the TX and the RX.

4.3.2 ITU-R Rain Attenuation Model

The ITU-R rain attenuation model specifically for terrestrial line-of-sight microwave links is given by Recommendation ITU-R P.530-10. This model gives the formula for the predicted attenuation due to rainfall based on the desired availability. Important parameters include specific attenuation, the regression coefficients computed from the ITU data library, and the rain rate. The regression coefficients are dependent on frequency and polarization.

The specific attenuation is given by

$$\gamma = kR^{\alpha} \tag{4.3}$$

In equation (4.3), γ is the specific attenuation due to rain in dB/km and R is the rain rate in mm/hr. For selected frequencies, the coefficients of K and α are listed in Table 4.1 [34]. coefficients are developed from scattering calculations and differ in value for different frequencies (1 to 1000 GHz) and polarization (horizontal or vertical). The values for these constants are already given in ITU-R P.838-3 . The link attenuation can be calculated by getting the sum of the specific attenuations in a given link path.

Table 4.1: The values of parameters k and α given by ITU-R

Frequency (GHz)	k_H	α_H	k_V	α_V
15	0.04481	1.1233	0.05008	1.044
18	0.07078	1.0818	0.07708	1.0025
23	0.1286	1.0214	0.1284	0.9630

To apply the ITU-R method, the first thing to determine is the 99.99% fade depth using the following formula:

$$Atten_{0:01} = kR^{dr} \tag{4.4}$$

which is the same as equation (4.3) but with the additional parameters d and r. Parameter d is the link distance in kilometer, while r is the distance factor given by:

$$r = \frac{1}{1 + \frac{d}{d_0}} \tag{4.5}$$

where

$$d_0 = 35e^{-0.015R} \tag{4.6}$$

is the effective path length.

$Atten_{0:01}$ will give the expected rain attenuation when the rain rate is equal to the rain rate that occurs only 0.01% of the time. This can equivalently be the rain fade margin when you want a microwave link that is available 99.99% of the time. The R(0:01) rain rate may be obtained directly from local rainfall data, or if not available, it is given in ITU-R P.837-4 [35]. For availabilities other than 99.99%, adjustments need to be done to $Atten_{0:01}$.

$$Atten_p = Atten_{0:01}[0.12_p - (0.546 + 0.043\log(p))] \tag{4.7}$$

$$Atten_p = Atten_{0:01}[0.07_p - (0.855 + 0.139\log(p))] \tag{4.8}$$

Equation (4.7) is for areas with latitude greater than 30^o North or South of the equator, while Eq. (4.8) is for latitudes below 30^o North or South of the equator. The variable p is the desired probability (100 - availability) expressed as percentage.

ITU rain regions for the Middle East, Europe and Africa, and Scandinavia is shown in Figure 4.5 [34].

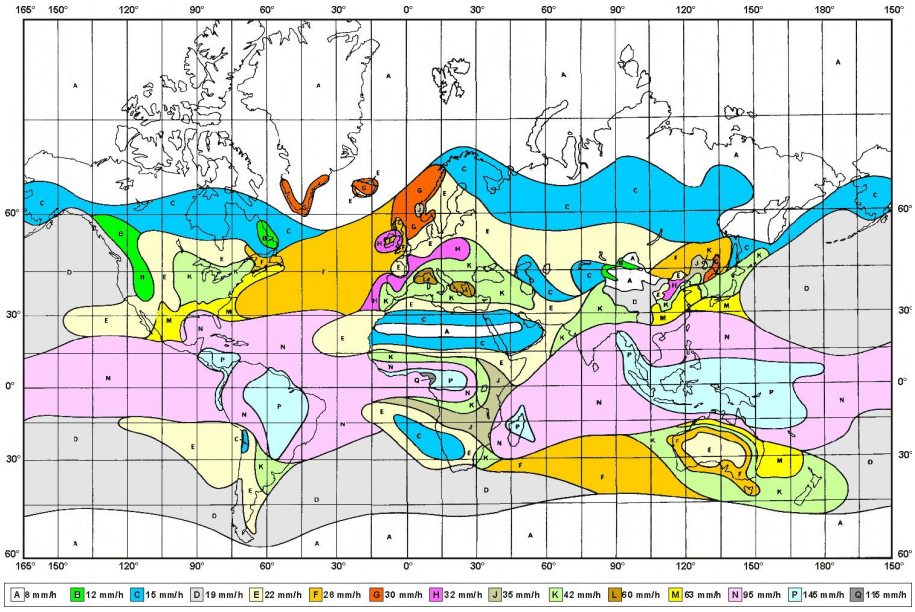

Figure 4.5: ITU Rain Rate Map Zone [34]

4.3.3 Crane Global Model

The Crane Global Model was developed by Robert K. Crane. It uses the same regression coefficients as the ITU-R model. The general formula of the Crane Model is different from that of the ITU-R, as well as the R(0:01) for different regions in the world. The attenuation model is given by:

$$Atten = \begin{cases} kR^{\alpha}\left(\frac{e^{y\delta R}-1}{y} + \frac{(e^{zd}-e^{z\delta R}e^{0.83-0.17\ln(R)}\delta(R))}{z}\right), & \text{for } \delta(R) < d < 22.5 \\ kR^{\alpha}\left(\frac{e^{y\delta}}{y} - 1\right), & \text{for } 0 < d < \delta(R). \end{cases} \tag{4.9}$$

where d is the link distance in kilometer, and

$$\delta(R) = 3.8 - 0.6\ln(R) \tag{4.10}$$

$$y = \alpha\left(\frac{0.83 - 0.17\ln(R)}{\delta(R)} + 0.26 - 0.03\ln(R)\right) \tag{4.11}$$

$$z = \alpha(0.026 - 0.03\ln(R)) \tag{4.12}$$

The ITU-R model is valid for link distances up to 60 km while the Crane Global Model is valid for link distances up to 22.5 km [36]. In general, the Crane model gives a higher attenuation prediction than the ITU-R model.

4.4 Adapting the Selected Propagation Models

When providing coverage of a long distance, it becomes necessary to consider the earths curvature and radius. Therefore, one of our key research contribution is to adapt the three selected empirical propagation models to additionally consider the elevation angle in predicting the coverage at various microwave altitudes. This adaptation does not only offer LoS service connectivity and coverage but also Out-of-Sight service to receivers that would suffering from outage or low connectivity as a result of their distance. This adaptation is expected to reduce the path loss [37]. The distance D of the selected propagation models is computed based on elevation angle θ as follows:

$$\cos\theta = \frac{E_r}{E_r + H} \tag{4.13}$$

$$\theta = \cos^{-1}\frac{E_r}{E_r + H} \tag{4.14}$$

$$D = \theta.E_r \tag{4.15}$$

$$D = 2E_r[\cos^{-1}(\frac{E_r}{E_r + H} * \cos\theta) - \theta] \tag{4.16}$$

Where:

- H and E_r are the Earths radius.
- θ is the elevation angle.

Each of the three selected models predicts values of path. Calculating path loss is useful for monitoring system performance, network planning and coverage to achieve good reception. RSS helps to estimate the coverage range when the signal weakens, RSS depends on transmitter power (P_t), path loss (P_L), transmitter antenna gains $G(h_t)$, receiver antenna gains $G(h_r)$ as well as (L) connector, cable loss and environment factors [38] [39]. The optimum Microwave altitude and coverage footprint can be derived from the path loss results. Coverage footprint in all three models is based on an elevation angle from a receivers location which is a significant departure from current empirical models .

In order to give a brief description of the propagation models algorithm, a flowchart is given in Figure 4.6; where PL is calculated at each chosen distance across different environments.

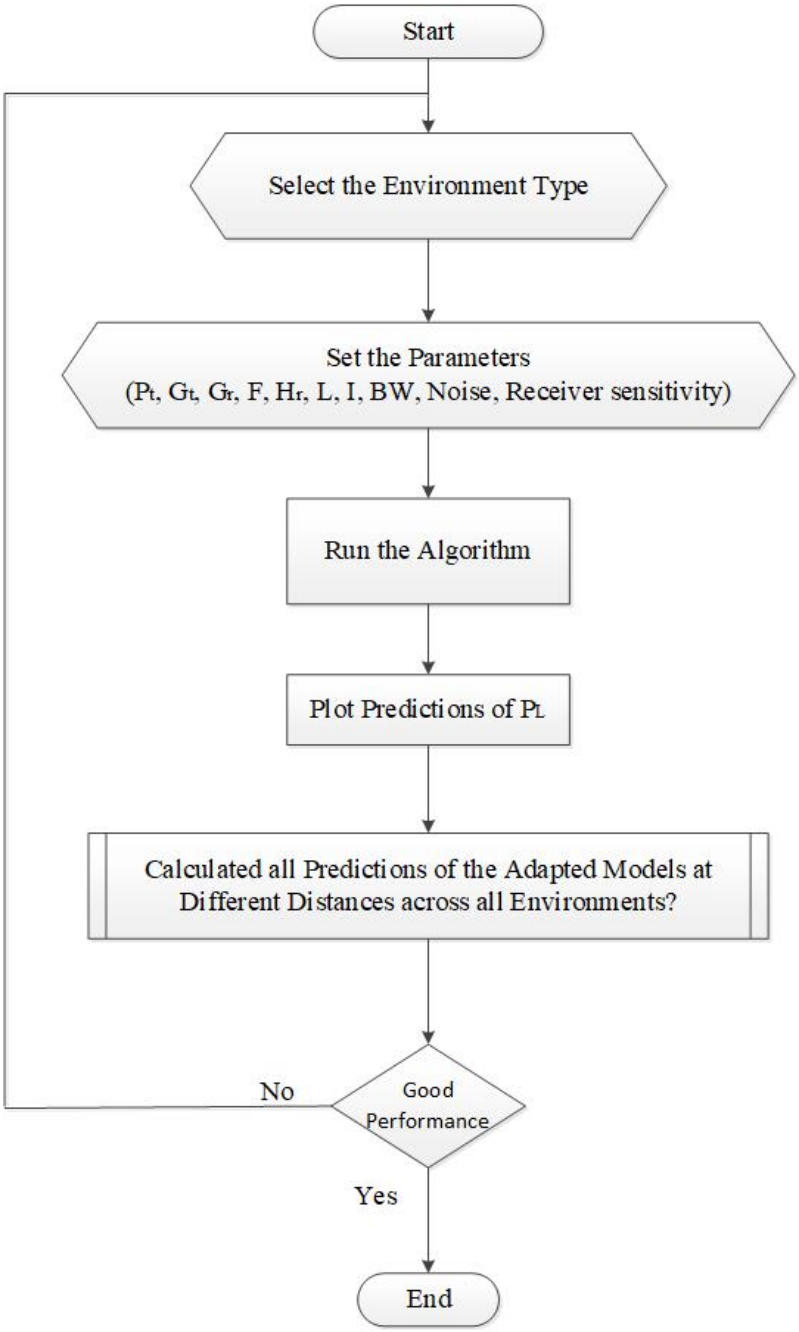

Figure 4.6: Flowchart of the propagation models algorithms

The prediction of propagation path loss can be primarily considered as a regression issue. In point of fact, information about transmitter, receiver, buildings, frequency, etc. represents the inputs and the propagation loss represents the outcome to be calculated see Figure 4.7. The main purpose is to find a suitable input vector x and an estimate $f(x)$ that best approximates the propagation loss. Learning machines, which are vital tools for settling regression problems, can be efficiently applied for securing a dependable prediction of wave propagation [24]

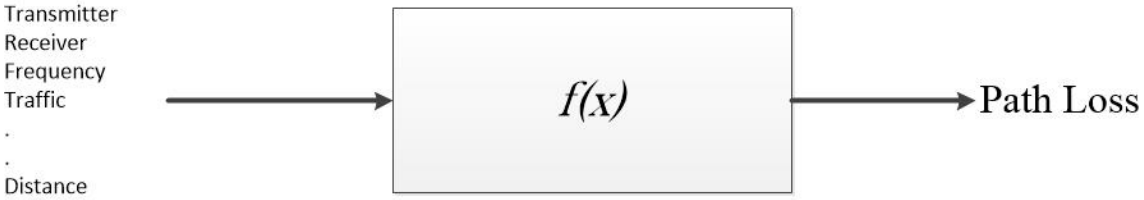

Figure 4.7: Path loss prediction as a regression problem

4.5 Optimizing a Propagation Model

ML techniques and algorithms are used for data analytics to obtain valuable information from complex and large data that allow making a smart decision. The learning concept is based on learning from the internal pattern of the data, where data can adjust their internal parameters accordingly. The optimization phase here aims to highlight the architecture of the optimization framework that achieves wider wireless coverage and better QoS for network planning for point to point connectivity using microwave link [40], as Figure 4.8 shows. To optimize, we deploy a supervised learning algorithm that trains the NN to evolve an optimized model for each selected distance.

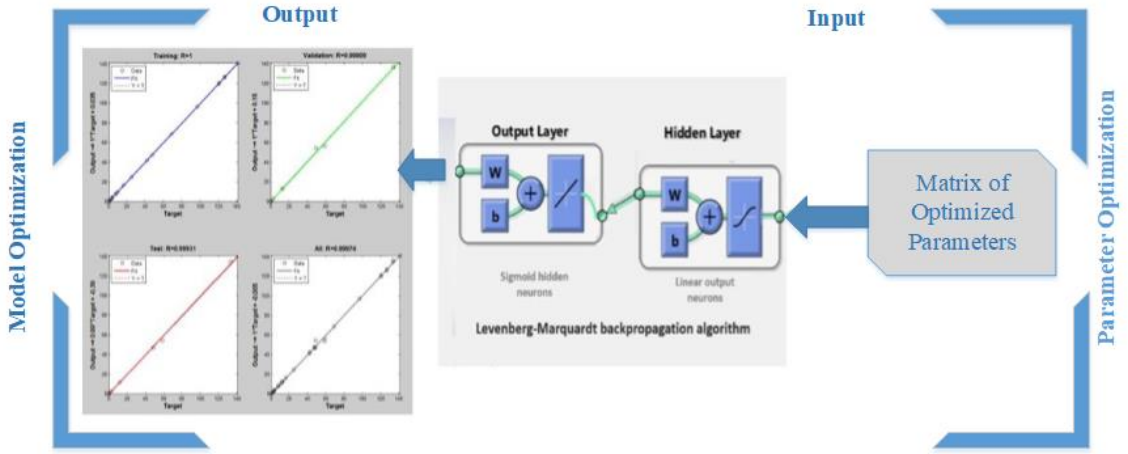

Figure 4.8: Machine Learning optimization Framework using Neural Nets

4.5.1 NN Feed Forward Fitting Tool optimization

The next step in optimization use the Levenberg Marquardt backpropagation as shown in Figure 4.9, using the NN Feed Forward Fitting Tool in MATLAB to evaluate the performance of the optimized set of parameters with the adapted selected simulated model. The NN fitting tool in MATLAB supports data selection, network creation and training, and network performance evaluation using Mean Square Error (MSE) and regression analysis. In the model optimization stage, all input entered to the NN Feed Forward Fitting Tool [41] [42]. The process of optimization uses two scenarios, the first scenario populated with the selected parameters (distance, frequencies, and transmitting power) and the the second one populated with the

selected parameters (distance, frequencies, and transmitting power) in addition to one of the three adapted propagation model which ITU-R p.530 model.

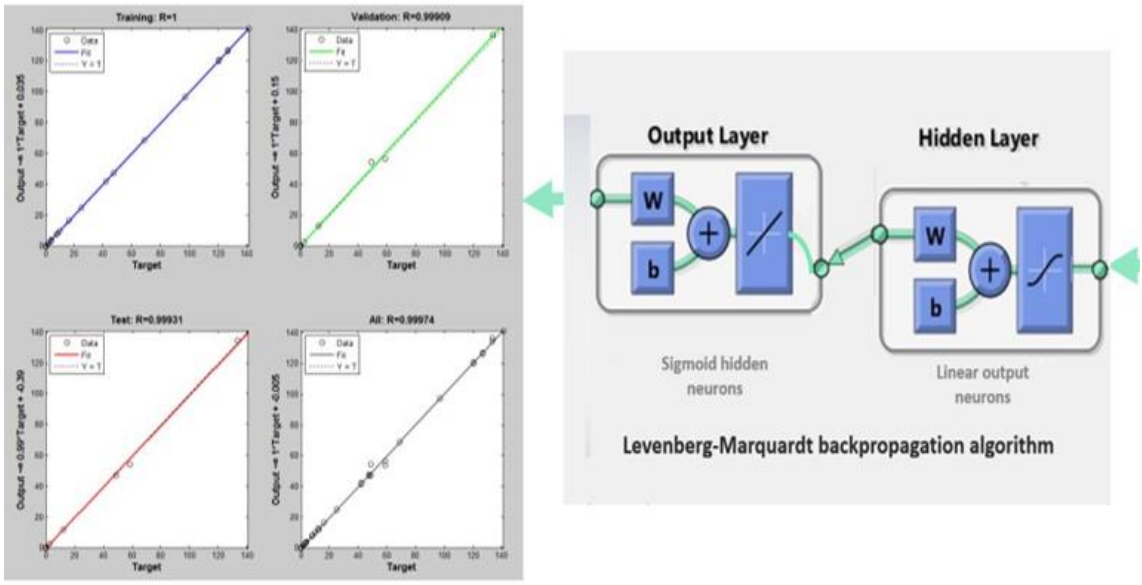

Figure 4.9: The Levenberg-Marquardt Backpropagation Algorithm

Another design decision is the choice of the training function. The Levenberg-Marquardt backpropagation algorithm uses the Hessian matrix approximation of Newton's method, which is regarded as faster and more accurate near an error minimum [41]. meanwhile, the scalar μ decreases after each drop-in performance function, which means the performance function is continuously reduced at each iteration of the algorithm. The Hessian matrix can be approximated as:

$$H = JT^J \tag{4.17}$$

The gradient is calculated as:

$$g = J^T e \tag{4.18}$$

The Hessian matrix approximation of Newton's method is as:

$$xk + 1 = xk - \left[JT^J \mu J\right]^{-}1 J^T e \tag{4.19}$$

Where:

- J: is a Jacobian matrix which composed of first values of the network errors in consideration of the assigned weights and biases.

- e: is a vector of network errors.

The Jacobian matrix can be computed via a backpropagation technique that is less complex than the Hessian matrix. The available input data-set and target data-set are randomly divided into three sets; (1)training which makes offerings to the network while training, and in turn the network is tuned in response to errors, hence, calculating the gradient and updating the weights and biases; (2) validation which measures network generalization and stops training when generalization halts improving; (3) Testing which delivers an autonomous measure of performance during and after training, thus with no effect on training [41] [42].

The flowchart in Figure 4.10 describes the process of how the Levenberg Marquardt algorithm of the NN fitting process going using MSE and regression analysis. This incorporates, selecting data, creating and training a network, and evaluating performance.

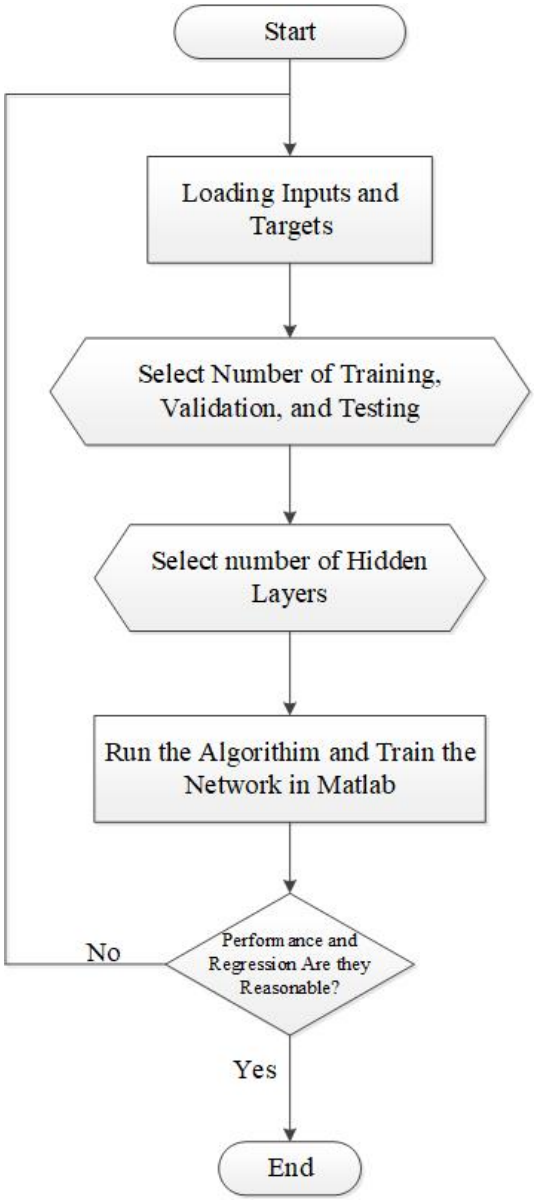

Figure 4.10: Flowchart of NN Feed Forward Fitting Tool optimization

4.6 Implementation of the Selected Models

The three adapted propagation models have been simulated under the same conditions using MATLAB. PL is computed based using each propagation model formula. Comparative results of selected models are illustrated in Figure 4.11, to Figure 4.16.

4.6.1 Model Validation

In order to know which model has better results for Palestine area and then use the selected model as ANN input . It is important to evaluate the performance of propagation model considered. The Mean Square Error (MSE) [43] was calculated to estimate the better model for path loss prediction in Palestine. The best model for optimization was decided using equation 4.20.

$$MSE = \frac{1}{n}\sum_{t=1}^{n}(P_{mt} - P_{Rt})^2 \tag{4.20}$$

Where: P_{mt} is the mean value of measured data, P_{Rt} is the mean value of predicted path loss, n is the number of data points.

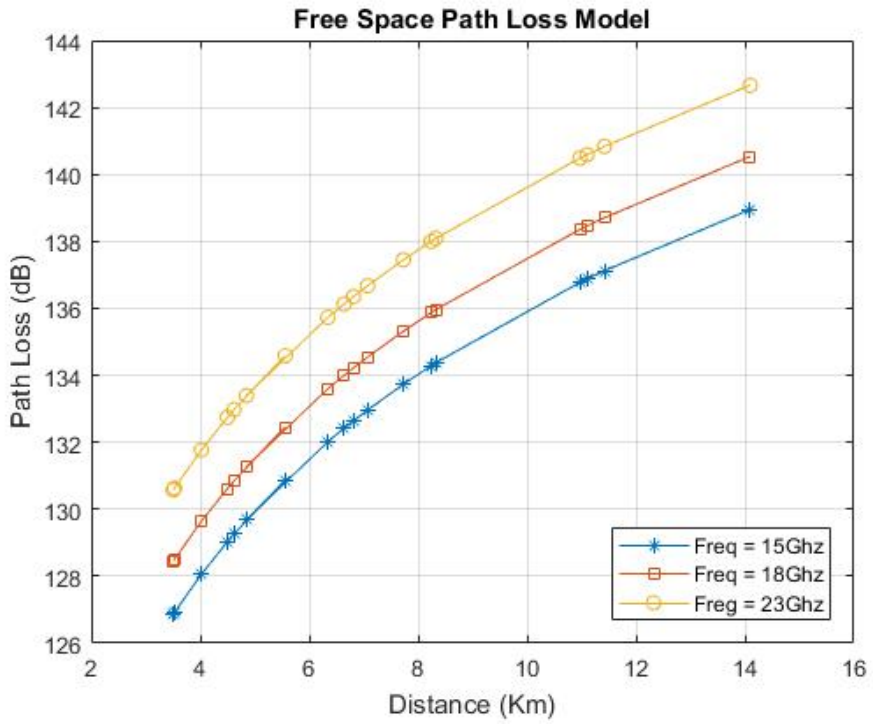

Figure 4.11: Implementation of Free Space Path loss Model.

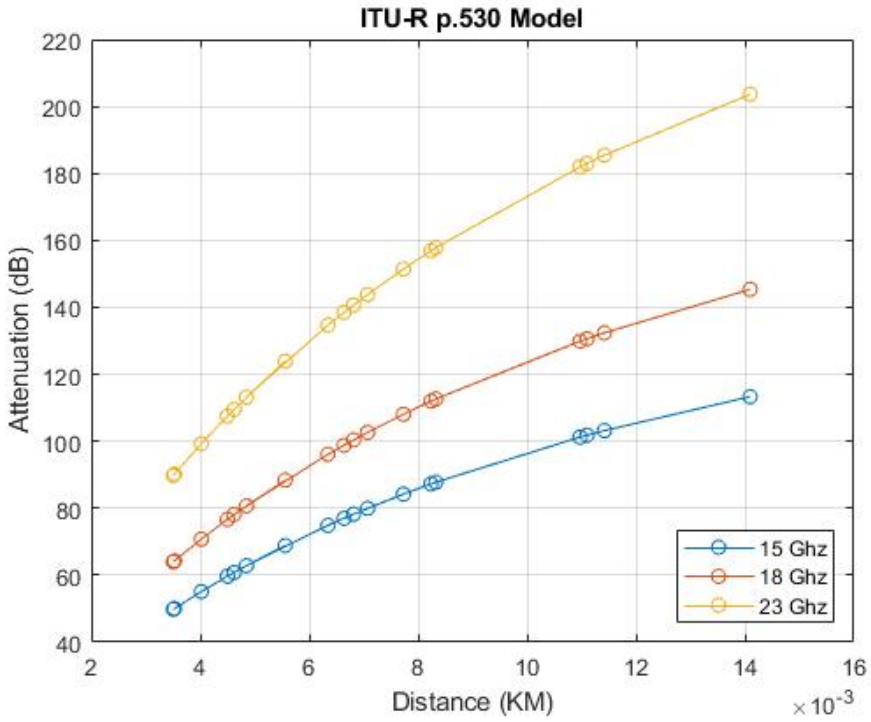

Figure 4.12: Implementation of ITU-R Attenuation Model.

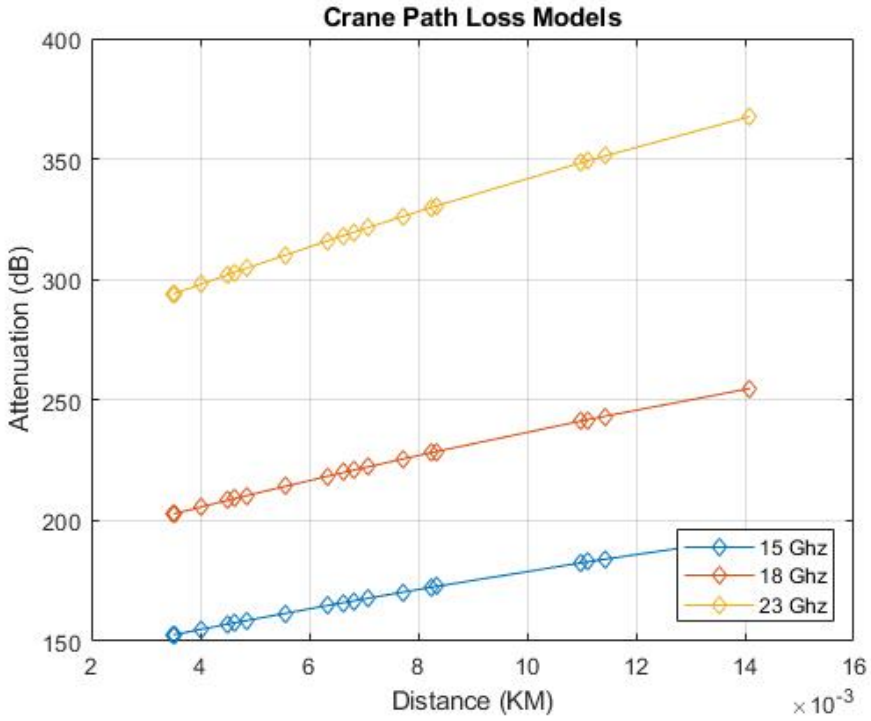

Figure 4.13: Implementation of Crane Attenuation Model.

Figure 4.14: A comparison between the Three Models at Frequency 15GHz.

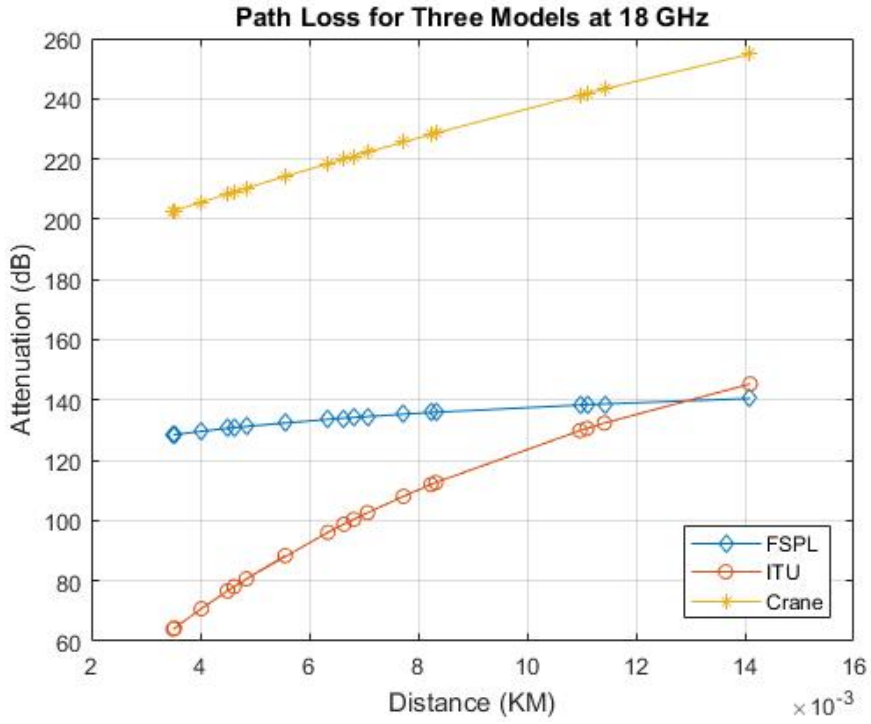

Figure 4.15: A comparison between the Three Models at Frequency 18GHz.

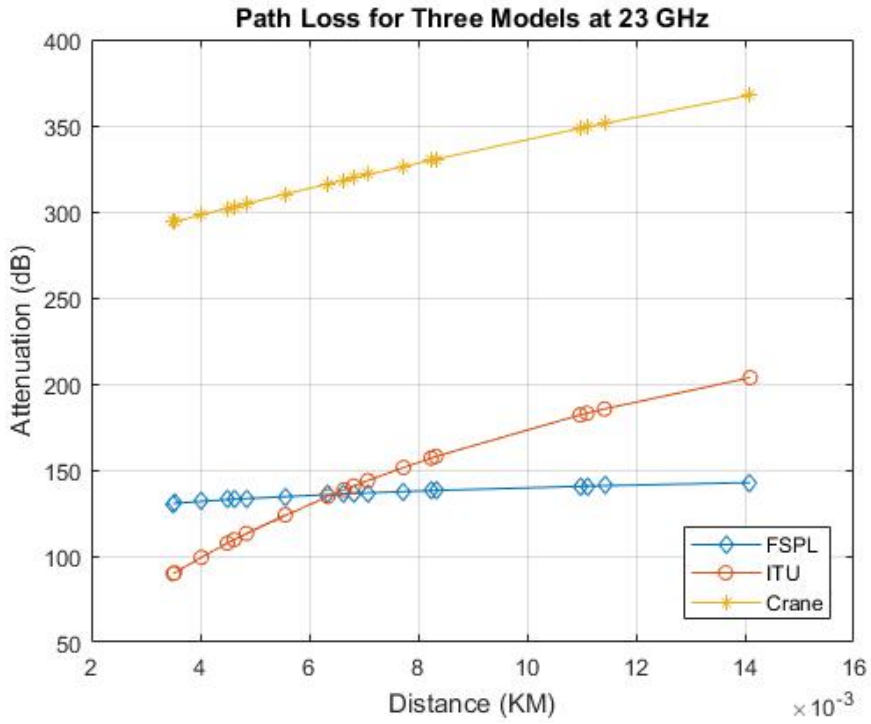

Figure 4.16: A comparison between the Three Models at Frequency 23GHz.

In Figures 4.11, 4.12, and 4.13 represent the relation between selected model (FSPL, ITU-R p.530, and Crane) respectively at different frequencies with distance, it obvious that the less attenuation at frequency 15G.

In Figures 4.14, 4.15, and 4.16 represent a comparison between FSPL, ITU-R p.530, and Crane at frequency 15G, 18G, and 23G respectively at different distance, ITU model recorded the lowest attenuation in all cases.

4.7 Implementation of the Optimized Model

The optimization process takes as input the selected empirical adapted propagation model predictions at several microwave distances, frequencies and transmitting power as scenario 1. It then deploys the Levenberg Marquardt backpropagation algorithm using the NN Feed Forward Fitting Tool to evaluate the performance of the optimized set of parameters against of the selected adapted models.

4.7.1 Implementation of the NN Feed Forward

The output of the predictions obtained from the selected model adding frequency, Tx power and distance parameters used as input to NN Feed Forward fitting tool in scenario one. In scenario two frequency, Tx power and distance parameters are used as input to NN Feed Forward fitting tool. The optimization process uses the Levenberg-Marquardt backpropagation algorithm alongside the NN Feed Forward Fitting Tool to evaluate the performance of the evolved set of parameters. Figures

4.17 through to 4.20 depict its implementation using the NN MATLAB toolbox.

Figures 4.17, 4.18, and Table 4.2 show the percentage of Training, Validation, and Testing, as well as assigning the optimum number of hidden layers needing to be adjusted several times in order to obtain optimal performance and regression. Figures 4.19 and 4.20 show training and evaluation. Validation uses regression plotting to determine the optimal number of iterations during which validation produces a minimal value. After initial training of the NN model, the performance changes after each training iteration. This training set and validation set decreases continuously to the point where overfitting happens, and thus the error rate increases. Understanding the NN training performance, Regression plots, and Error Histogram plot for Training data can give additional verification of network performance.

Table 4.2: Percentage of Training, Validation, Testing, and Input Output parameters

Parameter	**Value**
DataSet	31103
Percentage of Training	70%
Percentage of Validation	15%
Percentage of Testing	15%
Input for scenario #1	4
Input for scenario #2	3
Output	1
Hidden Layers	2, 4, 6, 8, 10

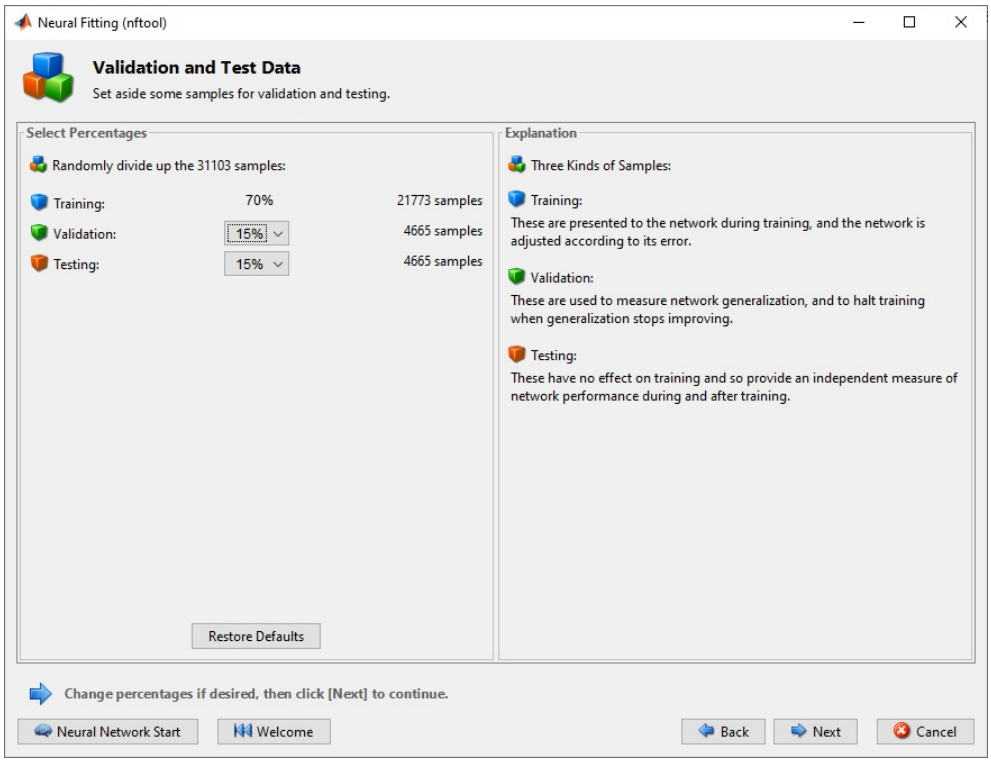

Figure 4.17: Input and target vectors settings using the MATLAB NN fitting tool.

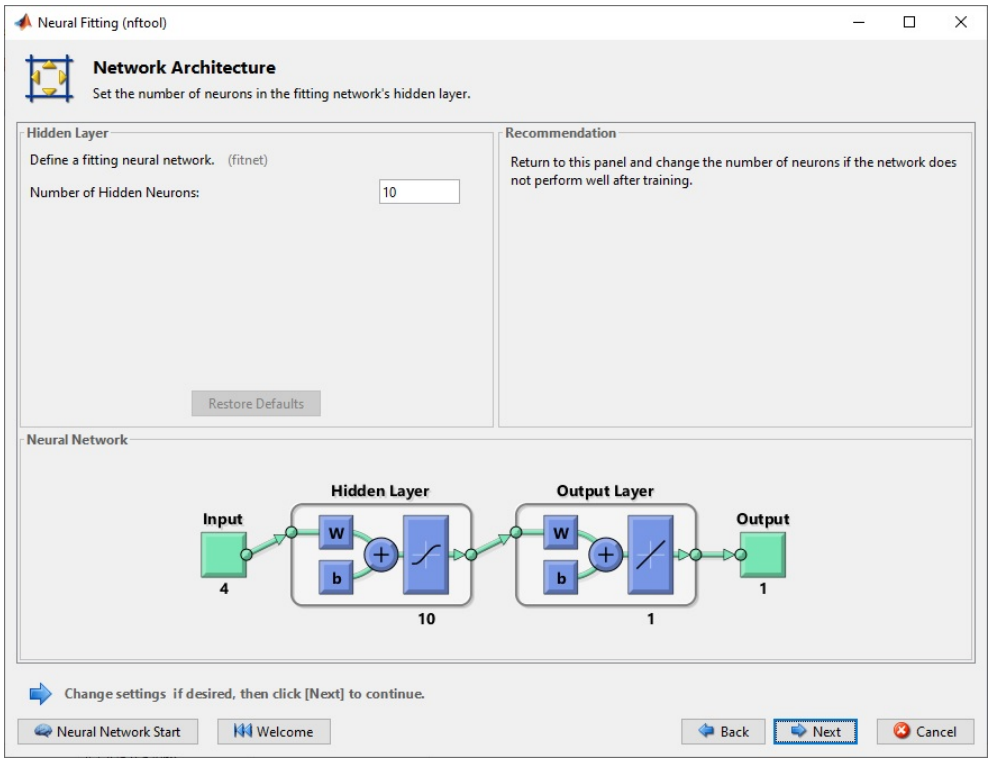

Figure 4.18: Defining optimum number of Neurons using the MATLAB NN fitting tool.

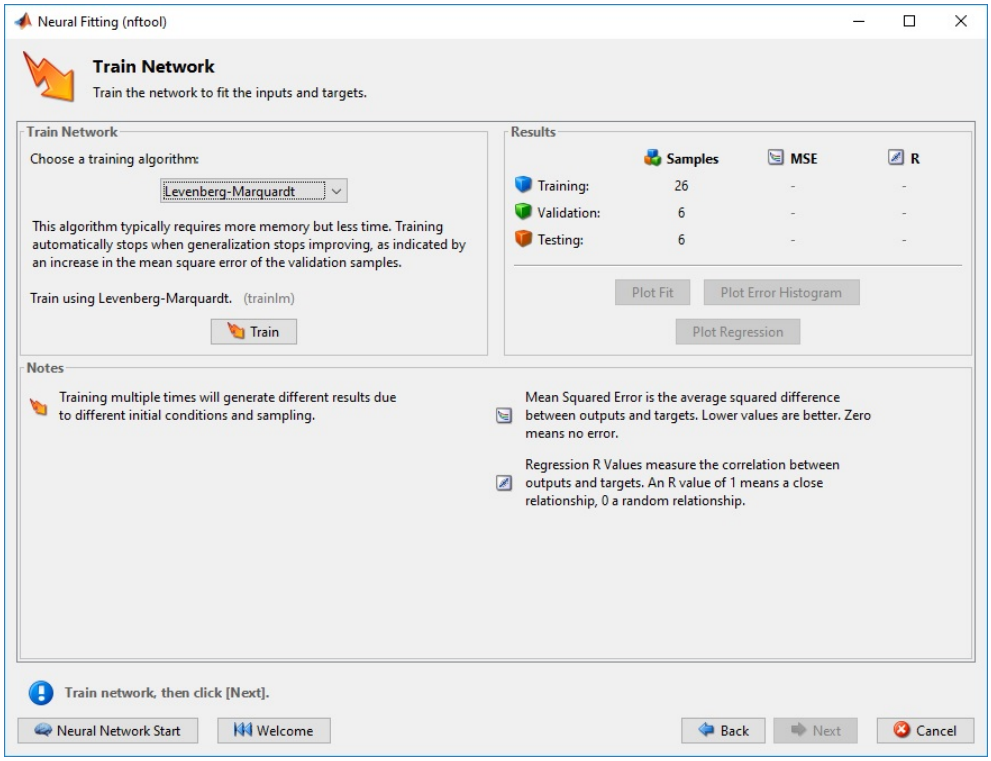

Figure 4.19: Training and measuring MSE using the MATLAB NN fitting tool.

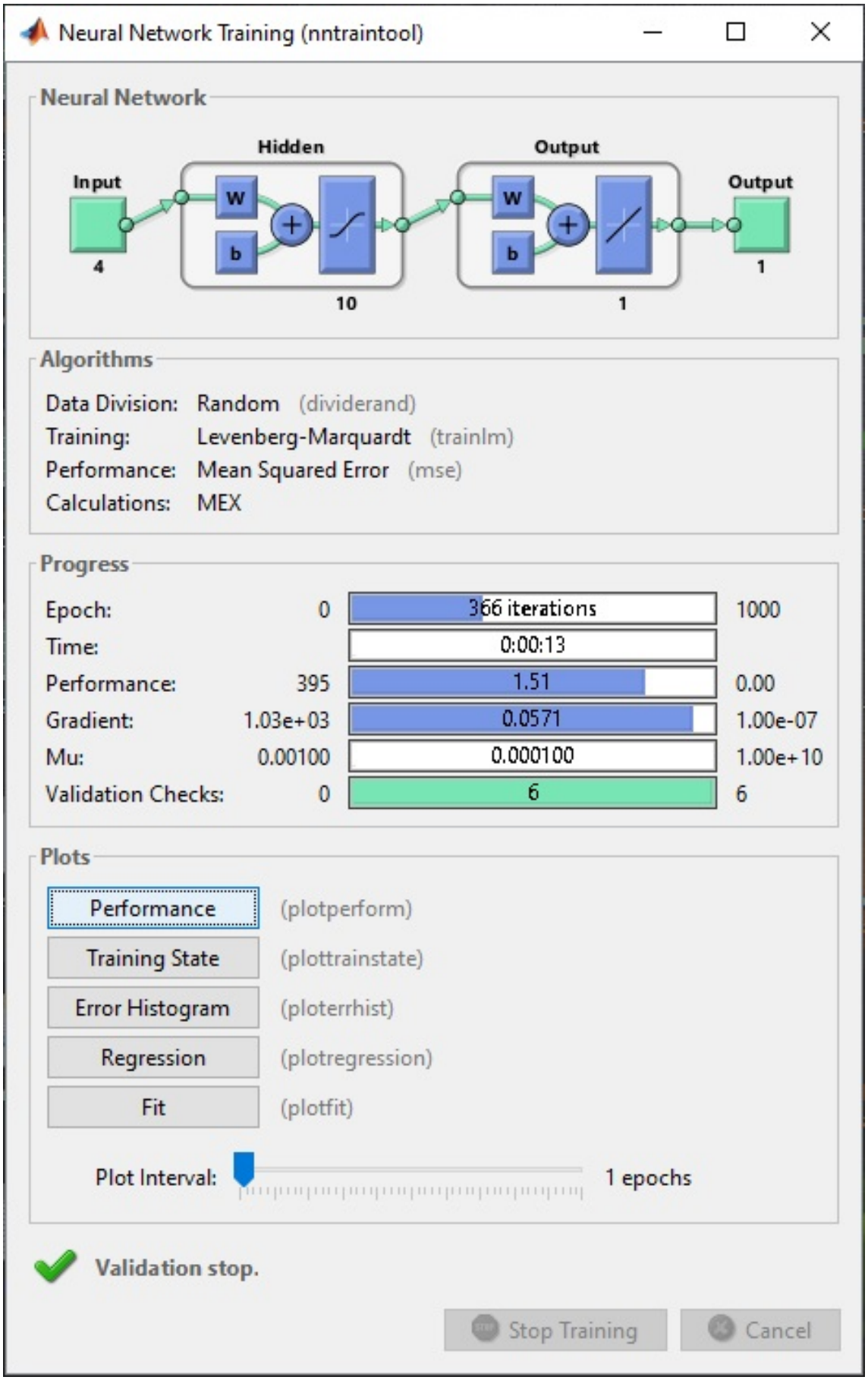

Figure 4.20: Evaluating parameter performance using the MATLAB NN fitting tool.

Chapter 5

Experimental Evaluation

Contents

5.1 Results and Discussion 46

5.1.1 Descriptive statistics of scenario One 46

5.1.2 Descriptive statistics of scenario Two 53

5.1.3 Regression Model 58

5.1 Results and Discussion

This section introduces and analyzes multiple tests to test the efficiency and robustness of ANN, the terrain profile data and the path loss data collected from extensive survey measurements. Additionally, the efficiency results of the ANN models obtained in the experimental process is described and discussed. In addition, an optimum ANN model was defined based on predictive precision and generalization capabilities. Finally, a comparative study of the predictive results of the evolved ANN model and ITU-R p530 model was carried out to validate the choice of feed-forward network approach as the optimal option for predictions of path loses.

5.1.1 Descriptive statistics of scenario One

The reported results in table 5.1, shows the descriptive statistics dispersion, distribution of the data and central tendency for path loss (P), and hidden layers (Hidden =2 (H2), Hidden =4 (H4), Hidden =6 (H6), Hidden =8 (H8) and Hidden =10 (H10)).

- Scenario One: A multi-layered FFNN architecture comprising four input neurons and one output neuron, as seen in Figure 5.1, has been developed for model training and creation. Data on the pre-processed path loss collected from nodes along the nineteen sites is compiled, sorted, and ultimately separated into data set training and data set checking. The data-sets for training and research are stored in matrix form with respectively 21773 and 4665 instances. Testing of data collection generated from code instances not included in the data set of the study. The data-set research was generated to determine

the ANN models' generalization capability. The data-sets input variables contain transmitting power, distance, frequencies, and path loss of model ITU-R p.530. For the defined input vector matrix the single target output of the ANN model is the corresponding path loss value. The complete data set for training was divided into 70% training, 15% validation, and 15% sub-data-set testing.

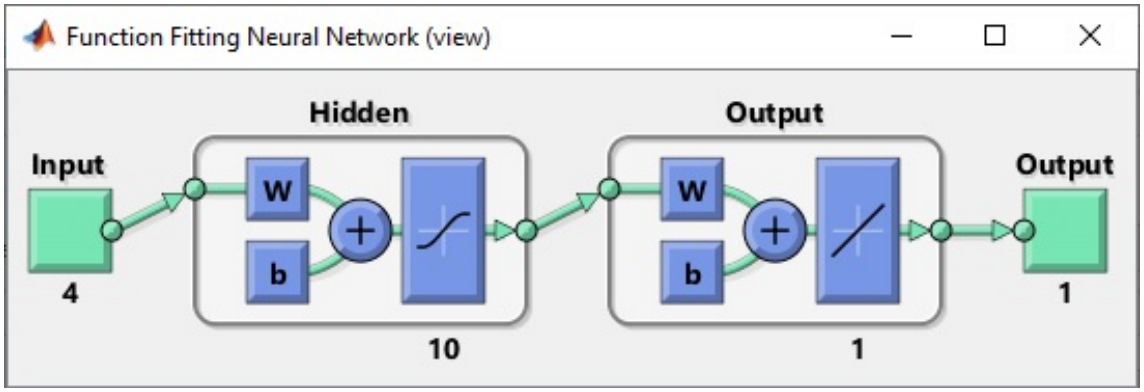

Figure 5.1: ANN model diagram.

Table 5.1: Descriptive statistics for output variables in training, testing, and validation data-set at different layers

Layers	Descriptive		Training		Testing		Validation	
			Statistic	Std. Error	Statistic	Std. Error	Statistic	Std. Error
P	Mean		-57.1982777	0.03200849	-57.1028939	0.06761833	-57.26403	0.0697834
	95% Confidence Interval for Mean	Lower Bound	-57.2610167		-57.2354578		-57.4008385	
		Upper Bound	-57.1355387		-56.97033		-57.1272216	
	5% Trimmed Mean		-56.8793595		-56.7717816		-56.9436108	
	Median		-56.1		-56.1		-56.1	
	Variance		22.307		21.329		22.717	
	Std. Deviation		4.72306993		4.6183863		4.76626232	
	Minimum		-80.3		-81.9		-79.1	
	Maximum		-51.2		-51.5		-51.2	
	Range		29.1		30.4		27.9	
	Interquartile Range		4		4		3.7	
	Skewness		-1.365	0.017	-1.443	0.036	-1.377	0.036
	Kurtosis		0.785	0.033	1.209	0.072	0.825	0.072
H2	Mean		-0.00006	0.00861489	0.0103469	0.01912315	-0.0048897	0.01894741
	95% Confidence Interval for Mean	Lower Bound	-0.0169458		-0.0271435		-0.0420356	
		Upper Bound	0.0168258		0.0478374		0.0322562	
	5% Trimmed Mean		-0.1857648		-0.1833462		-0.1862622	
	Median		-0.19441		-0.19441		-0.1944	
	Variance		1.616		1.706		1.675	
	Std. Deviation		1.27118482		1.30612678		1.29412323	
	Minimum		-2.90344		-1.86085		-1.7034	
	Maximum		18.53915		18.39656		26.3887	
	Range		21.44259		20.25741		28.0921	
	Interquartile Range		0.66216		0.66216		0.6621	
	Skewness		5.481	0.017	5.325	0.036	6.872	0.036
	Kurtosis		42.211	0.033	39.602	0.072	79.523	0.072
H4	Mean		0.0100907	0.00851543	0.0223818	0.01888514	0.0003796	0.01875761
	95% Confidence Interval for Mean	Lower Bound	-0.0066002		-0.014642		-0.0363942	
		Upper Bound	0.0267815		0.0594056		0.0371533	
	5% Trimmed Mean		-0.1705469		-0.1656184		-0.1763896	
	Median		-0.15313		-0.15313		-0.1531	
	Variance		1.579		1.664		1.641	
	Std. Deviation		1.25650942		1.28987049		1.28115957	
	Minimum		-3.10573		-2.12828		-1.9057	
	Maximum		18.27172		18.19427		26.5507	
	Range		21.37745		20.32255		28.4564	
	Interquartile Range		0.66142		0.6		0.6614	
	Skewness		5.492	0.017	5.358	0.036	6.9	0.036
	Kurtosis		42.614	0.033	40.31	0.072	81.35	0.072
H6	Mean		-0.0012468	0.00851575	0.011407	0.01887753	-0.0103922	0.01875148
	95% Confidence Interval for Mean	Lower Bound	-0.0179383		-0.0256019		-0.047154	
		Upper Bound	0.0154447		0.0484159		0.0263695	
	5% Trimmed Mean		-0.1816247		-0.176344		-0.1868448	
	Median		-0.18099		-0.18099		-0.181	
	Variance		1.579		1.662		1.64	
	Std. Deviation		1.25655694		1.28935074		1.28074128	
	Minimum		-3.12453		-2.09816		-1.9245	
	Maximum		18.30184		18.17547		26.5493	
	Range		21.42637		20.27363		28.4738	
	Interquartile Range		0.61717		0.6		0.6172	
	Skewness		5.505	0.017	5.366	0.036	6.917	0.036
	Kurtosis		42.76	0.033	40.386	0.072	81.643	0.072
H8	Mean		0.0065962	0.00851596	0.0192786	0.01887638	-0.0027424	0.01875357
	95% Confidence Interval for Mean	Lower Bound	-0.0100957		-0.017728		-0.0395083	
		Upper Bound	0.0232881		0.0562852		0.0340234	
	5% Trimmed Mean		-0.1751784		-0.1696882		-0.18069	
	Median		-0.182		-0.182		-0.182	
	Variance		1.579		1.662		1.641	
	Std. Deviation		1.2565875		1.28927173		1.28088362	
	Minimum		-3.13587		-2.09971		-1.9359	
	Maximum		18.30029		18.16413		26.5703	
	Range		21.43616		20.26384		28.5062	
	Interquartile Range		0.61771		0.6		0.6177	
	Skewness		5.515	0.017	5.372	0.036	6.925	0.036
	Kurtosis		42.77	0.033	40.345	0.072	81.643	0.072
H10	Mean		0.0007586	0.00851609	0.0133129	0.01887864	-0.0080367	0.01875046
	95% Confidence Interval for Mean	Lower Bound	-0.0159336		-0.0236981		-0.0447965	
		Upper Bound	0.0174508		0.050324		0.0287231	
	5% Trimmed Mean		-0.1804286		-0.1752029		-0.1854018	
	Median		-0.1722		-0.1722		-0.1722	
	Variance		1.579		1.663		1.64	
	Std. Deviation		1.25660723		1.28942605		1.2806716	
	Minimum		-3.13943		-2.08319		-1.9394	
	Maximum		18.31681		18.16057		26.5369	
	Range		21.45624		20.24376		28.4763	
	Interquartile Range		0.61099		0.6		0.611	
	Skewness		5.518	0.017	5.375	0.036	6.925	0.036
	Kurtosis		42.832	0.033	40.399	0.072	81.614	0.072

The results reveal that P (Path loss) that been reported under training, testing and validation have mean -57.198, -57.102 and -57.264 respectively. And median with -56.1, -56.1 and -56.1. Hence In these results, the mean path loss that is required to reach the target are -57.198, -57.102 and -57.264 respectively. And the median of path loss is -56.1. The data appear to be skewed to the right, which explains why the mean is greater than the median. Moreover, for Skewness is that if the number is greater than +1 or lower than 1, this is an indication of a substantially skewed distribution and the reported results indicate the path loss has substantially skewed distribution for training, testing and validation by -1.365, -1.443 and -1.377 respectively. For kurtosis, the general guideline is that if the number is greater than +1, the distribution is too peaked. Likewise, a kurtosis of less than 1 indicates a distribution that is too flat. while the reported results reveal that Kurtosis more than zero and less than one; 0.785 for training, 0.209 for testing and 0.825 for validation, these results insure that the path loss the distribution is not too peak neither not flat within the accepted range which is not very narrow distribution with most of the responses in the center. Interestingly, the path loss has a high standard deviation under validation approximately by 4.76 compare with training 4.72 and testing 4.61. This indicates high volatility in the path loss during the tested time and unstable electromagnetic signals and shows better under testing.

The results reveal that H2 that been reported under training, testing and validation have mean -0.00006, 0.01034 and -0.00488 respectively. And median with -0.19441, -0.1944 and -0.1944. Hence In these results, the data appear to be skewed to the left, which explains why the median is greater than the mean. Moreover, for Skewness is that if the number is greater than +1 or lower than 1, this is an indication of a substantially skewed distribution and the reported results indicate the H2 has substantially skewed distribution for training, testing and validation by 5.481, 5.325 and 6.872 respectively. For kurtosis, the general guideline is that if the number is greater than +1, the distribution is too peaked. Likewise, a kurtosis of less than 1 indicates a distribution that is too flat. While the reported results reveal that Kurtosis more than one; 42.211 for training, 39.602 for testing and 79.523 for validation, these results insure that the H2 the distribution is too peaked which is very narrow distribution with most of the responses in the center. Interestingly, the H2 has a high standard deviation under testing approximately by 1.30 compare with training 1.27 and validation 1.29. This indicates high volatility in the H2 during the tested time and unstable electromagnetic signals and shows better under testing.

The results reveal that H4 that been reported under training, testing and validation have mean 0.0100907, 0.0223818 and 0.0003796 respectively. And median with -0.15313, -0.15313 and -0.1531. Hence In these results, the data appear to be skewed to the left, which explains why the median is greater than the mean. Moreover, for Skewness is that if the number is greater than +1 or lower than 1, this is an indication of a substantially skewed distribution and the reported results indicate the H4 has substantially skewed distribution for training, testing and validation by 5.492, 5.358 and 6.9 respectively. For kurtosis, the general guideline is that if the number is greater than +1, the distribution is too peaked. Likewise, a kurtosis of less than 1 indicates a distribution that is too flat. While the reported results reveal that Kurtosis more than one; 42.614 for training, 40.31 for testing and 81.35 for

validation, these results insure that the H4 the distribution is too peaked which is very narrow distribution with most of the responses in the center. Interestingly, the H4 has a high standard deviation under testing approximately by 1.25 compare with training 1.29 and validation 1.28. This indicates high volatility in the H4 during the tested time and unstable electromagnetic signals and shows better under testing.

The results reveal that H6 that been reported under training, testing and validation have mean -0.000012468, 0.011407 and -0.103922 respectively. And median with -0.18099, -0.18099and -0.181. Hence In these results, the data appear to be skewed to the left, which explains why the median is greater than the mean. Moreover, for Skewness is that if the number is greater than +1 or lower than 1, this is an indication of a substantially skewed distribution and the reported results indicate the H6 has substantially skewed distribution for training, testing and validation by 5.505, 5.366 and 6.917 respectively. For kurtosis, the general guideline is that if the number is greater than +1, the distribution is too peaked. Likewise, a kurtosis of less than 1 indicates a distribution that is too flat. While the reported results reveal that Kurtosis more than one; 42.76 for training, 40.386 for testing and 81.643 for validation, these results insure that the H6 the distribution is too peaked which is very narrow distribution with most of the responses in the center. Interestingly, the H6 has a high standard deviation under testing approximately by 1.25 compare with training 1.29 and validation 1.28. This indicates high volatility in the H6 during the tested time and unstable electromagnetic signals and shows better under testing.

The results reveal that H8 that been reported under training, testing and validation have mean 0.0065962, 0.0192786 and -0.0027424 respectively. And median with -0.182, -0.182 and -0.182. Hence In these results, the data appear to be skewed to the left, which explains why the median is greater than the mean. Moreover, for Skewness is that if the number is greater than +1 or lower than 1, this is an indication of a substantially skewed distribution and the reported results indicate the H8 has substantially skewed distribution for training, testing and validation by 5.515, 5.372 and 6.925 respectively. For kurtosis, the general guideline is that if the number is greater than +1, the distribution is too peaked. Likewise, a kurtosis of less than 1 indicates a distribution that is too flat. While the reported results reveal that Kurtosis more than one; 42.77 for training, 40.345 for testing and 81.643 for validation, these results insure that the H8 the distribution is too peaked which is very narrow distribution with most of the responses in the center. Interestingly, the H8 has a high standard deviation under testing approximately by 1.25 compare with training 1.29 and validation 1.28. This indicates high volatility in the H8 during the tested time and unstable electromagnetic signals and shows better under testing.

The results reveal that H10 that been reported under training, testing and validation have mean 0.0007586, 0.0133129 and -0.0080367 respectively. And median with -0.1722 , -0.1722 and -0.1722. Hence In these results, the data appear to be skewed to the left, which explains why the median is greater than the mean. Moreover, for Skewness is that if the number is greater than +1 or lower than 1, this is an indication of a substantially skewed distribution and the reported results indicate the H10 has substantially skewed distribution for training, testing and validation by 5.518, 5.375 and 6.925 respectively. For kurtosis, the general guideline is that if the

number is greater than +1, the distribution is too peaked. Likewise, a kurtosis of less than 1 indicates a distribution that is too flat. While the reported results reveal that Kurtosis more than one; 42.832 for training, 40.399 for testing and 81.614 for validation, these results insure that the H10 the distribution is too peaked which is very narrow distribution with most of the responses in the center. Interestingly, the H10 has a high standard deviation under testing approximately by 1.25 compare with training 1.29 and validation 1.28. This indicates high volatility in the H10 during the tested time and unstable electromagnetic signals and shows better under testing.

Figures 5.2, 5.3, and 5.4 illustrate the histogram (Skewness) distribution for training, testing and validation Data-set respectively at hidden layers 2, 4, 6, 8, and 10.

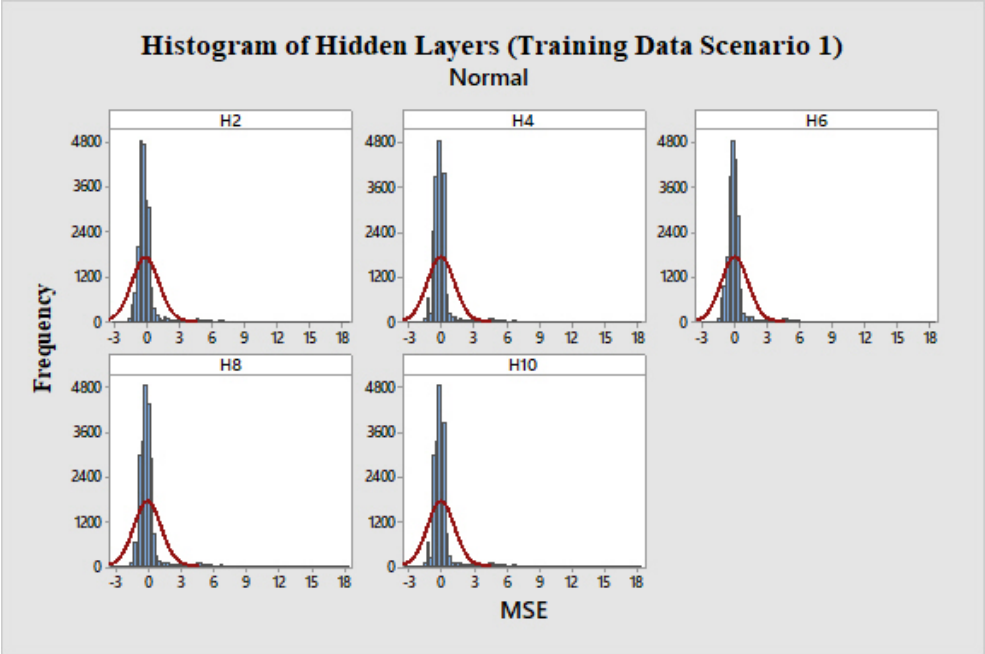

Figure 5.2: Histogram of hidden layers at training

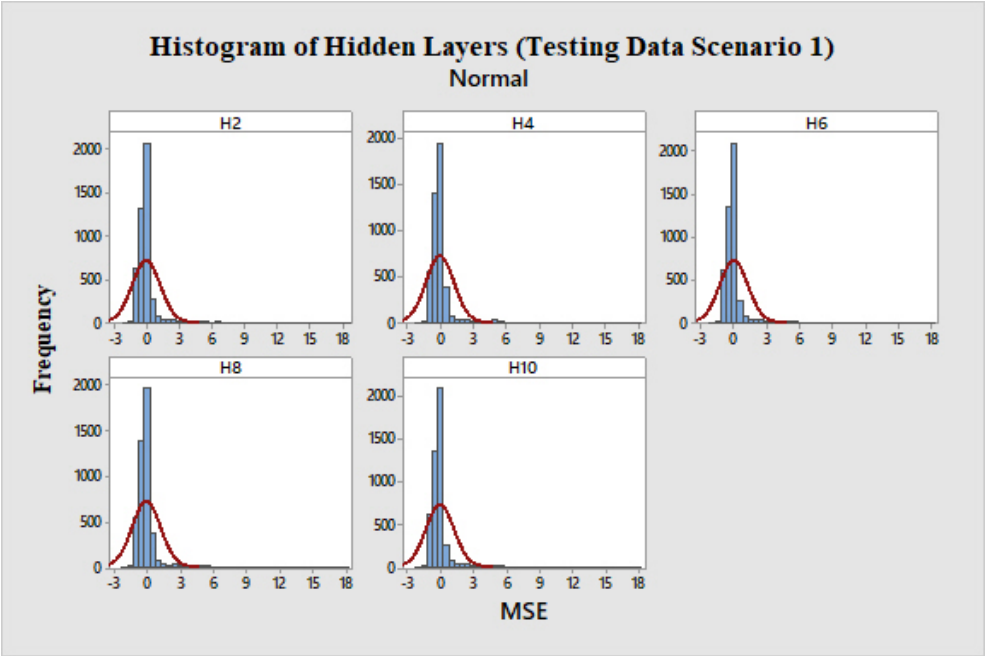

Figure 5.3: Histogram of hidden layers at testing

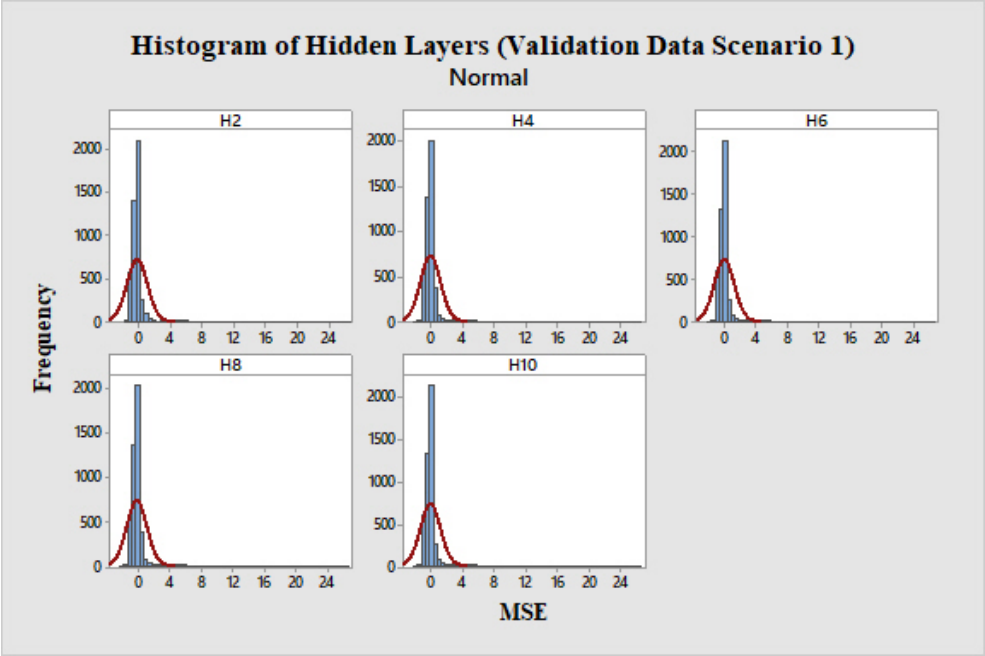

Figure 5.4: Histogram of hidden layers at validation

5.1.2 Descriptive statistics of scenario Two

The reported results in table 5.2, shows the descriptive statistics dispersion,distribution of the data and central tendency for path loss (P), and hidden layers (Hidden =2 (H2), Hidden =4 (H4), Hidden =6 (H6), Hidden =8 (H8) and Hidden =10 (H10))

- Scenario Two: As seen in Figure 5.5, a multi-layered FFNN architecture, containing three inputs and one neuron, was planned for model training and creation. The data-set of pre-processed path failure collected from nodes along the nineteen sites was compiled, categorized, and then split into data-set training and data-set checking. The data-sets for training and research are stored in matrix form with respectively 21773 and 4665 instances. Data-set practice consisted of data instances not used in the data-set instruction. The data-set research was generated to determine the ANN models' generalization capability. The data-sets input variables include transmitting power, distance, and frequencies. For the defined input vector matrix the single target output of the ANN model is the corresponding path loss value. The complete data set for training was divided into 70% training, 15% validation, and 15% sub-dataset testing.

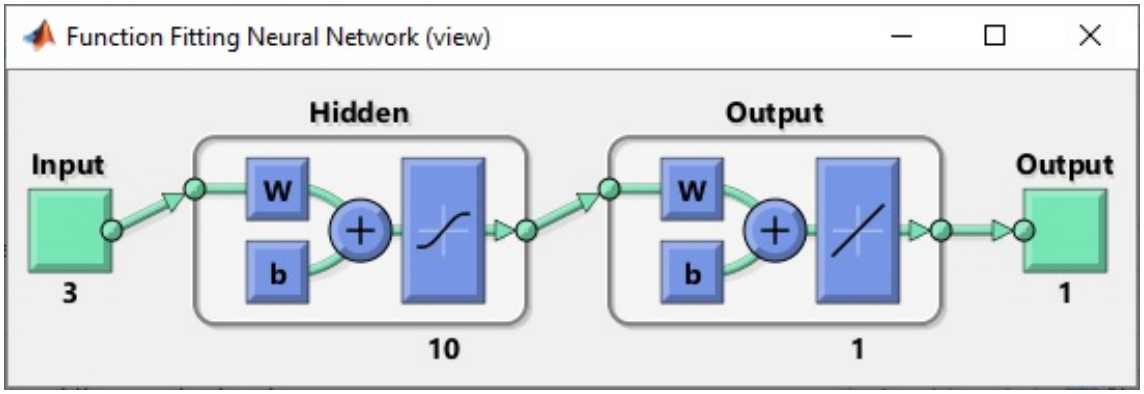

Figure 5.5: ANN model diagram

Table 5.2: descriptive statistics for output variables in training, testing, and validation data-set at different layers.

Layers	Descriptive		Training		Testing		Validation	
			Statistic	Std. Error	Statistic	Std. Error	Statistic	Std. Error
P	Mean		-57.1665044	0.03174634	-57.2692495	0.03152303	-57.6723694	0.03371586
	95% Confidence Interval for Mean	Lower Bound	-57.2287295		-57.3310369		-57.738455	
		Upper Bound	-57.1042792		-57.2074621		-57.6062839	
	5% Trimmed Mean		-56.8430403		-56.9588952		-57.403352	
	Median		-56.1		-56.2		-56.5	
	Variance		21.943		21.635		24.751	
	Std. Deviation		4.6843873		4.65132936		4.97500309	
	Minimum		-80.3		-80.3		-81.9	
	Maximum		-51.2		-51.2		-51.2	
	Range		29.1		29.1		30.7	
	Interquartile Range		4		3.6		3.9	
	Skewness		-1.391	0.017	-1.357	0.017	-1.159	0.017
	Kurtosis		0.906	0.033	0.9	0.033	0.182	0.033
H2	Mean		0.0047666	0.00870275	0.004105	0.00793077	-0.0092262	0.00767158
	95% Confidence Interval for Mean	Lower Bound	-0.0122914		-0.0114399		-0.024263	
		Upper Bound	0.0218246		0.0196499		0.0058107	
	5% Trimmed Mean		-0.178458		-0.1477325		-0.1529631	
	Median		-0.1596373		-0.12232		-0.12232	
	Variance		1.649		1.369		1.281	
	Std. Deviation		1.28415032		1.17021203		1.1319929	
	Minimum		-2.72532		-2.72532		-3.12633	
	Maximum		26.51621		26.51621		26.51621	
	Range		29.24153		29.24153		29.64253	
	Interquartile Range		0.66568		0.52416		0.56268	
	Skewness		5.727	0.017	6.699	0.017	6.573	0.017
	Kurtosis		49.706	0.033	67.847	0.033	67.676	0.033
H4	Mean		-0.0058832	0.00860779	-0.0050287	0.00782355	-0.0135084	0.00758181
	95% Confidence Interval for Mean	Lower Bound	-0.0227551		-0.0203634		-0.0283693	
		Upper Bound	0.0109886		0.0103061		0.0013525	
	5% Trimmed Mean		-0.1793152		-0.1458903		-0.147421	
	Median		-0.1763912		-0.1763422		-0.1763422	
	Variance		1.613		1.333		1.252	
	Std. Deviation		1.2701378		1.15439192		1.11874733	
	Minimum		-3.0934		-3.0934		-3.0934	
	Maximum		26.54633		26.54633		26.54633	
	Range		29.63973		29.63973		29.63973	
	Interquartile Range		0.60333		0.56785		0.56785	
	Skewness		5.493	0.017	6.393	0.017	6.275	0.017
	Kurtosis		47.073	0.033	64.149	0.033	63.977	0.033
H6	Mean		0.0051171	0.00833153	0.0043677	0.00750361	-0.0009805	0.00723058
	95% Confidence Interval for Mean	Lower Bound	-0.0112133		-0.0103399		-0.015153	
		Upper Bound	0.0214475		0.0190753		0.0131919	
	5% Trimmed Mean		-0.1457937		-0.1104041		-0.1168752	
	Median		-0.1720079		-0.1095196		-0.1095196	
	Variance		1.511		1.226		1.138	
	Std. Deviation		1.22937371		1.10718287		1.06692131	
	Minimum		-4.15344		-4.15344		-4.55344	
	Maximum		26.21615		26.21615		26.21615	
	Range		30.36959		30.36959		30.76959	
	Interquartile Range		0.65211		0.58549		0.52272	
	Skewness		5.006	0.017	5.713	0.017	5.658	0.017
	Kurtosis		42.539	0.033	57.903	0.033	58.173	0.033
H8	Mean		-0.0052898	0.00833138	-0.0054394	0.0075046	-0.0084641	0.00723146
	95% Confidence Interval for Mean	Lower Bound	-0.0216199		-0.020149		-0.0226383	
		Upper Bound	0.0110403		0.0092702		0.0057101	
	5% Trimmed Mean		-0.1543457		-0.1184119		-0.1226306	
	Median		-0.1532864		-0.1087716		-0.1087716	
	Variance		1.511		1.226		1.139	
	Std. Deviation		1.2293509		1.10732949		1.06705126	
	Minimum		-4.19539		-4.19539		-4.59539	
	Maximum		26.25989		26.25989		26.25989	
	Range		30.45528		30.45528		30.85528	
	Interquartile Range		0.64579		0.53899		0.53899	
	Skewness		4.967	0.017	5.663	0.017	5.601	0.017
	Kurtosis		42.303	0.033	57.541	0.033	57.782	0.033
H10	Mean		-0.0002612	0.00833284	0.0013149	0.00750559	-0.0056053	0.00723421
	95% Confidence Interval for Mean	Lower Bound	-0.0165942		-0.0133966		-0.0197849	
		Upper Bound	0.0160718		0.0160264		0.0085743	
	5% Trimmed Mean		-0.1499044		-0.1126059		-0.1200555	
	Median		-0.1298247		-0.1125068		-0.1125068	
	Variance		1.512		1.227		1.139	
	Std. Deviation		1.22956727		1.10747462		1.06745673	
	Minimum		-4.3067		-4.3067		-4.7067	
	Maximum		26.27893		26.27893		26.27893	
	Range		30.58563		30.58563		30.98563	
	Interquartile Range		0.63589		0.59884		0.58153	
	Skewness		4.967	0.017	5.671	0.017	5.588	0.017
	Kurtosis		42.375	0.033	57.722	0.033	57.723	0.033

The results reveal that P (Path loss) that been reported under training, testing and validation have mean -57.166, -57.269 and -57.672 respectively. And median with -56.1, -56.2 and -56.5. Hence In these results, the mean path loss that is required to reach the target are -57.166, -57.269, and -57.672 respectively. And the median of path loss is -56.1, -56.2, and -56.5. The data appear to be skewed to the right, which explains why the mean is greater than the median. Moreover, for Skewness is that if the number is greater than +1 or lower than 1, this is an indication of a substantially skewed distribution and the reported results indicate the path loss has substantially skewed distribution for training, testing and validation by -1.391, -1.357 and -1.159 respectively. For kurtosis, the general guideline is that if the number is greater than +1, the distribution is too peaked. Likewise, a kurtosis of less than 1 indicates a distribution that is too flat. while the reported results reveal that Kurtosis more than zero and less than one; 0.906 for training, 0.9 for testing and 0.182 for validation, these results insure that the path loss the distribution is not too peak neither not flat within the accepted range which is not very narrow distribution with most of the responses in the center. Interestingly, the path loss has a high standard deviation under validation approximately by 4.97 compare with training 4.68 and testing 4.65. This indicates high volatility in the path loss during the tested time and unstable electromagnetic signals and shows better under testing.

The results reveal that H2 that been reported under training, testing and validation have mean 0.0047666, 0.004105 and -0.0092262 respectively. And median with -0.1596373, -0.12232 and -0.12232. Hence In these results, the data appear to be skewed to the left, which explains why the median is greater than the mean. Moreover, for Skewness is that if the number is greater than +1 or lower than 1, this is an indication of a substantially skewed distribution and the reported results indicate the H2 has substantially skewed distribution for training, testing and validation by 5.727, 6.699 and 6.573 respectively. For kurtosis, the general guideline is that if the number is greater than +1, the distribution is too peaked. Likewise, a kurtosis of less than 1 indicates a distribution that is too flat. While the reported results reveal that Kurtosis more than one; 49.706 for training, 67.847 for testing and 67.676 for validation, these results insure that the H2 the distribution is too peaked which is very narrow distribution with most of the responses in the center. Interestingly, the H2 has a high standard deviation under testing approximately by 1.28 compare with training 1.17 and validation 1.13. This indicates high volatility in the H2 during the tested time and unstable electromagnetic signals and shows better under testing.

The results reveal that H4 that been reported under training, testing and validation have mean -0.0058832 , -0.0050287 and -0.0135084 respectively. And median with -0.1763912, -0.1763422 and -0.1763422 . Hence In these results, the data appear to be skewed to the left, which explains why the median is greater than the mean. Moreover, for Skewness is that if the number is greater than +1 or lower than 1, this is an indication of a substantially skewed distribution and the reported results indicate the H4 has substantially skewed distribution for training, testing and validation by 5.493, 6.393 and 6.275 respectively. For kurtosis, the general guideline is that if the number is greater than +1, the distribution is too peaked. Likewise, a kurtosis of less than 1 indicates a distribution that is too flat. While the reported results reveal that Kurtosis more than one 47.073 for training, 64.149 for testing and 63.977 for

validation, these results insure that the H4 the distribution is too peaked which is very narrow distribution with most of the responses in the center. Interestingly, the H4 has a high standard deviation under testing approximately by 1.27 compare with training 1.15 and validation 1.11. This indicates high volatility in the H4 during the tested time and unstable electromagnetic signals and shows better under testing.

The results reveal that H6 that been reported under training, testing and validation have mean -0.0051171 , 0.0043677 and -0.0009805 respectively. And median with -0.1720079, -0.1095196 and -0.1095196. Hence In these results, the data appear to be skewed to the left, which explains why the median is greater than the mean. Moreover, for Skewness is that if the number is greater than +1 or lower than 1, this is an indication of a substantially skewed distribution and the reported results indicate the H6 has substantially skewed distribution for training, testing and validation by 5.006, 5.713 and 5.658 respectively. For kurtosis, the general guideline is that if the number is greater than +1, the distribution is too peaked. Likewise, a kurtosis of less than 1 indicates a distribution that is too flat. While the reported results reveal that Kurtosis more than one 42.539 for training, 57.903 for testing and 58.173 for validation, these results insure that the H6 the distribution is too peaked which is very narrow distribution with most of the responses in the center. Interestingly, the H6 has a high standard deviation under testing approximately by 1.23 compare with training 1.10 and validation 1.06. This indicates high volatility in the H6 during the tested time and unstable electromagnetic signals and shows better under testing.

The results reveal that H8 that been reported under training, testing and validation have mean –0.0052898 , -0.0054394 and -0.0084641 respectively. And median with -0.1532864 , -0.1087716 and -0.1087716. Hence In these results, the data appear to be skewed to the left, which explains why the median is greater than the mean. Moreover, for Skewness is that if the number is greater than +1 or lower than 1, this is an indication of a substantially skewed distribution and the reported results indicate the H8 has substantially skewed distribution for training, testing and validation by 4.967, 5.663 and 5.601 respectively. For kurtosis, the general guideline is that if the number is greater than +1, the distribution is too peaked. Likewise, a kurtosis of less than 1 indicates a distribution that is too flat. While the reported results reveal that Kurtosis more than one 42.303 for training, 57.541 for testing and 57.782 for validation, these results insure that the H8 the distribution is too peaked which is very narrow distribution with most of the responses in the center. Interestingly, the H8 has a high standard deviation under testing approximately by 1.23 compare with training 1.10 and validation 1.06. This indicates high volatility in the H8 during the tested time and unstable electromagnetic signals and shows better under testing.

The results reveal that H10 that been reported under training, testing and validation have mean —0.0002612 , 0.0013149 and -0.0056053 respectively. And median with -0.1298247 , -0.1125068 and -0.1125068 . Hence In these results, the data appear to be skewed to the left, which explains why the median is greater than the mean. Moreover, for Skewness is that if the number is greater than +1 or lower than 1, this is an indication of a substantially skewed distribution and the reported results indicate the H10 has substantially skewed distribution for training, testing and validation by 4.967, 5.671 and 5.588 respectively. For kurtosis, the general guideline

is that if the number is greater than +1, the distribution is too peaked. Likewise, a kurtosis of less than 1 indicates a distribution that is too flat. While the reported results reveal that Kurtosis more than one 42.375 for training, 57.722 for testing and 57.723 for validation, these results insure that the H10 the distribution is too peaked which is very narrow distribution with most of the responses in the center. Interestingly, the H10 has a high standard deviation under testing approximately by 1.23 compare with training 1.10 and validation 1.06. This indicates high volatility in the H10 during the tested time and unstable electromagnetic signals and shows better under testing.

Figures 5.6, 5.7, and 5.8 illustrate the histogram (Skewness) distribution for training, testing and validation Data-set respectively at hidden layers 2, 4, 6, 8, and 10.

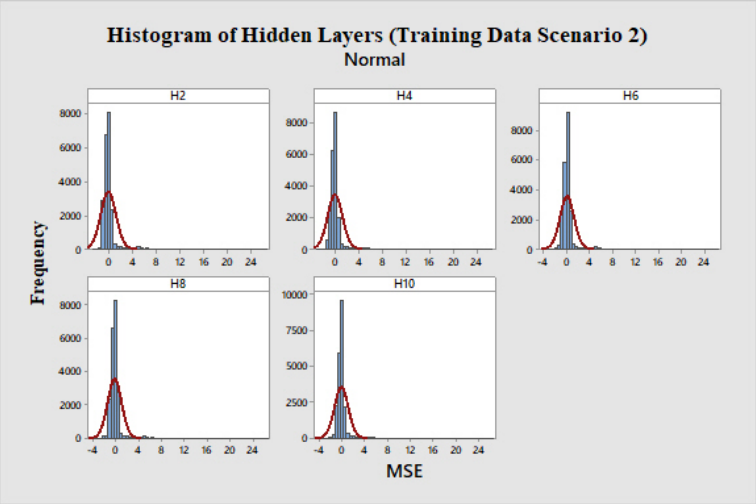

Figure 5.6: Histogram of hidden layers at training

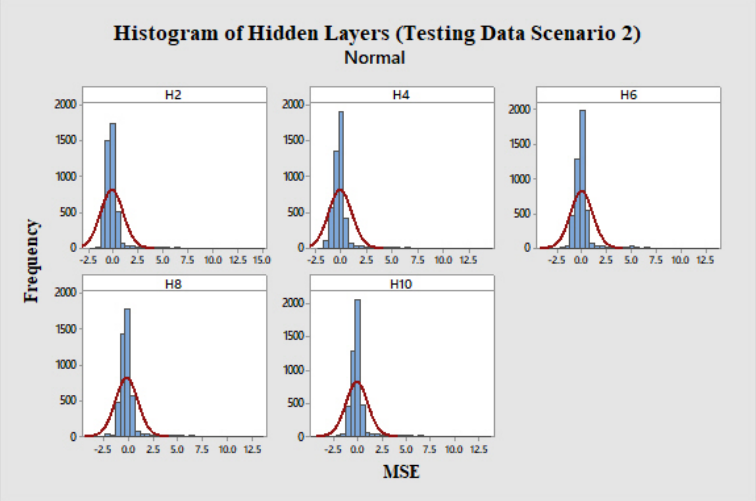

Figure 5.7: Histogram of hidden layers at testing

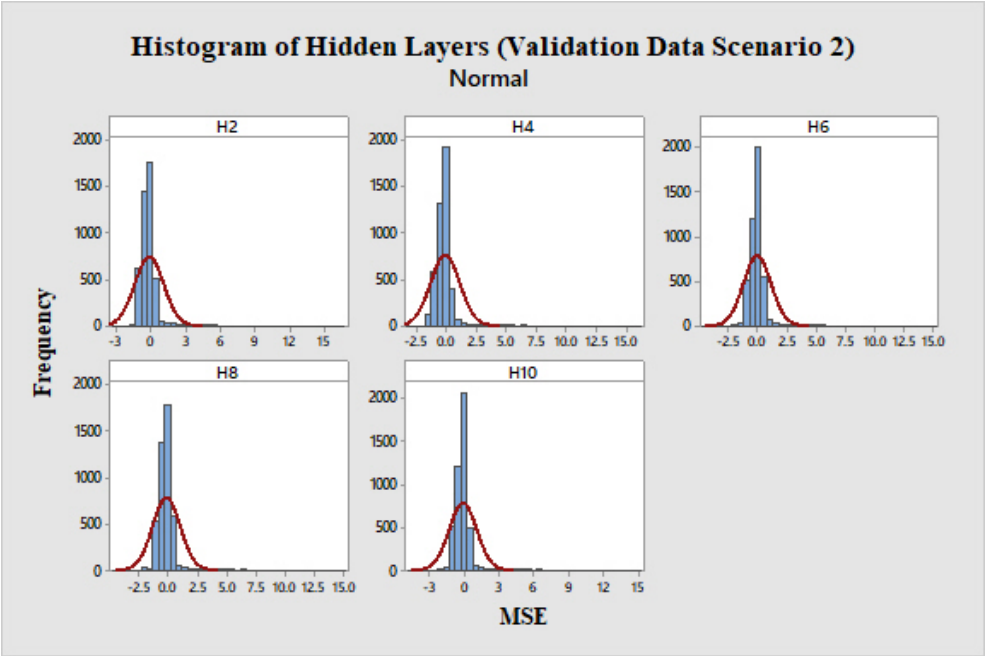

Figure 5.8: Histogram of hidden layers at validation

5.1.3 Regression Model

The study uses regression analysis to predict the value of a path loss (P) based on the values of different layers, and to study the impact of changes in layers used H2, H4, H6, H8, and H10 on the path loss. Therefore, this results shows the effects of each layers on path loss regarding the magnitude and direction. For training, testing and validation in two different scenarios, as reported in table 5.3.

Table 5.3: Scenario one path loss prediction based on different layers

scenario#1	Training				Testing				Validation			
	C	Beta	R Square	F	C	Beta	R Square	F	C	Beta	R Square	F
H2	-57.198*	-0.269*	0.072	1701.46*	-57.092*	-0.287*	0.082	417.143*	-57.26*	-0.273	0.075	376.347*
H4	-57.188*	-0.27*	0.073	1712.49*	-57.08*	-0.288*	0.083	421.615*	-57.26*	-0.276	0.076	385.994*
H6	-57.2*	-0.264*	0.07	1631.03*	-57.091*	-0.282*	0.08	403.486*	-57.27*	-0.27	0.073	367.567*
H8	-57.192*	-0.26*	0.067	1573.34*	-57.084*	-0.278*	0.077	390.562*	-57.26*	-0.266	0.071	355.273*
H10	-57.198*	-0.266*	0.071	1655.45*	-57.089*	-0.284*	0.081	408.873*	-57.27*	-0.272	0.074	372.576*

Note: * represent significant at 1% level, F represents F-test the model fitness.

The reported results in scenario one, reveal the relationship between the path loss and different layers. In training H2 has reduce the path loss approximately by 26.9%, and statistically significant at 1% level. Furthermore, R-square indicates that H2 in training explain the path loss in the electromagnetic by 7.2%. Almost similar in validation H2 has reduce the path loss approximately by 27.3%, and statistically significant at 1% level. Furthermore, R-square indicates that H2 in validation explain the path loss in the electromagnetic by 7.5%. while the results under testing have more efficiency in reducing the path loss in the electromagnetic, in testing H2 has reduce the path loss approximately by 28.7%, and statistically significant at 1% level. Furthermore, R-square indicates that H2 in testing explain the path loss in the electromagnetic by 8.2%. Turning to layer 4 (H4), in training H4 has reduce the path loss approximately by 27%, and statistically significant at 1% level.

Furthermore, R-square indicates that H4 in training explain the path loss in the electromagnetic by 7.3%. Almost similar in validation H4 has reduce the path loss approximately by 27.6%, and statistically significant at 1% level. Furthermore, R-square indicates that H4 in validation explain the path loss in the electromagnetic by 7.6%. while the results under testing have more efficiency in reducing the path loss in the electromagnetic, in testing H4 has reduce the path loss approximately by 28.8%, and statistically significant at 1% level. Furthermore, R-square indicates that H4 in testing explain the path loss in the electromagnetic by 8.3%. Turning to layer 6 (H6), in training H6 has reduce the path loss approximately by 26.4%, and statistically significant at 1% level. Furthermore, R-square indicates that H6 in training explain the path loss in the electromagnetic by 7%. Almost similar in validation H6 has reduce the path loss approximately by 27%, and statistically significant at 1% level. Furthermore, R-square indicates that H6 in validation explain the path loss in the electromagnetic by 7.3%. While the results under testing have more efficiency in reducing the path loss in the electromagnetic, in testing H6 has reduce the path loss approximately by 28.2%, and statistically significant at 1% level. Furthermore, R-square indicates that H6 in testing explain the path loss in the electromagnetic by 8%.

In training H8 has reduce the path loss approximately by 26%, and statistically significant at 1% level. Furthermore, R-square indicates that H8 in training explain the path loss in the electromagnetic by 6.7%. Almost similar in validation H8 has reduce the path loss approximately by 26.6%, and statistically significant at 1% level. Furthermore, R-square indicates that H8 in validation explain the path loss in the electromagnetic by 7.1%. While the results under testing have more efficiency in reducing the path loss in the electromagnetic, in testing H8 has reduce the path loss approximately by 27.8%, and statistically significant at 1% level. Furthermore, R-square indicates that H8 in testing explain the path loss in the electromagnetic by 7.7%. Turning to layer 10 (H10), in training H10 has reduce the path loss approximately by 26.6%, and statistically significant at 1% level. Furthermore, R-square indicates that H10 in training explain the path loss in the electromagnetic by 7.1%. Almost similar in validation H10 has reduce the path loss approximately by 27.2%, and statistically significant at 1% level. Furthermore, R-square indicates that H10 in validation explain the path loss in the electromagnetic by 7.4%. While the results under testing have more efficiency in reducing the path loss in the electromagnetic, in testing H10 has reduce the path loss approximately by 28.4%, and statistically significant at 1% level. Furthermore, R-square indicates that H10 in testing explain the path loss in the electromagnetic by 8.1%.

Table 5.4: scenario one testing data under different frequency.

scenario#1	15Ghz				18Ghz				23 Ghz			
	C	Beta	R Square	F	C	Beta	R Square	F	C	Beta	R Square	F
H2	-54.843	-0.95*	0.903	5950.738*	-62.028	-0.33*	0.109	167.746	-55.119	-0.615*	0.378	1611.207*
H4	-55.096	-0.972*	0.945	10990.88*	-61.787	-0.193*	0.037	53.283	-55.126	-0.577*	0.333	1324.018*
H6	-55.066	-0.971*	0.944	10633.16*	-61.803	-0.181*	0.033	46.661	-55.146	-0.573*	0.328	1294.835*
H8	-55.067	-0.972*	0.944	10781.76*	-61.799	-0.177*	0.031	44.074	-55.134	-0.567*	0.321	1255.886*
H10	-55.051	-0.971*	0.943	10542.05*	-61.796	-0.183*	0.033	47.469	-55.149	-0.572*	0.327	1288.195*

Note: * represent significant at 1% level, F represents F-test the model fitness.

The reported results in scenario one, reveal the relationship between the path loss and different layers under 15 GHz highly effective in reducing the path loss in electromagnetic among the different layers as shown in table 4 the range of Beta between 95% to 97.1% and statically significant at 1% level, with high R-square ranged between 90.3% to 94.5%. Compare with the path loss of electromagnetic under 18 GHz the range of beta between 17.7% to 33% and statistically significant, with weak R-square range between 3.1% to 10.9%. Moreover, the results under 23GHz shows slightly good performance compare with 18GHz, indicate the range of beta between 57.2% to 61.5% and statically significant and R-square ranged between 32.1% to 37.8%.

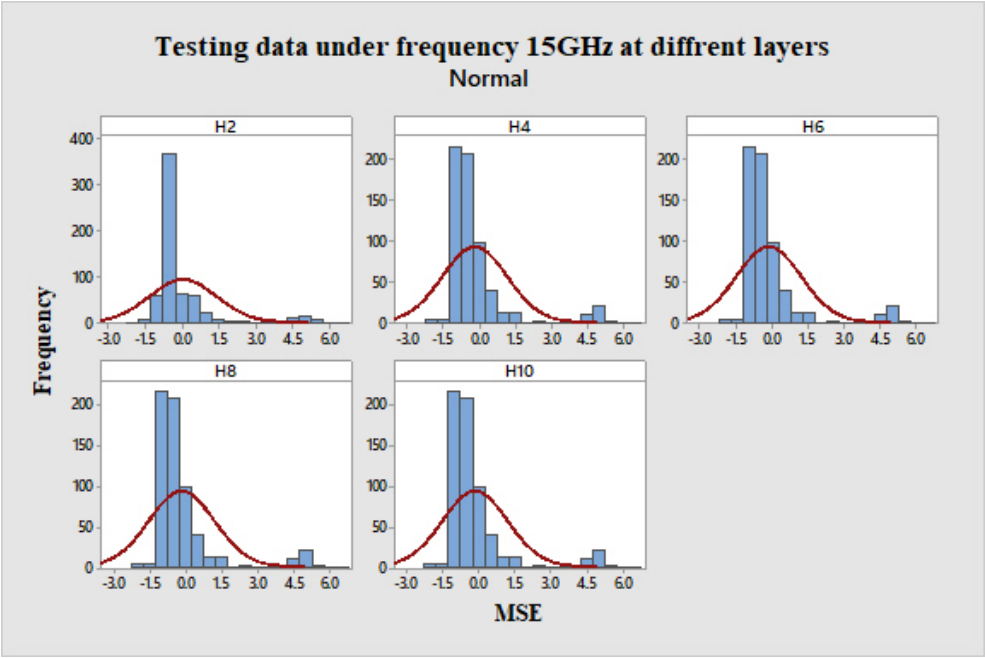

Figure 5.9: Histogram of scenario one testing data under 15GHz frequency

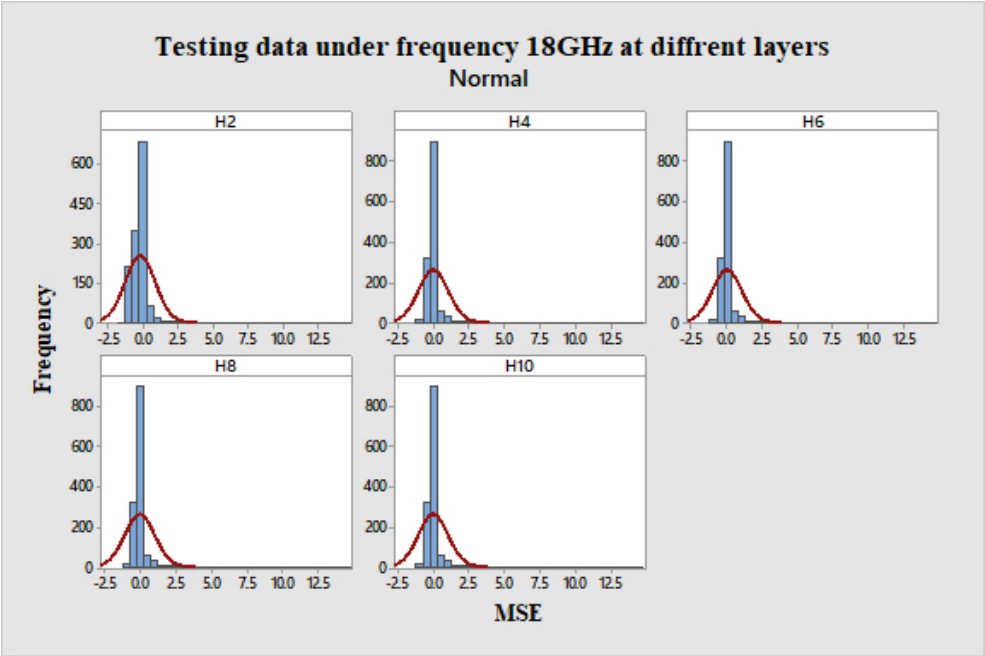

Figure 5.10: Histogram of scenario one testing data under 18GHz frequency

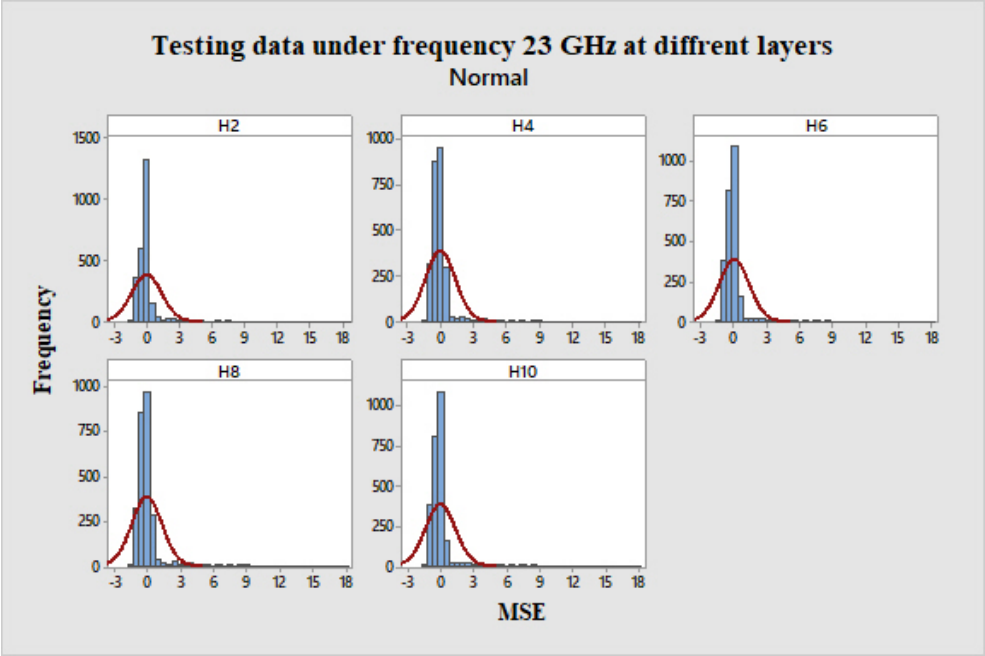

Figure 5.11: Shows Histogram of scenario one testing data under 23GHz frequency

Table 5.5: Scenario two path loss prediction based on different layers.

scenario#2	Training				Testing				Validation			
	C	Beta	R Square	F	C	Beta	R Square	F	C	Beta	R Square	F
H2	-57.162*	-0.277*	0.077	1813.6*	-57.265	-0.255*	0.065	1510.872*	-57.682	-0.235*	0.055	1274.489*
H4	-57.172*	-.274*	0.075	1768.503*	-57.274	-0.25*	0.063	1453.745*	-57.686	-0.229*	0.053	1206.409*
H6	-57.161*	-0.262*	0.069	1610.21*	-57.265	-0.237*	0.056	1301.008*	-57.682	-0.217*	0.047	1074.194*
H8	-57.172*	-0.268*	0.072	1681.031*	-57.275	-0.243*	0.059	1365.369*	-57.681	-0.223*	0.05	1139.457*
H10	-57.167*	-0.262*	0.069	1610.145*	-57.268	-0.236*	0.056	1285.938*	-57.678	-0.216*	0.047	1067.347*

Note: * represent significant at 1% level, F represents F-test the model fitness.

The reported results in scenario two reveal the relationship between the path loss and different layers. In training and testing H2 have reduced the path loss approximately by 27.7%, and 25.5% respectively. In addition, statistically significant at 1% level. Furthermore, R-square indicates that H2 in training and testing explain the path loss in the electromagnetic by 7.7% and 6.5% respectively. These results under training and testing have more efficiency in reducing the path loss in the electromagnetic. While the results under validation have less efficiency in reducing the path loss in the electromagnetic, in validation H2 has reduce the path loss approximately by 23.5%, and statistically significant at 1% level. Furthermore, R-square indicates that H2 in validation explain the path loss in the electromagnetic by 5.5%. Turning to layer 4 (H4), in training and testing H4 have reduced the path loss approximately by 27.4%, and 25% respectively. In addition, statistically significant at 1% level. Furthermore, R-square indicates that H4 in training and testing explain the path loss in the electromagnetic by 7.5% and 6.3% respectively. These results under training and testing have more efficiency in reducing the path loss in the electromagnetic. While the results under validation have less efficiency in reducing the path loss in the electromagnetic, in validation H4 has reduce the path loss approximately by 22.9%, and statistically significant at 1% level. Furthermore, R-square indicates that H4 in validation explain the path loss in the electromagnetic by 5.3%.

In training and testing H6 have reduced the path loss approximately by 26.2%, and 23.7% respectively. In addition, statistically significant at 1% level. Furthermore, R-square indicates that H6 in training and testing explain the path loss in the electromagnetic by 6.9% and 5.6% respectively. These results under training and testing have more efficiency in reducing the path loss in the electromagnetic. While the results under validation have less efficiency in reducing the path loss in the electromagnetic, in validation H6 has reduce the path loss approximately by 21.7%, and statistically significant at 1% level. Furthermore, R-square indicates that H6 in validation explain the path loss in the electromagnetic by 4.7%.

In training and testing H8 have reduced the path loss approximately by 26.8%, and 24.3% respectively. In addition, statistically significant at 1% level. Furthermore, R-square indicates that H8 in training and testing explain the path loss in the electromagnetic by 7.2% and 5.9% respectively. These results under training and testing have more efficiency in reducing the path loss in the electromagnetic. While the results under validation have less efficiency in reducing the path loss in the electromagnetic, in validation H8 has reduce the path loss approximately by 22.3%, and statistically significant at 1% level. Furthermore, R-square indicates that H8 in validation explain the path loss in the electromagnetic by 5%. In training and testing

H10 have reduced the path loss approximately by 26.2%, and 23.6% respectively. In addition, statistically significant at 1% level. Furthermore, R-square indicates that H10 in training and testing explain the path loss in the electromagnetic by 6.9% and 5.6% respectively. These results under training and testing have more efficiency in reducing the path loss in the electromagnetic. While the results under validation have less efficiency in reducing the path loss in the electromagnetic, in validation H10 has reduce the path loss approximately by 21.6%, and statistically significant at 1% level. Furthermore, R-square indicates that H10 in validation explain the path loss in the electromagnetic by 4.7%.

Note: * represent significant at 1% level, F represents F-test the model fitness.

The reported results in scenario two, reveal the relationship between the path loss and different layers under 15 GHz highly effective in reducing the path loss in electromagnetic among the different layers as shown in table 6 the range of Beta between 86.9% to 96% and statically significant at 1% level, with high R-square ranged between 75.5% to 93%. Compare with the path loss of electromagnetic under 18 GHz the range of beta between 17.5% to 19.1% and statistically significant, with weak R-square range between 3% to 3.7%. Moreover, the results under 23Ghz shows slightly good performance compare with 18 GHz, indicate the range of beta between 49.3% to 50.8% and statically significant and R-square ranged between 24.3% to 25.8%.

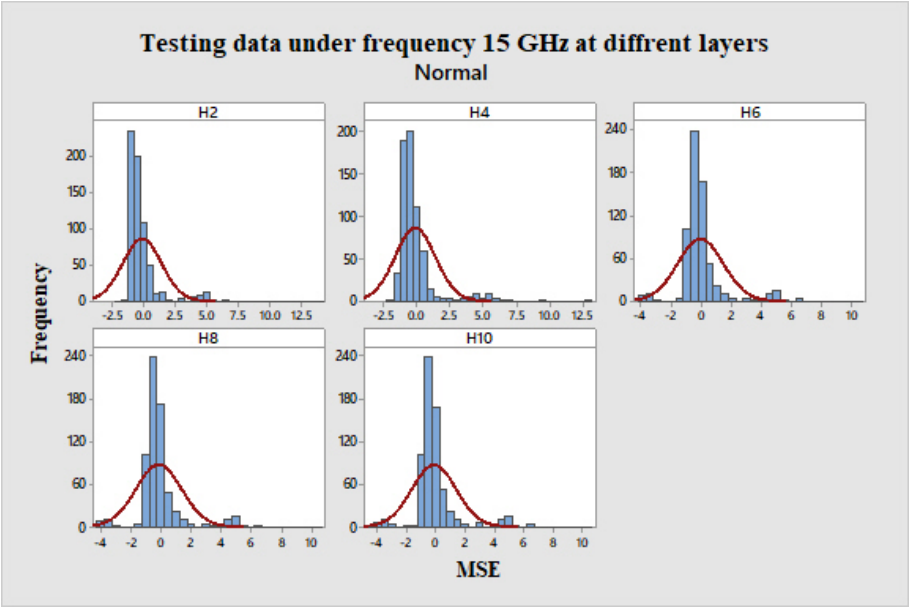

Figure 5.12: Histogram of scenario two testing data under frequency 15GHz

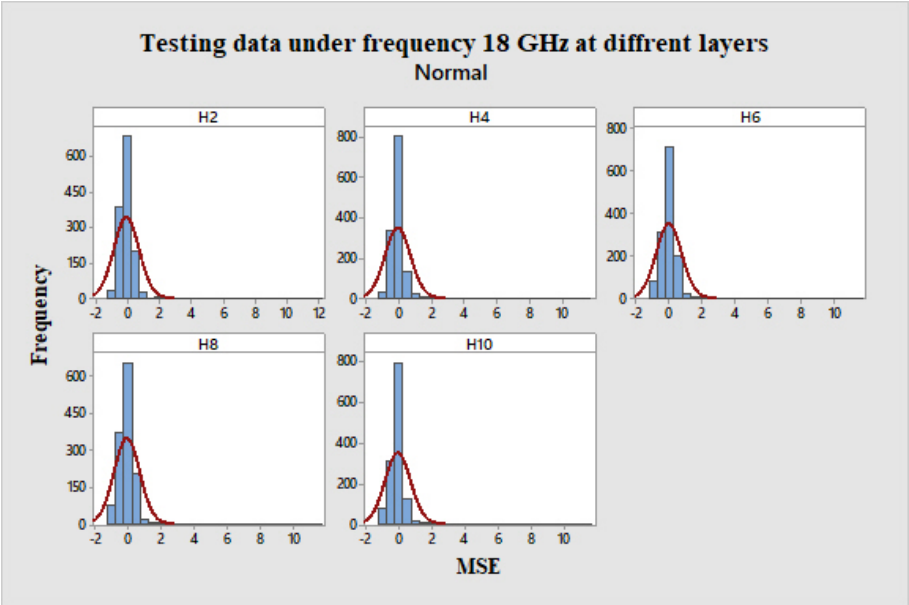

Figure 5.13: Histogram of scenario two testing data under frequency 18GHz

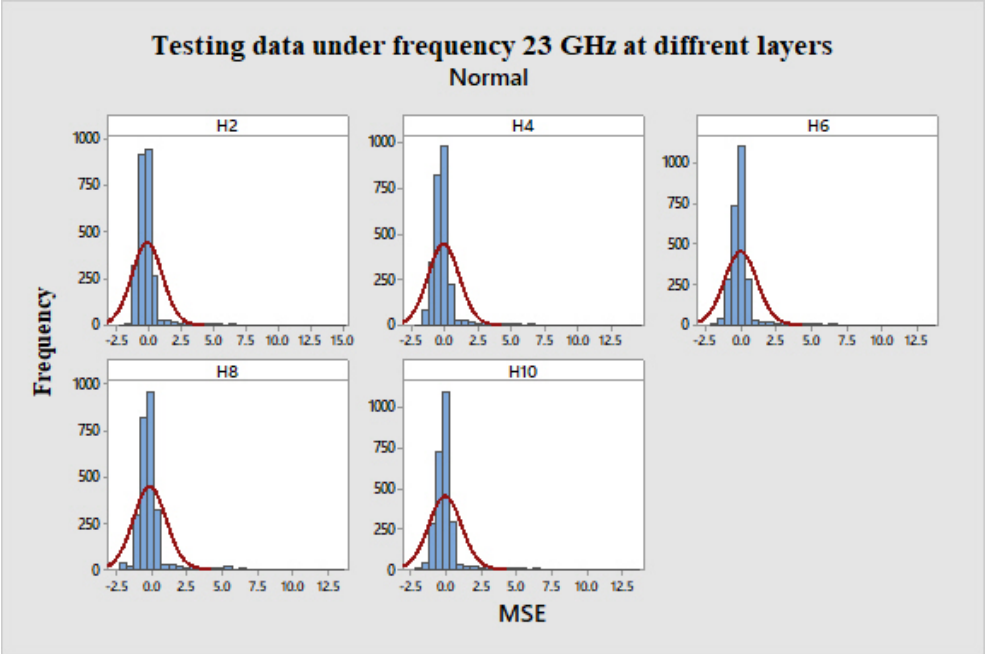

Figure 5.14: Histogram of scenario two testing data under frequency 23GHz

The performance of the developed machine learning model under hidden layer 4 proved to be optimal in terms of prediction accuracy and generalization ability when compared to those all tested "layers 2, 6, 8, and 10" and with widely used empirical models (FSPL, ITU-R p.530, and Crane). Figure 5.15 illustrates Absolute Error study of the predictive results of the evolved ANN model and theoretical models was carried out to validate the choice of feed-forward network approach as the optimal option for predictions of path loses.

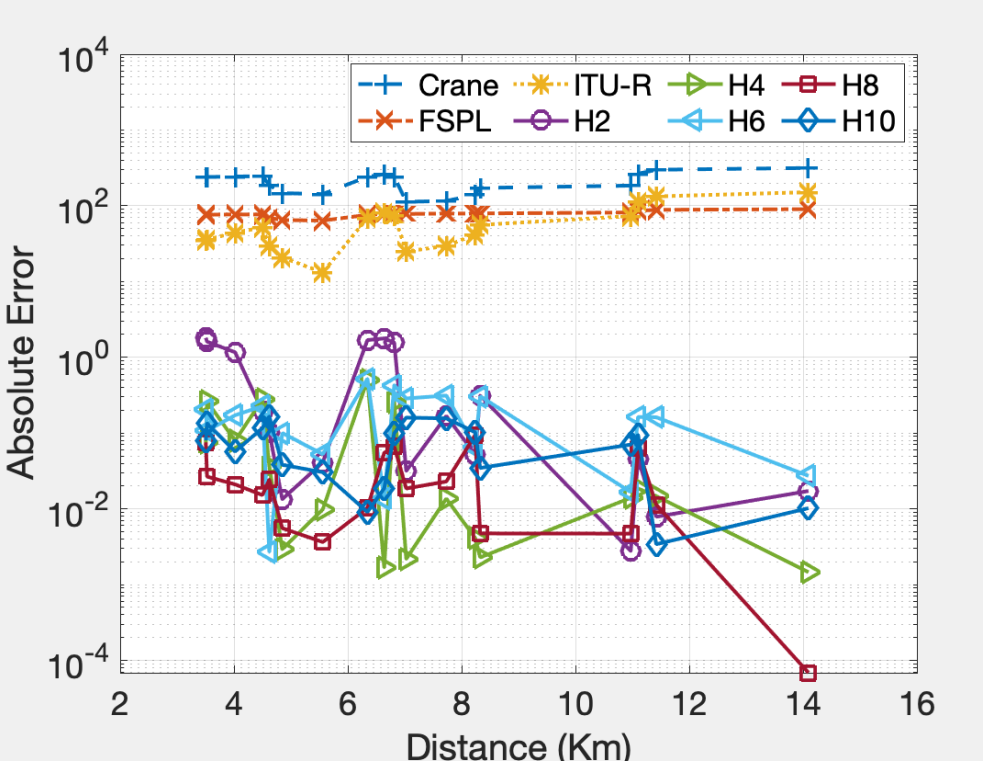

Figure 5.15: Absolute Error of the predictive results ANN model and Theoretical models

Based on Mean Squared Error (MSE), as shown in Figure 5.16 the performance of the ANN models was evaluated. Results of the ANN processes showed that the least predictive error occurred in the FNN architecture which employs a tangent activation mechanism and 4 hidden neurons. Experimental findings revealed a significant increase in performance metrics for the training data set: MSE dropped from 70.8 to 0.0032 dB. The assessment of the predictions provided by the optimized ANN model also revealed substantial changes with respect to the generalization capacity.

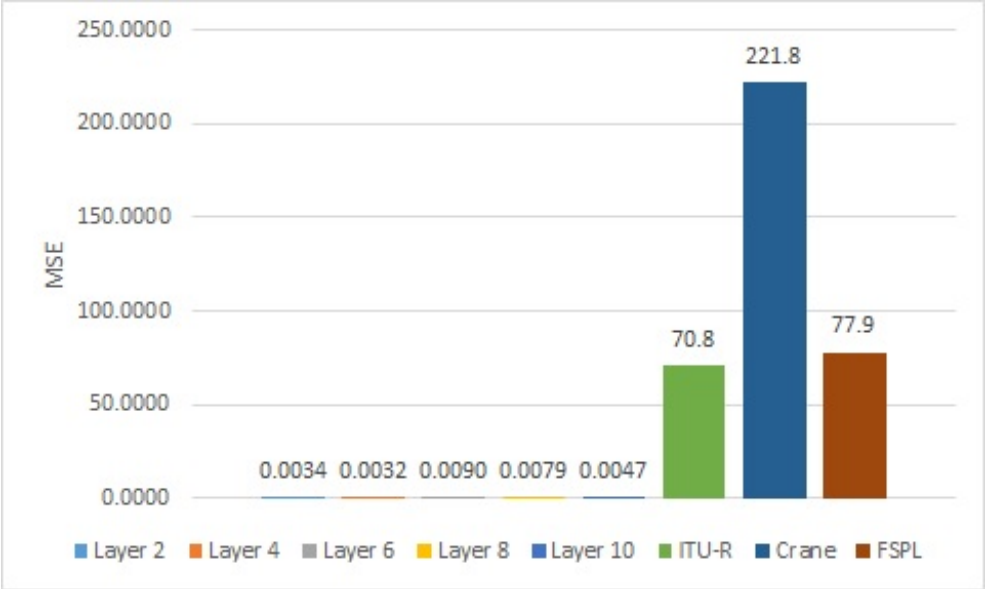

Figure 5.16: Mean squared error (MSE), for ANNs models and theoretical models

Chapter 6

Conclusion and Perspectives

The main part of this thesis demonstrated a machine learning approach to generate optimized path loss models, reflecting the specific characteristics of a given environment, based on traces from real past Data-Set obtained from PalTel and Jawwal. and adapt the three selected empirical propagation models to additionally consider the elevation angle in predicting the coverage at various microwave distances.

There is no generic propagation model which can suit every environment and provide accurate predictions other than those models which have been custom-designed for that. Thus, the ML optimization considered.

6.1 Conclusion

The data collected on the field profile and Path Loss data was introduced and analyzed in scenario 1 using regression test measurements. The findings of the machine learning models obtained in the experiment phase were also described and explored. Also, a predictive precision and generalization capabilities model was established based on the optimum model, by using a regression model and calculating each layer's vulnerability (beta) in electromagnetic path loss. A descriptive study of the prediction outcomes and the performance of ANN with different number of hidden layers was performed. This is to validate the choice of feed-forward network approach to enhance the estimation of path loss predictions. Finally, the performances of the models were evaluated based on the regression coefficient and (R) metrics. The results of the machine learning processes showed that the ANN with four hidden layers architecture produces the least prediction error. This means that the proposed ANN model with four hidden layers represents the optimum model among all tested parameters including other path loss models. In summary, the performance of the developed machine learning model with four hidden layers is the best path loss estimator in terms of prediction accuracy and generalization ability.

6.2 Perspectives

The work in this thesis can be extended in future to include the following research topics, which were not covered in this thesis due to lack of time:

- In this work, only three frequencies band have been considered in extending the footprint and achieving a low PL. Additional frequency bands may be considered for inclusion in the optimal model, which in turn may enhance RSS and maximize throughput especially for areas with limited coverage but significant number of users. One such frequency band is 28GHz/47GHz which may be shared with satellites. Another such frequency band is 60GHz, which is dedicated for 5G WiGig.
- The optimized model in this work only includes parameters for outdoor propagation, i.e. FSPL and large-scale fading, at different altitudes. Therefore, future R&D may include parameters in relation to calculating indoor propagation, i.e. small-scale fading, building penetration loss.
- Integrating live geolocations sourced from google maps may provide a more realistic background to the environmental considerations whilst assessing propagation model performance.

Appendices

Appendix A

Antenna Specification

Antenna is the part of a transmission or receiving network designed to radiate electromagnetic waves or to receive them. The ability to concentrate and shape the radiated power in space is an essential property of an antenna; it stimulates power in certain desired directions, and suppresses power in other directions. There are several different kinds of antennas and their mechanical forms; each type is uniquely designed for particular purposes. Tables A.1, A.2 and A.3 show antennas specification used in JAWWAL at 15 GHz, 18GHz, and 23GHz respectively.

Table A.1: Antennas specification used in JAWWAL at 15 GHz

Frequency band	15GHz			
diameter Size(m)	0.3m	0.6m	0.9m	1.2m
Frequency range (GHz)	14.40 - 15.35			
Gain (Low-band) (dBi)	31.9	37.2	40.5	42.9
Gain (Mid-band) (dBi)	32.4	37.5	40.9	43.1
Gain (High-band) (dBi)	32.5	37.6	41.1	43.3
Half power beam width (deg)	4.4	2.4	1.6	1.2
Cross-polar discrimination (dB)	30	30	30	30
Front-to-back ratio (dB)	60	65	69	71
VSWR/Return loss (dB)	1.3:1/17.7	1.3:1/17.7	1.3:1/17.7	1.3:1/17.7
ETSI compliance	Class 3	Class 3	Class 3	Class 3
FCC compliance	N/A	N/A	N/A	N/A

Table A.2: Antennas specification used in JAWWAL at 18 GHz

Frequency band	18GHz			
diameter Size(m)	0.3m	0.6m	0.9m	1.2m
Frequency range (GHz)	17.70 - 19.70			
Gain (Low-band) (dBi)	33.7	39.4	42.4	44.7
Gain (Mid-band) (dBi)	34.7	39.7	43.5	45.2
Gain (High-band) (dBi)	34.5	40.5	44.1	45.7
Half power beam width (deg)	3.2	2	1.3	0.9
Cross-polar discrimination (dB)	30	30	30	30
Front-to-back ratio (dB)	62	69	71	73
VSWR/Return loss (dB)	1.3:1/17.7	1.3:1/17.7	1.3:1/17.7	1.3:1/17.7
ETSI compliance	Class 3	Class 3	Class 3	Class 3
FCC compliance	Cat B2	Cat A	Cat A	Cat A

Table A.3: Antennas specification used in JAWWAL at 23 GHz

Frequency band	23GHz			
diameter Size(m)	0.3m	0.6m	0.9m	1.2m
Frequency range (GHz)	21.20 - 23.60			
Gain (Low-band) (dBi)	35.8	41.4	44.5	46
Gain (Mid-band) (dBi)	35.8	41.6	44.9	46.3
Gain (High-band) (dBi)	35.9	41.6	45.4	46.9
Half power beam width (deg)	2.7	1.6	1	0.7
Cross-polar discrimination (dB)	30	30	30	30
Front-to-back ratio (dB)	60	65	69	70
VSWR/Return loss (dB)	1.3:1/17.7	1.3:1/17.7	1.3:1/17.7	1.3:1/17.7
ETSI compliance	Class 3	Class 3	Class 3	Class 3
FCC compliance	Cat A	Cat A	Cat A	Cat A

Bibliography

[1] A. Neskovic, N. Neskovic, and G. Paunovic, "Modern approaches in modeling of mobile radio systems propagation environment," *IEEE Communications Surveys & Tutorials*, vol. 3, no. 3, pp. 2–12, 2000.

[2] A. B. Carlson, "Communication systems: an introduction to signals and noise in electriocal communication," 2002.

[3] O. Bouchet, H. Sizun, C. Boisrobert, and F. De Fornel, *Free-space optics: propagation and communication*, vol. 91. John Wiley & Sons, 2010.

[4] P. R. Karmel, G. D. Colef, G. D. Colef, and R. L. Camisa, *Introduction to electromagnetic and microwave engineering*, vol. 53. John Wiley & Sons, 1998.

[5] J. M. Sandri, "Microwave backhaul as a business: taking the next step [microbusiness]," *IEEE Microwave Magazine*, vol. 10, no. 5, pp. 34–46, 2009.

[6] Y. Zhang, J. Wen, G. Yang, Z. He, and J. Wang, "Path loss prediction based on machine learning: Principle, method, and data expansion," *Applied Sciences*, vol. 9, no. 9, p. 1908, 2019.

[7] E. Ostlin, H.-J. Zepernick, and H. Suzuki, "Macrocell path-loss prediction using artificial neural networks," *IEEE Transactions on Vehicular Technology*, vol. 59, no. 6, pp. 2735–2747, 2010.

[8] C. Phillips, D. Sicker, and D. Grunwald, "A survey of wireless path loss prediction and coverage mapping methods," *IEEE Communications Surveys & Tutorials*, vol. 15, no. 1, pp. 255–270, 2013.

[9] G. R. MacCartney, M. K. Samimi, and T. S. Rappaport, "Omnidirectional path loss models in new york city at 28 ghz and 73 ghz," in *Personal, Indoor, and Mobile Radio Communication (PIMRC), 2014 IEEE 25th Annual International Symposium on*, pp. 227–231, IEEE, 2014.

[10] M. Born and E. Wolf, *Principles of optics: electromagnetic theory of propagation, interference and diffraction of light*. Elsevier, 2013.

[11] H. Sizun and P. de Fornel, *Radio wave propagation for telecommunication applications*. Springer, 2005.

[12] R. Freeman, "Radio system design for telecommunications, hoboken," 2007.

[13] J. U. A. J. M. Akura, "A high performance model for rainfall effect on radio signals,"

[14] T. Tamir, "Radio wave propagation along mixed paths in forest environments," *IEEE Transactions on Antennas and Propagation*, vol. 25, no. 4, pp. 471–477, 1977.

[15] A. Al-Hourani and S. Kandeepan, "Cognitive relay nodes for airborne lte emergency networks," in *2013, 7th International Conference on Signal Processing and Communication Systems (ICSPCS)*, pp. 1–9, IEEE, 2013.

[16] I. Recommendation, "530-13," propagation data and prediction methods required for the design of terrestrial lineof-sight systems"," *International Telecommunication Union*, 2009.

[17] P. Harley, "Short distance attenuation measurements at 900 mhz and 1.8 ghz using low antenna heights for microcells," *IEEE Journal on Selected Areas in Communications*, vol. 7, no. 1, pp. 5–11, 1989.

[18] H. Xia, H. L. Bertoni, L. R. Maciel, A. Lindsay-Stewart, and R. Rowe, "Radio propagation characteristics for line-of-sight microcellular and personal communications," *IEEE Transactions on antennas and propagation*, vol. 41, no. 10, pp. 1439–1447, 1993.

[19] R. Luebbers, "Finite conductivity uniform gtd versus knife edge diffraction in prediction of propagation path loss," *IEEE Transactions on Antennas and Propagation*, vol. 32, no. 1, pp. 70–76, 1984.

[20] K. Pahlavan and A. H. Levesque, *Wireless information networks*, vol. 93. John Wiley & Sons, 2005.

[21] P. Valtr, M. Fencl, V. Bares, and P. Pechac, "Comparison of measured and theoretically predicted rain attenuation at 32 ghz and 38 ghz," 2018.

[22] A. Neskovic, N. Neskovic, and D. Paunovic, "Indoor electric field level prediction model based on the artificial neural networks," *IEEE Communications Letters*, vol. 4, no. 6, pp. 190–192, 2000.

[23] J. O. Eichie, O. D. Oyedum, M. O. Ajewole, and A. M. Aibinu, "Comparative analysis of basic models and artificial neural network based model for path loss prediction," *Progress In Electromagnetics Research*, vol. 61, pp. 133–146, 2017.

[24] M. Piacentini and F. Rinaldi, "Path loss prediction in urban environment using learning machines and dimensionality reduction techniques," *Computational Management Science*, vol. 8, no. 4, pp. 371–385, 2011.

[25] S. Shrestha and D.-Y. Choi, "Rain attenuation over terrestrial microwave links in south korea," *IET Microwaves, Antennas & Propagation*, vol. 11, no. 7, pp. 1031–1039, 2017.

[26] M. Ahuna, T. Afullo, and A. Alonge, "Rain attenuation prediction using artificial neural network for dynamic rain fade mitigation," *SAIEE Africa Research Journal*, vol. 110, no. 1, pp. 11–18, 2019.

[27] A. Krenker, J. Bešter, and A. Kos, "Introduction to the artificial neural networks," *Artificial Neural Networks: Methodological Advances and Biomedical Applications. InTech*, pp. 1–18, 2011.

[28] K. Gurney, *An introduction to neural networks*. CRC press, 2014.

[29] B. Krose and P. Smagt, "An introduction to neural network . the university of amsterdam," *Amesterdam, Netherland*, 1996.

[30] A. Krenker, M. Volk, U. Sedlar, J. Bešter, and A. Kos, "Bidirectional artificial neural networks for mobile-phone fraud detection," *Etri Journal*, vol. 31, no. 1, pp. 92–94, 2009.

[31] C. A. Oroza, Z. Zhang, T. Watteyne, and S. D. Glaser, "A machine-learning-based connectivity model for complex terrain large-scale low-power wireless deployments," *IEEE Transactions on Cognitive Communications and Networking*, vol. 3, no. 4, pp. 576–584, 2017.

[32] A. B. Zineb and M. Ayadi, "A multi-wall and multi-frequency indoor path loss prediction model using artificial neural networks," *Arabian Journal for Science and Engineering*, vol. 41, no. 3, pp. 987–996, 2016.

[33] T. S. Rappaport, "Wireless communications–principles and practice, (the book end)," *Microwave Journal*, vol. 45, no. 12, pp. 128–129, 2002.

[34] Z.-w. Zhao, M.-g. Zhang, and Z.-s. Wu, "Analytic specific attenuation model for rain for use in prediction methods," *International Journal of Infrared and millimeter waves*, vol. 22, no. 1, pp. 113–120, 2001.

[35] P. García, J. García, J. Riera, and A. Benarroch, "Slant-path propagation experiment at ka-band in madrid," 2007.

[36] G. D. Abrajano and M. Okada, "Determining rain location through microwave mesh network signal attenuation," in *TENCON 2012 IEEE Region 10 Conference*, pp. 1–6, IEEE, 2012.

[37] S. Khaleefa, S. Alsamhi, and N. Rajput, "Tethered balloon technology for telecommunication, coverage and path loss," in *2014 IEEE Students' Conference on Electrical, Electronics and Computer Science*, pp. 1–4, IEEE, 2014.

[38] L. Reynaud and T. Rasheed, "Deployable aerial communication networks: challenges for futuristic applications," in *Proceedings of the 9th ACM symposium on Performance evaluation of wireless ad hoc, sensor, and ubiquitous networks*, pp. 9–16, ACM, 2012.

[39] W. L. Tan, P. Hu, and M. Portmann, "Experimental evaluation of measurement-based sinr interference models," in *2012 IEEE International Symposium on a World of Wireless, Mobile and Multimedia Networks (WoWMoM)*, pp. 1–9, IEEE, 2012.

[40] Y. Lin and H. Ye, "Input data representation for self-organizing map in software classification," in *2009 Second International Symposium on Knowledge Acquisition and Modeling*, vol. 2, pp. 350–353, IEEE, 2009.

[41] V. Jain, A. Singh, V. Chauhan, and A. Pandey, "Analytical study of wind power prediction system by using feed forward neural network," in *2016 International Conference on Computation of Power, Energy Information and Commuincation (ICCPEIC)*, pp. 303–306, IEEE, 2016.

[42] J. C. D. Angeles and E. P. Dadios, "Neural network-based path loss prediction for digital tv macrocells," in *2015 International Conference on Humanoid, Nanotechnology, Information Technology, Communication and Control, Environment and Management (HNICEM)*, pp. 1–9, IEEE, 2015.

[43] V. Erceg, L. J. Greenstein, S. Y. Tjandra, S. R. Parkoff, A. Gupta, B. Kulic, A. A. Julius, and R. Bianchi, "An empirically based path loss model for wireless channels in suburban environments," *IEEE Journal on selected areas in communications*, vol. 17, no. 7, pp. 1205–1211, 1999.